EVALUATION OF MODELLING STRATEGIES FOR BEHAVIOR OF REINFORCED CONCRETE BRIDGE COLUMNS UNDER MONOTONIC AND CYCLIC LOADING
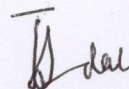
TARUTAL GHOSH MONDAL

CE13M1023

A Dissertation Submitted to

Indian Institute of Technology Hyderabad

In Partial Fulfilment of the Requirements for

The Degree of Master of Technology

भारतीय प्रौद्योगिकी संस्थान हैदराबाद
Indian Institute of Technology Hyderabad

DEPARTMENT OF CIVIL ENGINEERING

INDIAN INSTITUTE OF TECHNOLOGY HYDERABAD, INDIA

JUNE, 2016

Declaration

I declare that this written submission represents my ideas in my own words, and where others' ideas or words have been included, I have adequately cited and referenced the original sources. I also declare that I have adhered to all principles of academic honesty and integrity and have not misrepresented or fabricated or falsified any idea/data/fact/source in my submission. I understand that any violation of the above will be a cause for disciplinary action by the Institute and can also evoke penal action from the sources that have thus not been properly cited, or from whom proper permission has not been taken when needed.
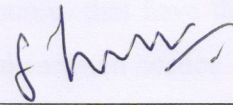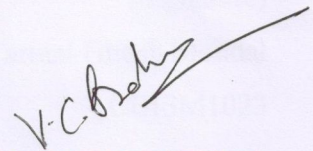
(Signature)
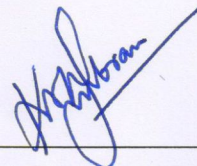
Tarutal Ghosh Mondal

CE13M1023

Approval Sheet

This thesis entitled "*Evaluation of Modelling Strategies for Behaviour of Reinforced Concrete Bridge Columns under Monotonic and Cyclic Loading*" by TARUTAL GHOSH MONDAL is approved for the degree of Master of Technology from IIT Hyderabad.

Dr. S. Suriya Prakash

Advisor

Dr. C. P. Vyasarayani

Co-Advisor and External Examiner

Prof. K. V. L. Subramaniam

Internal Examiner

Dr. Anil Agarwal

Internal Examiner

Acknowledgements

I would like to express my highest appreciation to my supervisor, Dr. S. Suriya Prakash, who gave me the opportunity to work in this interesting area and for the patient guidance, encouragement and advice he has provided through my time as his student. His effort in supporting me throughout the work was invaluable.

I have been lucky to be supervised by Dr. C. P. Vyasarayani who cared so much about my work and responded to my queries promptly. I also would like to thank Dr. Anil Agarwal for his precious guidance that represented a constant source of help and encouragement throughout the work. I really appreciate the discussions we have had.

ABSTRACT

Torsional loadings can significantly affect the flow of internal forces and deformation capacity of RC columns. This, if not considered in design, can influence the performance of vital components of bridges and consequently impact the daily operation of the transportation system. Moreover, presence of torsional loading increases the possibility of brittle shear dominated failure which may result in fatal catastrophe. However, a review of previously published studies indicates that the torsional behaviour of reinforced concrete members has not been studied in as much depth as the behaviour under flexure and shear. The present study focuses on filling this knowledge gap existing in this important area of research. A finite element study is conducted to understand the overall behaviour of reinforced concrete columns under monotonic torsional loading. Influence of different parameters like reinforcement ratio and level of axial compression, internal shear flow distribution in the cross section and sequence of failure progression for square and circular columns were investigated. On the other hand, recent bridge failures due to earthquakes around world have renewed interest in understanding the nonlinear dynamic behaviour of existing and new bridge structures. Analysis of reinforced concrete bridge columns under cyclic loading requires proper identification and calibration of suitable hysteresis models. Columns being the most critical components of a bridge structure, knowledge on the hysteresis behaviour of bridge columns are of primary importance in determining the earthquake response of bridges. This study aims at predicting the flexural hysteresis behaviour of RC bridge columns using Bouc - Wen type model. Experimental data from literature is used for validation of the proposed modelling approach. A good correlation was observed between the observed behaviour and the predicted values. A polygonal hysteresis model is also developed to predict the response of circular RC columns under cyclic torsional loading. Unloading and reloading rules are proposed based on statistical analysis of experimental data. The prediction of the model compared favourably with measured values.

CONTENTS

LIST OF FIGURES

LIST OF TABLES

CHAPTER 1
INTRODUCTION

1.1 GENERAL

The damages observed after earthquakes has indicated that torsional oscillations are often the cause of distress in buildings and bridges. Reinforced concrete (RC) bridge columns with irregular three-dimensional bridge configurations can result in significant torsional moments in addition to axial, bending, and shear forces during earthquake events. The addition of torsion is more likely in skewed or horizontally curved bridges, bridges with unequal spans or column heights, and bridges with outrigger bents. Torsion in bridges with outrigger bents occurs due to eccentricity of reaction force developed in the footing due to lateral movement of superstructure under seismic vibration (Fig. 1.1(a)). In skewed bridges, the collision between bridge deck and abutment may cause inplane rotation of superstructures and consequently induces torsion in the bridge columns (Fig. 1.1(b)).
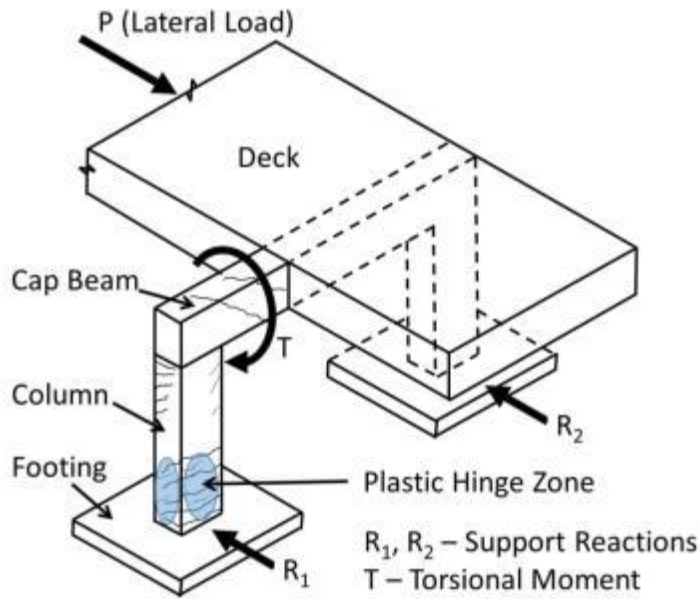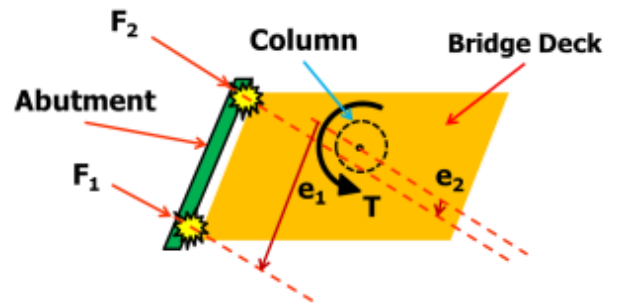
(a) Outrigger Bent   (b) Skew Bridge Deck

Fig. 1.1 Torsion in Bridge Structures

Torsion effects due to rotation of the superstructure can be significant when shear keys restrain the bridge superstructure at the abutment, and/or if there is a significant decrease in the torsion stiffness in relation to the bending stiffness of the column. Construction of bridges with these configurations is often unavoidable due to site constraints. The force produced in bridge columns due to dead and live loads is primarily axial. Bridges near the earthquake epicentre can be subjected to a significant vertical load (Saadeghvaziri and Fouch 1990), which is typically neglected in design. Lateral seismic loads will cause the single-column bents to translate laterally and rotate slightly when the bridge abutment has significant stiffness. Spread footings and pile footings have adequate torsional restraint to be considered when they are fixed against rotation. As such, the superstructure rotation will cause compatibility torsion in the columns. The load on the columns will, therefore, include axial compression, shear, flexure

and torsion. Axial loads can be considered constant in absence of a vertical component due to near field effects, while other loads act cyclically.

The possibility of significant torsional loadings was illustrated in an analytical study carried out to investigate the seismic torsion response of skewed bridge piers by Tirasit and Kawashima (2006). The results from their analysis show that pounding between skewed bridge deck and abutments takes place which results in inplane deck rotation increasing seismic torsion in skewed bridge piers. Moreover, they found that the consideration of the locking of bearing movement after failure can extremely amplify the seismic torsion in skewed bridge piers. This necessitates a clear understanding of the effect of torsion combined with bending, shear and axial compression on the behaviour of bridge columns.

1.2 LITERATURE REVIEW

Seismic torsion in bridges in the past earthquakes has been documented (Goel and Chopra 1994), analytically investigated (Isakovic et al. 1998, Meng and Lui 2000, Hurtado 2009, Tirasit and Kawashima 2005, Mondal and Prakash 2015c) and experimentally measured (Johnson et al. 2006, Nelson et al. 2007) by different researchers.

Hsu (1968a) tested 53 beams under pure torsion. The major variables of his experiments were – i) Amount of reinforcement, ii) Solid section versus hollow section, iii) Ratio of volume of longitudinal bars to volume of hoop bars, iv) Grade of concrete, v) Scale effects, vi) Depth-to-width ratio of cross section, vii) Spacing of longitudinal bars, and vii) Spacing of hoops. Some notable findings of his work are –

- Pre-cracking behaviour of reinforced concrete elements is identical to plain concrete elements. Saint – Venant theory cannot predict the post cracking response of RC sections.

- An RC section is said to be under-reinforced if the reinforcement yields prior to crushing of concrete in compression. If crushing of concrete occurs before yielding of reinforcement, then the section is called over-reinforced.

- The concrete in the core does not contribute to ultimate capacity of the section significantly.

- Hoop spacing has minimal effect on the ultimate capacity of RC sections with identical volumetric ratio of hoops.

Lampert and Collins (1972) showed through experimental and analytical studies that space truss model can accurately predict the torsional strength of RC sections with low reinforcement ratio. However, the model becomes unconservative for high reinforcement ratio.

Mitchell and Collins (1974) introduced 'diagonal compression field theory' to deal with this unconservatism and suggested that prediction of the proposed model matches the post cracking experimental response accurately. In the same line, Hsu and Moy (1985) presented 'softened truss model' which is equally competent in predicting the behaviour of RC sections subjected to torsional loading. The two theories are based on slightly different assumptions on concrete behaviour and thickness of shear flow zone. They are more accurate than space truss model but at the same time more complicated to implement.

Most of the investigations in the past focused solely on the ultimate torsional strength of RC members ignoring the overall torque – twist behaviour. Hsu (1968a) observed that before

cracking the torsional behaviour of reinforced concrete members is similar to plain concrete members with small increase in strength with increasing reinforcement. After cracking torsional stiffness drops suddenly and follows a short plateau till peak and thereafter encounters a gradual fall in resistance till failure (Lampert 1973, Mitchell and Collins 1974, Rabbat and Collins 1978, Hsu and Moy 1985). Lampert (1973) derived a theoretical expression for post cracking secant stiffness based on space truss model. However, Lampert's expression cannot follow the complete torque – twist curve as in case of diagonal compression field theory proposed by Mitchell and Collins or softened truss model proposed by Hsu. Few other models were proposed in the same line by Leung and Schnobrich (1987), Rahal and Collins (1996) and Cocchi and Volpi (1996) to predict the overall torsional behaviour of reinforced concrete sections.

Investigations have revealed that cyclic torsional loading reduces the strength and stiffness of a reinforced concrete member based on the displacement history of the member. Jakobsen et al. (1984) tested six reduced scale RC box columns under cyclic torsion with and without constant axial compression. His key findings are summarised below.

- Failure initiated by spalling of concrete in the corner.

- Just after cracking significant stiffness degradation took place.

- Load repetition at current maximum twist level caused stiffness reduction proceeding at decreasing rate.

- Load repetition below current maximum twist level did not affect the stiffness perceptibly.

- Axial compressive load and increased reinforcement ratio delayed the stiffness degradation.

Venkappa and Pandit (1987) conducted cyclic torsion tests on 16 reinforced concrete beams and made the following observations.

- Pre-cracking response was linear and was marked by absence of residual strains.

- The response after cracking was marked by nonlinearity of strains and progressive degradation of stiffness with successive loading cycle.

- The number of cycle causing failure declines sharply with increasing peak torque. Faster loading rate also has a similar influence on the number of loading cycle.

- Preloading under cyclic torsion significantly lowers the stiffness of an RC specimen.

Besides, several investigations were focused on the response of square (Ogata et al. 2000, Hsu and Wang 2000, Hsu and Liang 2003, Nagata et al. 2004, Otsuka et al. 2004, Tirasit and Kawashima 2005, Mondal and Prakash 2015b), oblong (McLean and Buckingham 1994, Hurtado 2009) and circular (Hurtado 2009, Prakash et al. 2012, Mondal and Prakash 2015a) columns subjected to cyclic and combined torsional loading. Nevertheless, information is scarce on several issues, such as, the effect of increasing the transverse reinforcement ratio, longitudinal reinforcement ratio, geometry of the cross section and the effect of axial compression on the torsional response of RC bridge columns.

A review of previous studies indicates that, hysteresis modelling approaches adopted by different researchers in the past are predominantly of two types, namely – polygonal hysteresis models (PHM) and smooth differential models (SDM). In polygonal hysteresis models, the response of an entity is represented by a set of path defining piecewise linear or nonlinear functions. One of the best known polygonal hysteresis models available in literature

is Clough and Johnston (1966) model, which is characterized by a bilinear primary curve. It considers strain hardening in post yielding regime and takes into account stiffness degradation under load reversals. Takeda model (Takeda et al. (1970)) represents a tri-linear primary curve marked by a stiffness change at cracking point. It is governed by some loading – unloading rules formulated based on experimental observations. In the pivot hysteresis model developed by Dowell et al. (1998), the envelope curve under monotonic loading has four branches characterized by elastic stiffness, strain hardening, strength degradation and linearly decreasing residual strength. The loading and unloading are governed by two pivot points which determine the level of softening with increasing displacement and the degree of pinching on load reversal. Other notable works on PHM include Fukada (1969), Aoyama (1971), Atalay and Penzien (1975), Nakata et al. (1978), Mansur and Hsu (2005), and Tirasit and Kawashima (2007). The PHMs are governed by some empirical laws derived on the basis of experimental observations representing a certain range of the parameters that influence the behaviour under cyclic loading. Utility of the models beyond that range of guiding parameters requires careful verification. Therefore, the PHMs are not generic and they lack the versatility of being applied to different structural systems and loading protocols. This limitation of PHM led to the development of smooth differential models where the response of a member to a reversed cyclic loading is represented by a set of ordinary differential equations. Among all SDMs studied previously, the one proposed by Bouc (1967) and Wen (1976, 1980) is most widely used owing to its versatility and robustness. It is also computationally efficient and mathematically tractable. The model was subsequently modified by Baber and Noori (Baber and Wen 1981, Baber and Noori 1985, 1986) to include the effect of system degradation and pinching and the improved model is popularly known as Bouc - Wen - Baber - Noori (BWBN) model. In the past, Bouc - Wen type models have been used to predict the cyclic response of different structural systems such as, masonry walls (Clarke 2005), torsional – shear buildings (Omrani et al. 2010), reinforced

concrete beams and beam-column joints (Kunnath et al. 1997, Sengupta and Li 2013), concrete piles (Lin et al. 2002) and base isolation devices (Ismail et al. 2010). However, only limited studies have focused on predicting the flexural hysteresis behaviour of RC bridge columns.

On the other hand, all the PHMs mentioned above were developed for shear and flexure and are incapable of predicting the behaviour under torsion owing to high degree of pinching and degradation involved in torsional loading. Very few researchers have, in deed, focused on the analytical modelling of the hysteresis behaviour exhibited by RC members under cyclic torsion. Tirasit and Kawashima (2007) and Wang et al. (2014) have recently proposed some PHMs for RC columns under torsional loading. In both of the studies, a semi-empirical primary curve was used, where the yield torsional moment was estimated using space truss analogy and post-yield behaviour was obtained from empirical relations derived on the basis of experimental observations. However, application of these models is limited to specimens having similar geometric and reinforcement configurations as those used for formulation of the models. Validation of the models outside that range of test variables remained a scope of future work.

1.3 MOTIVATION

It is essential to expand the knowledge on the behaviour of RC members so that the effects of torsion can be clearly understood for developing rational design provisions. A few finite element studies in the recent years looked at the response of RC columns subjected to combined loading (Mullapudi and Ayoub 2009, Belarbi et al. 2009, Prakash et al. 2010). However, the existing FE models have the limitation of not predicting the post peak behaviour accurately. Moreover, the previously proposed models were validated with test data on global behaviour of the specimens alone, with complete disregard to local behaviours like strain in

the reinforcement. In addition to that, influence of different sectional parameters (e.g. reinforcement ratio and cross sectional shape), internal stress distribution and failure mechanism of the members were not adequately investigated from FE perspective. To fill this knowledge gap in this area, a FE model is generated in this study to accurately predict the global as well as local behaviour of RC columns under combined torsion and axial compression. A number of square and circular columns experimentally tested under torsion with various transverse reinforcement ratios and level of axial compression (Prakash 2009, Tirasit and Kawasima 2007a, 2007b) were analysed using full scale nonlinear finite element models. The finite element analysis results for overall torque – twist behaviour and localised values of strains in the rebar compared favourably with the test results. After calibration of the developed model, a parametric study was carried out to study the effect of cross sectional shape, transverse reinforcement ratio and increasing axial compression. Apart from that, the FE study presented in this thesis provides a valuable insight in to the progression of failure of columns under combined torsion and axial compression. Thickness of shear flow zone and shear stress distribution across the cross section are also investigated which are rather difficult to measure experimentally. This brings in an important contribution of this study as these parameters were not previously investigated in a detailed manner.

On the other hand, collapse of many important bridges around the world caused by recent earthquakes has put forth the necessity to assess the seismic vulnerability of the existing bridge columns. Seismic analysis of reinforced concrete (RC) structures requires hysteresis models that can accurately predict strength, stiffness, and ductility characteristics of the members under cyclic loading. Bridge columns should be properly designed to adequately dissipate seismic energy through inelastic deformation under vibrations during earthquakes. The level of accuracy of seismic design depends on the accuracy of the hysteresis model.

Owing to all these reasons it is of utmost importance to have a proper hysteresis model which can accurately predict the cyclic behaviour of RC members considering strength and stiffness degradation along with the pinching effects. However, very few investigations in the past have focused on development of analytical model which can accurately predict the response of RC bridge columns under cyclic loading. The present study focuses on filling this knowledge gap existing in this field by proposing a hysteresis model which accurately predicts the cyclic behaviour of RC columns of any cross-section, reinforcement ratio, and aspect ratio.

1.4 OBJECTIVE AND SCOPE

The objectives of this study are –

- To develop a FE model to predict the behaviour of RC columns under monotonic torsional loading.

- To investigate the influence of transverse reinforcement ratio, axial compression on torsional strength and stiffness of RC members.

- To determine the sectional distribution of shear stress and thereby to estimate the thickness of shear flow for square and circular sections at different stages of monotonic torsional loading.

- To predict the damage distribution and failure progression in RC columns under torsional loading through FE study.

- To develop an analytical model to accurately predict the hysteretic behaviour of RC columns of different cross sections, reinforcement ratio and level of axial compression under cyclic flexure and torsion.

The scopes of this study are summarised below –

❖ Finite Element Analysis

- The scope of this study is limited to square and circular columns only. Columns with other shapes of cross section are a scope of future study.

- Longitudinal reinforcement ratio was not a variable in the specimen considered for this study. Future studies should focus on the influence of longitudinal reinforcement ratio on torsional behaviour of RC columns.

- Columns specimens used in this study were tested under zero or low level of axial compression. So, column behaviour under torsional loading with high level of axial compression was not investigated. However, it may be investigated in details in a future study.

❖ Bouc – Wen Based Hysteresis Modelling

- The scope of this study is limited to circular columns only. Columns with other shapes of cross section are a scope of future study.

- This study focused on columns failing in flexure alone. Future study should focus on columns failing in shear, torsion and combined loading.

❖ Polygonal Hysteresis Modelling under Torsion

- The scope of this study is limited to circular columns only. Columns with other shapes of cross section are a scope of future study.

- Longitudinal reinforcement ratio was not a variable in the specimen considered for this study. Future studies should focus on validation of the developed model with specimens having different longitudinal reinforcement ratio

1.5 EXPERIMENTAL PROGRAM

1.5.1 Specimen Details

The specimens considered in this study for validation of the proposed finite element model include three columns (H/D(3)-T/M(∞)-1.32%, H/D(6)-T/M(∞)-0.73% and Missouri Square) tested at University of Missouri and another two columns (TP-91 and TP-92) tested in University of Tokyo. The details of the columns are listed in Table 1.1. The cross sectional details are shown in Fig. 1.2.

For calibration of the BWBN model, experimental results of five columns tested by Lehman and Moehle (2000) and three other columns tested by Saatcioglu and Baingo (1999) were considered. The reinforcement and geometric characteristics of the specimen considered in this study have been summarised in Table 1.2. Previous studies have shown that the parameters which significantly influence the inelastic cyclic response of reinforcement concrete bridge columns are the longitudinal and spiral reinforcement ratio, the axial load ratio and the column aspect ratio. It can be observed from Table 1.2 that, the specimens considered in this study for validation of BWBN model represent a wide range of the parameters mentioned above.

Table 1.1 Details of specimen used for validation of the proposed FE model

Specimen Id/ Parameters	H/D(3)- T/M(∞) − 1.32%	H/D(6)- T/M(∞)-0.73%	TP-91	TP-92	Missouri Square
Section Shape	Circular	Circular	Square	Square	Square
Diameter/Width (mm)	610	610	400	400	560
Clear Cover (mm)	25	25	27.5	27.5	38
Total Column Height (m)	2.74	4.55	1.75	1.75	3.35
Effective Column Height (m)	1.83	3.65	1.35	1.35	3.35

Cylinder Strength of Concrete (MPa)	27.97	37.90	28.3	28.4	34.6
Longitudinal Steel Yield Strength (MPa)	462	462	354	354	512
Transverse Steel Yield Strength (MPa)	457	457	328	328	454
Transverse Steel Ratio (percentage)	1.32	0.73	0.79	0.79	1.32
Longitudinal Steel Ratio (percentage)	2.1	2.1	1.27	1.27	2.13
Axial Force (kN)	600.51	600.51	0	160	0

Table 1.2 Details of specimen used for validation of BWBN model

Specimen Name $Test - H/D - \rho_l - \rho_t - P_{Axial}$	ρ_l (%)	ρ_t (%)	H (m)	D (mm)	Concrete Strength (MPa)	H/D	Axial (kN)	Yield Strength of Long. Bar (MPa)	Yield Strength of Transv. Bar (MPa)
Leh-H/D(4)- 1.5%- 0.72%-7.2%	1.5	0.72	2.4	610	31	4	654	462	607
Leh-H/D(4)- 0.75%- 0.72%-7.2%	0.75	0.72	2.4	610	31	4	654	462	607
Leh-H/D(4)- 2.98%- 0.72%-7.2%	2.98	0.72	2.4	610	31	4	654	462	607
Leh-H/D(8)- 1.5%- 0.72%-7.2%	1.5	0.72	4.8	610	31	8	654	462	607
Leh-H/D(10)- 1.5%- 0.72%-7.2%	1.5	0.72	6.1	610	31	10	654	462	607
Saat-H/D(6.58)- 3.28%-1.54%-21%	3.28	1.54	1.64	250	90	6.6	925	419	1000
Saat-H/D(6.58)- 3.28%-1.75%-42%	3.28	1.75	1.64	250	90	6.6	1850	419	580
Saat-H/D(6.58)- 3.28%-3.43%-42%	3.28	3.28	1.64	250	90	6.6	1850	419	420

(a) H/D(6)-T/M(∞)-0.73% and H/D(3)-T/M(∞)-1.32%

13 mm diameter
longitudinal bars

6 mm diameter ,
square ties
@ 50mm c/c

28 mm diameter
longitudinal bars

25 mm diameter
longitudinal bars

9 mm diameter ,
square ties @ 82mm c/c

9 mm diameter ,
Octagonal ties
@ 82mm c/c
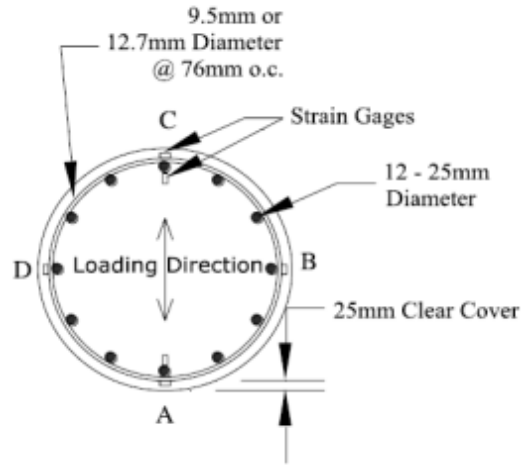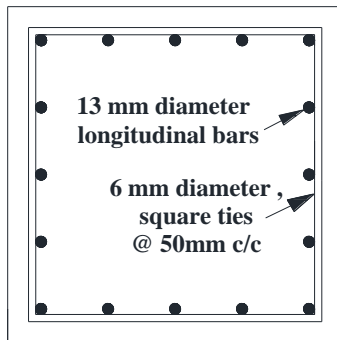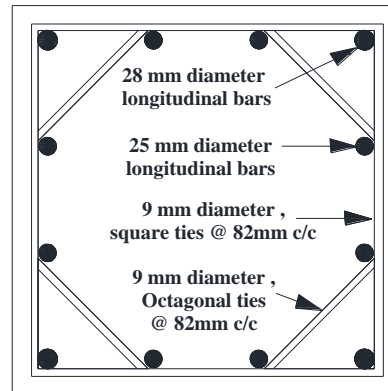
(b) TP-91 and TP-92   (c) Missouri Square

Fig. 1.2 Cross section of the specimens

1.5.2 Test Setup and Loading Protocol

Test data for the specimens tested in University of Missouri and University of Tokyo are obtained from Prakash (2009) and Tirasit and Kawasima (2007a, 2007b) respectively. As a part of these studies, several columns were tested under cyclic combined loading including torsion. The test setup for circular columns is shown in Fig. 1.3. Cyclic torsional loading was generated by controlling two horizontal servo-controlled hydraulic actuators. The axial compressive load was applied by a hydraulic jack on top of the load stubs. This jack transferred the axial load to the column via seven un-bonded high-strength pre-stressed steel strands. A number of instruments were used to measure the applied loads, deformations, and internal

23

strains. Electrical strain gages were attached to the surface of the longitudinal and transverse reinforcement to measure strains permitting study of the deformation of reinforcement under different loading conditions. The square columns had a similar test setup for applying cyclic torsion. However, in case of square columns, time varying axial compressive load was applied with the help of a vertical actuator attached to the top of the columns.
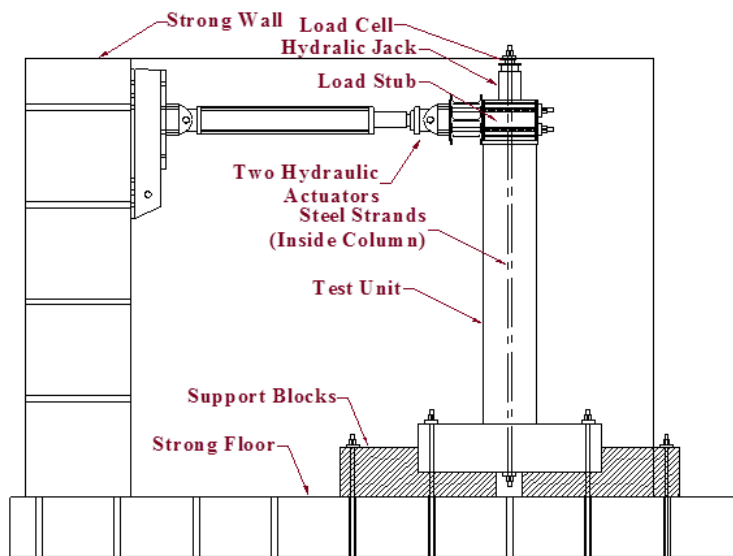
Fig. 1.3 Test set up

In the tests conducted by Lehman and Moehle (2000), the axial load was applied through a spreader beam using a post-tensioning rods placed on either side of the column. However, Saatcioglu and Baingo (1999) used two vertical actuators to apply constant level of axial compression throughout the test. The lateral displacement was applied using a servo-controlled hydraulic actuator that was attached to the top of the column. For the specimens tested by Saatcioglu and Baingo (1999), the lateral displacement history consisted of incrementally increasing deformation reversals. On the other hand, for the specimens tested by Lehman and Moehle (2000), the imposed displacement history included three cycles at each displacement level. For the post-yield displacement levels, a small displacement cycle was

imposed following the three main cycles. However, in this study only one cycle of each displacement level was considered for validation of the analytical model.

CHAPTER 2

BEHAVIOUR OF RC COLUMNS UNDER MONOTONIC TORSION: A FINITE ELEMENT STUDY

2.1 GENERAL

Finite element (FE) modelling of reinforced concrete structures under combined loading has received considerable attention in recent years. However, combination of torsion and axial compression is least studied until now in spite of its frequent occurrence in bridge columns under earthquake loading. This study aims at creating a nonlinear finite element model to predict the behaviour of reinforced concrete bridge columns under combined torsion and axial compression. A number of circular and square columns were analysed. The developed FE model was calibrated on local and global behaviour through comparison with test data. The overall torque–twist behaviour of the members was captured well by the developed FE models. The predicted values of strain in the longitudinal and transverse reinforcement matched closely with the experimental results. Increase in transverse steel ratio was found to increase the torsional capacity and limiting the damage of columns under torsion. It was further observed that at low level of axial compression the torsional capacity of columns is enhanced. In addition, the FE analysis showed a good agreement on the identification of the damage mechanism and the progression of failure. The shape of cross section is found to play a major role in distribution of torsional damage in the columns. Square columns exhibited a more localized damage due to presence of warping unlike in circular columns which exhibited a distributed damage along its length.

2.2 MATERIAL MODELS

2.2.1 Concrete

Concrete is a quasi-brittle material and has different behaviour in compression and tension. Smeared crack approach and damaged plasticity approach are generally used for nonlinear analysis of concrete. In the present study, damaged plasticity approach has been adopted as it offers a broad potential for matching the simulation results to experimental values (Fink et al. 2007). This is a continuum plasticity based isotropic damage model to represent the inelastic behaviour of concrete. This model is most suitable for the analysis of reinforced concrete structures subjected to monotonic or cyclic dynamic loading under low confining pressure. The details of this model can be found in Jankowiak and Lodygowski 2005, Kmiecik and Kaminski 2011 and ABAQUS Analysis User's Manual 6.11.

The values of Young's modulus and Poisson's ratio were provided as elastic properties. For the nonlinear part, compressive stress data is provided as a tabular function of inelastic (or crushing) strain to define the hardening behaviour of concrete under compression. The tension stiffening option was used to define the strain softening behaviour of concrete after cracking. Tension stiffening can be specified by means of post cracking yield stress and cracking strain values. It helps in approximately modelling the bond behaviour between steel and concrete. Absence of tension stiffening may lead to local cracking failure which may introduce temporary instability in overall response of the model. Hence, it is important to define tension stiffening from the perspective of numerical stability also. The variation of the damage variables with stress states were also specified under tension and compression. Recovery of tensile and compressive stiffness upon load reversal was assumed to be 0 and 95% respectively (ABAQUS Analysis User's Manual 6.11).

Compressive stress – strain model proposed by Vecchio and Collins (1986) was used for modelling concrete in this study. The behaviour is linearly elastic up to about 30% of the maximum compressive strength. Above this point, the stress increases gradually up to the maximum compressive strength. Once it reaches the maximum compressive strength, the curve descends into a softening region, and eventually crushing failure occurs when ultimate strain is reached.

The stress–strain curve for concrete under tension is approximately linearly elastic up to the maximum tensile strength. After this point, the concrete cracks and the strength decreases gradually to zero. Several tension stiffening models are available to model the strain softening observed in cracked concrete. Exponential model proposed by Greene (2006) has been used in this study to include the tension stiffening effect. The default values of the failure ratios were taken from literature (Kmiecik and Kamiński 2011 and Chaudhari and Chakrabarti 2012). The dilation angle was assumed to be 36 degree. The ratio of the ultimate biaxial compressive stress to the ultimate uniaxial compressive stress was taken as 1.16. Absolute value of the ratio of uniaxial tensile stress at failure to the uniaxial compressive stress at failure was assumed to be 0.1 though the default value is 0.09. A default value of 1/3 was considered for the ratio of the principal tensile stress value at cracking in plane stress, when the other non-zero principal stress component attains the ultimate compressive stress value, to the tensile cracking stress under uniaxial tension. The value of the viscosity parameter was assumed to be zero.

2.2.2 Reinforcement Steel

Stress – strain behaviour of steel was obtained from coupon tests. Results of coupon tests conducted on steel used for the circular columns are shown in Fig. 2.1. The same for other

specimens can be found in Tirasit (2006) and Prakash (2009). Behaviour under compression and tension were assumed to be identical. The yield strength of different steels has been shown in Table 1.1 (Chapter 1). Mass density was taken as 7800 kg/m3. Modulus of elasticity and Poisson's ratio were assumed to be 200000 MPa and 0.3 respectively.
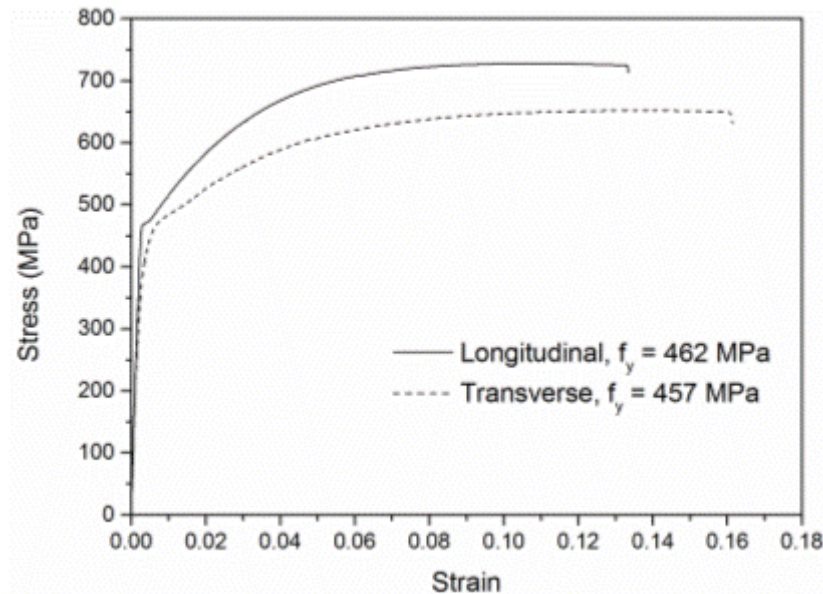
Fig. 2.1 Coupon test results for steel used in the circular columns

2.3 PROCEDURE: DYNAMIC EXPLICIT

Any quasi static problem can be solved as a dynamic one with sufficiently slow load increments to produce negligible inertial force. An explicit integration scheme available is used in this study owing to its advantages for highly nonlinear problems (Zimmermann 2001). Robustness in convergence behaviour, numerical stability, low computation cost and suitability for calculation in post failure range are the advantages of the explicit integration method. If dynamic analysis is adopted for static or quasi static procedure, the ratio of kinetic energy to

internal energy (ALLKE/ALLIE) must be less than 0.1 as recommended by Zimmermann (2001). This condition was satisfied for all the specimens considered in the present study.

2.4 STEEL – CONCRETE INTERFACE

The reinforcing steels were modelled as an embedded bar element. Separate truss elements can be used for modelling the reinforcement and they can be connected to the surrounding concrete elements via the interface elements. This approach is capable of representing the bond stress-slip relations between reinforcement and concrete. To improve the predictions, bond slip behaviour was modelled at the interface between longitudinal steel and concrete using a surfaced based contact interaction model. This Penalty interaction algorithm uses Coulomb friction model (ABAQUS Analysis User's Manual 6.11) for surface to surface interactions. The value of coefficient of friction was assumed to be 0.6 as suggested by Rabbat and Russell (1985). Shear stress limit was taken from Floros and Ingason (2013). Elastic slip stiffness was obtained from an equation proposed by Delso et al. (2011). Number of parametric studies was carried out to study the influence of bond on torsional behaviour. Incorporation of bond slip model did not produce appreciable improvement in the results when compared to perfect bond model. Hurtado (2009) observed that there was negligible slip during the testing of RC columns under torsion unlike in flexure where the slip is considerable. Hence, a perfect bond was considered for modelling the steel concrete interface in all the models to reduce the computational time and improve the accuracy of the predictions.

2.5 LOAD AND BOUNDARY CONDITIONS

One of the key aspects that influence a finite element solution significantly is the accurate estimation of load and boundary conditions. In the present study, all degrees of freedom were restrained at the bottom of the columns whereas the top was free to deform in any mode. The top surface was made rigid using rigid body constraint. Rigid body constraints allow to constrain the motion of regions of the assembly to the motion of a reference point. The relative positions of the regions that are part of the rigid body remain constant throughout the analysis. A reference point was created at the centre of the surface and was assigned as the rigid body reference point. Motion or constraints that are applied to the reference point are then applied to the entire rigid part. Angle of rotation was imposed monotonically at the reference point as a function of time in a tabular form. Constant magnitude of axial compressive load was also applied at the same reference point to simulate the test conditions of the experimental study.

2.6 MESHING

Accuracy of FE results greatly depend on the size of the mesh, kind of element used and order of approximation. Concrete was modelled with C3D8R element which is a 3 dimensional 8 noded brick element with 3 translational degree of freedom at each node. Rotational degrees of freedom are expressed in terms of the translational degrees of freedom. Reduced integration was used to get rid of excess stiffness due to shear locking. Hourglass control was adopted to eliminate the spurious modes. On the other hand, T3D2 element was used to model the rebars. It is a 2 noded 3 dimensional truss element with three translational degree of freedom at each node. Linear elements used in this study require finer mesh leading to increase in demand of computer capacity. However, this rise in capacity requirement is offset

by explicit integration scheme which is compatible to larger size of mesh. In order to determine the optimum mesh size for the FE model, a mesh sensitivity analysis was carried out using element aspect ratio of one. Number of elements was increased keeping the aspect ratio constant which resulted in smaller mesh sizes. This process was repeated successively until convergence of results was achieved.

2.7 RESULTS AND DISCUSSION

2.7.1 Validation of the Developed Model

Overall torque – twist behaviour of the test specimens are predicted by the developed finite element model and compared with experimental results in Fig. 2.1. The predictions of the FE model for overall torque – twist behaviour are found to be in good agreement with the experimental results. Efficacy of the model in predicting the cracking and ultimate torsional capacity of the tested columns is further illustrated in Table 2.1. FE model overestimates the cracking and ultimate torsional capacity, only to a limited extent. The overestimation can be attributed to size effect, material and geometric imperfections (Claeson and Johansson 1999) which are not considered in the FE model. The torsional stiffness predicted by the finite element model was close to the measured values, particularly in the pre-cracking and post-peak region. The predicted variation of longitudinal and transverse strain at the mid height of the columns with torsional moment showed a sound match with the experimental observations (Fig. 2.2). For both square and circular sections, the tie rebars was predicted to yield before the longitudinal rebars and the same was observed in the experiment. It demonstrates that the developed model is equally effective in predicting the local and the global behaviour of reinforced concrete members with fair accuracy.
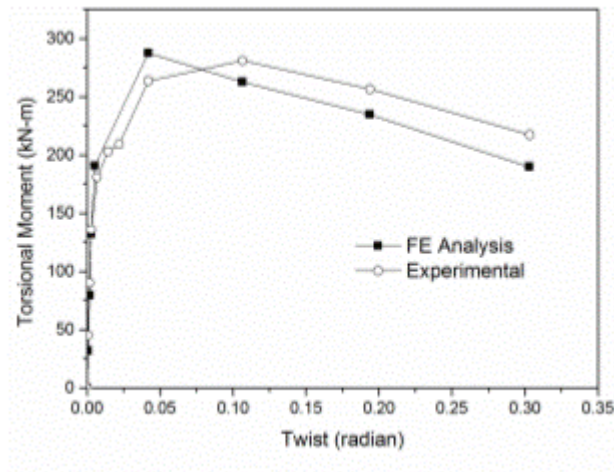
(a) H/D(6)-T/M(∞)-0.73%
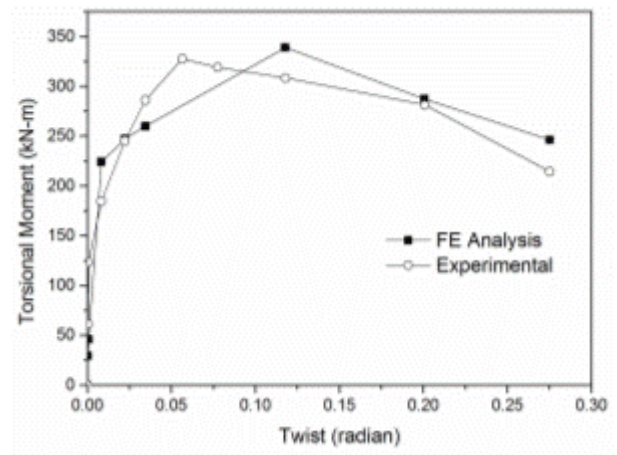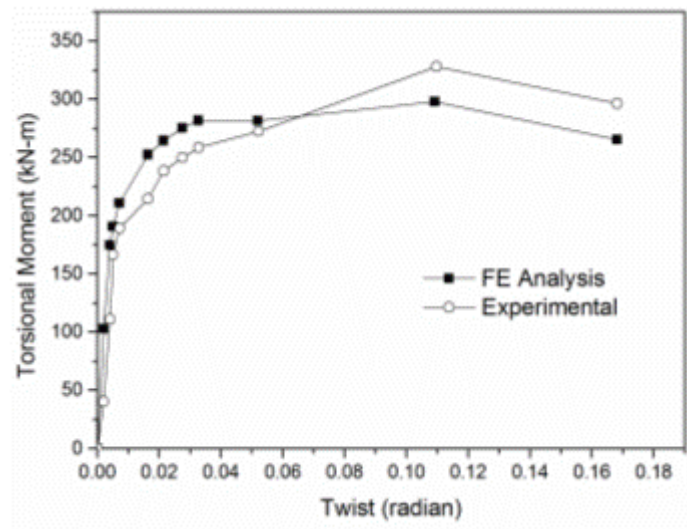
(b) H/D(3)-T/M(∞)-1.32%

(c) Missouri Square
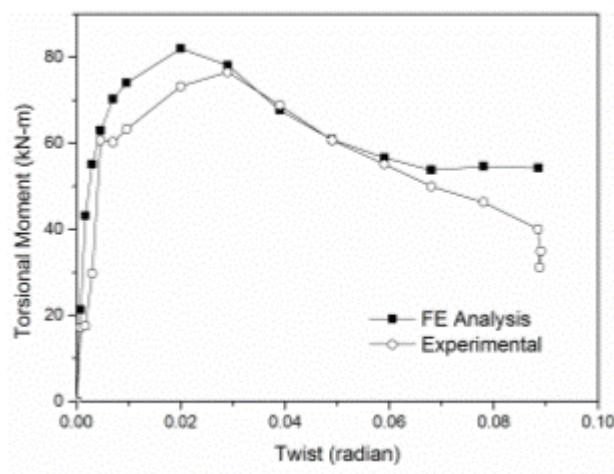
(d) TP-91
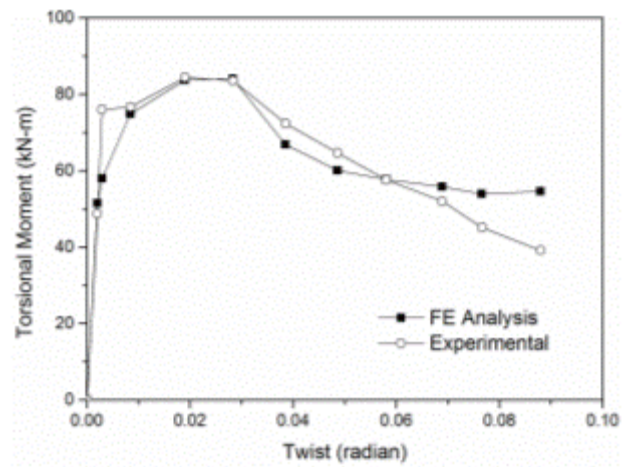
(e) TP-92

Fig. 2.1 Overall torque - twist behavior

Table 2.1 - Comparison of Predicted Values with Test Data

Specimen		TP-91	TP-92	H/D (6)-T/M (∞)-0.73%	H/D (3)-T/M (∞)-1.32%	Missouri-Square
Cracking Torque (kN-m)	FE Analysis (A)	62.9	58.0	190.7	224.1	212.3
	Experimental (B)	60.7	76.6	180.9	184.6	189.3
	A/B	1.04	0.76	1.05	1.21	1.12
Ultimate Torque (kN-m)	FE Analysis (A)	82.0	84.1	287.7	338.8	283.7
	Experimental (B)	76.6	84.4	281.1	327.5	328.0
	A/B	1.07	0.99	1.02	1.03	0.86
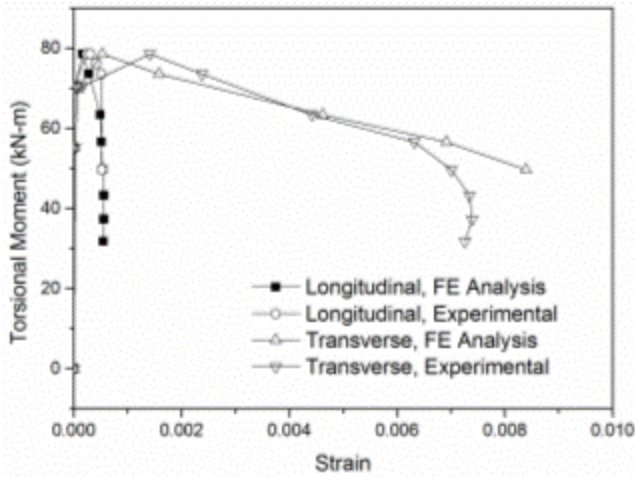
(a) TP-92
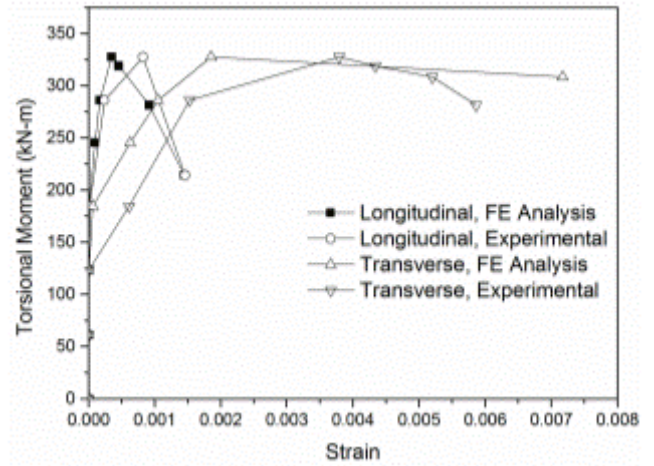
(b) H/D (3)-T/M (∞)-1.32%

Fig. 2.2 Strain in the rebars

2.7.2 Overall Torque – Twist Behaviour

Overall torque – twist behaviour of the square and circular columns is plotted in Fig. 2.1. The response is essentially linear in the pre-cracking range. After cracking, the torque – twist behaviour exhibits a short plateau followed by an increase in resistance at a tangential stiffness equal to a small fraction of the initial stiffness. Similar behaviour was observed in previous analytical studies using softened truss model (Hsu 1968a) and modified compression field theory (Mitchell and Collins 1974) which are used extensively for prediction of torsional

response of RC members. Failure of the columns subjected to torsion was governed by diagonal cracking leading to formation of torsional plastic hinge near the mid-height of the columns (Prakash et al. 2012).

2.7.3 Effect of Axial Compression

The tested square columns used for FE validation had an axial stress of 0 MPa and 1 MPa and the circular columns had a constant axial stress of 2 MPa. Effect of axial compression on the torsional behaviour of square and circular reinforced concrete columns is shown in Fig. 2.3. Presence of axial compressive load delays the tensile stresses in concrete arising from torsion. Thus, the cracking of concrete under diagonal tension is delayed. Consequently, cracking torsional capacity of RC members increases significantly in presence of low axial compressive load. Increased torsional moment with axial compressive load causes shear cracks spiralling around the column. This results in concrete compression field in the form of diagonal struts that will induce uniform tensile stress in longitudinal and transverse reinforcements. If some axial compression is applied together with torsional moment, and assuming that the column section is cracked due to applied torsion, the tension in the longitudinal steel induced by torsion will be reduced by the axial compression. Thus, the axial compression loading will produce an effect similar to that of increasing the longitudinal steel content in resisting the applied torsion. This results in increased torsional capacity of the section as observed in Fig. 2.4. A similar observation was recorded experimentally by Jakobsen et al. (1984) for box columns, Hurtado (2009) for circular columns and Bishara and Peir (1973) for square columns. More test results on columns with different sectional parameters in future studies should clarify the effect of axial compression on the torsional capacity of RC columns.
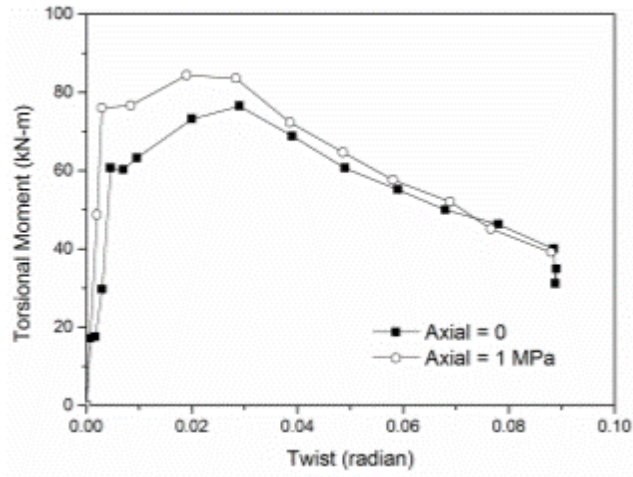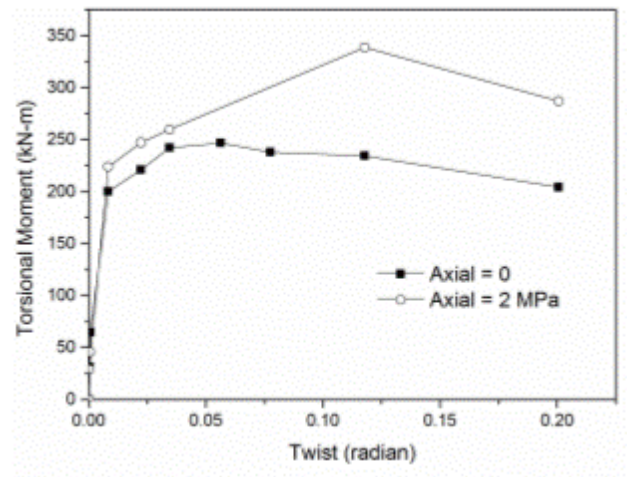
(a) Square Column   (b) Circular Column

Fig. 2.3 Effect of Axial Compression

2.7.4 Effect of Transverse Reinforcement

The effect of transverse reinforcement on the torsional moment - twist response of square and circular bridge columns was investigated and the results are shown in Fig. 2.4. The increase in transverse reinforcement ratio increased the peak torsional capacity of the columns as observed in Fig. 2.5. This is because, when an RC member is cracked due to applied torsion, apparent truss action is developed where the longitudinal and the transverse steel act as tensile links. In this way, the transverse reinforcements contribute to the torsional capacity of RC members. The twist at ultimate torsional moment was increased for square columns due to increased confinement and reduced softening by transverse reinforcement. However, the value of the same parameter was reduced for circular columns owing to the change in failure mode from ductile yield of reinforcement to brittle compressive failure of diagonal concrete strut. For square and circular columns, the variation in longitudinal and transverse strains with torsional moment for different transverse reinforcement ratio is compared in Fig. 2.6. It is observed that increase in transverse steel ratio increases the stiffness of the member thereby

limiting the strain levels in longitudinal as well as in transverse reinforcement which indicates less damage to the columns.
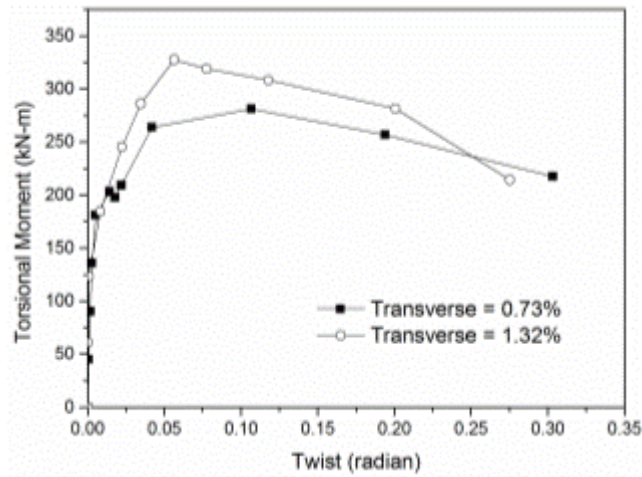
(a) Circular Column
(axial compression = 2 MPa)
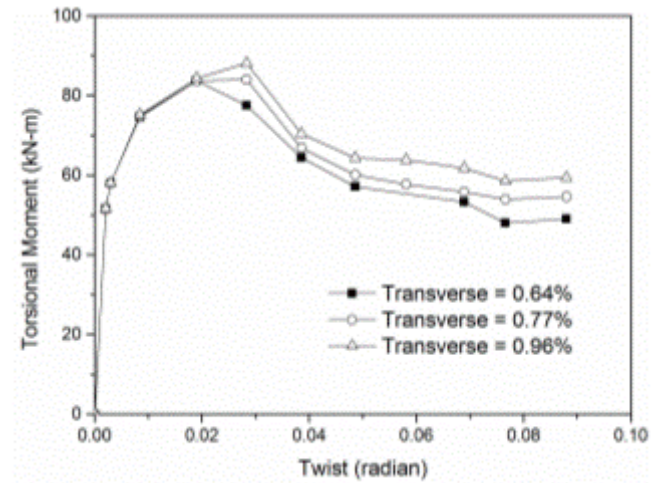
(b) Square Column
(axial compression = 1 MPa)

Fig. 2.4 Effect of Transverse Steel Ratio on Overall Torque – Twist Behavior
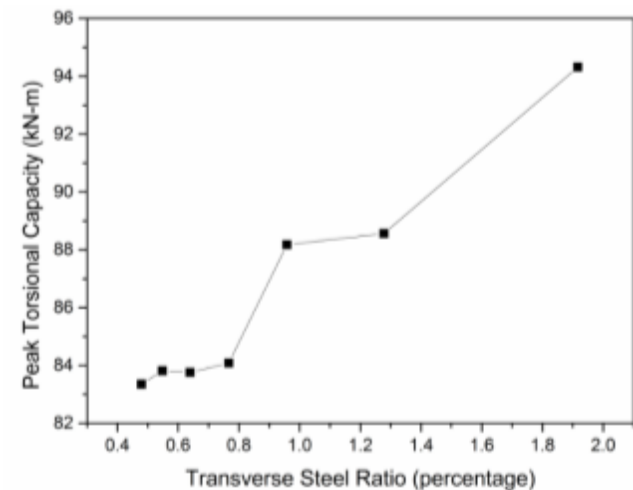
(a) Square Column
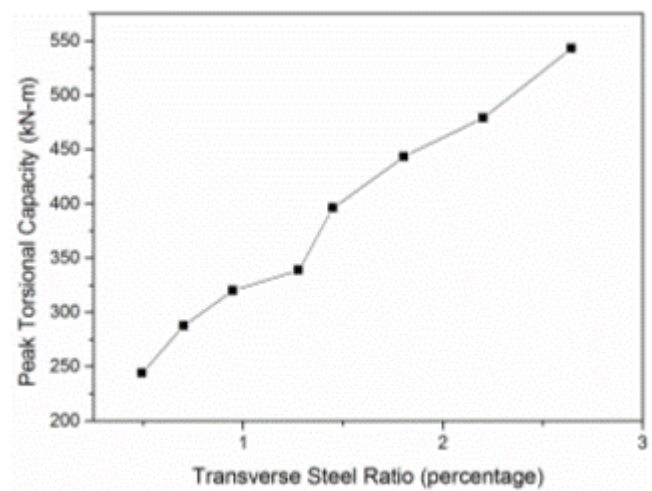
(b) Circular Column

Fig. 2.5 Effect of transverse steel ratio on peak torsional capacity
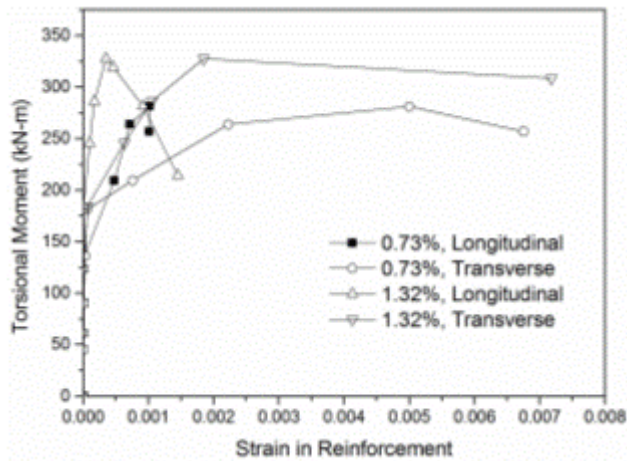
(a) Circular Column
(axial compression = 2 MPa)
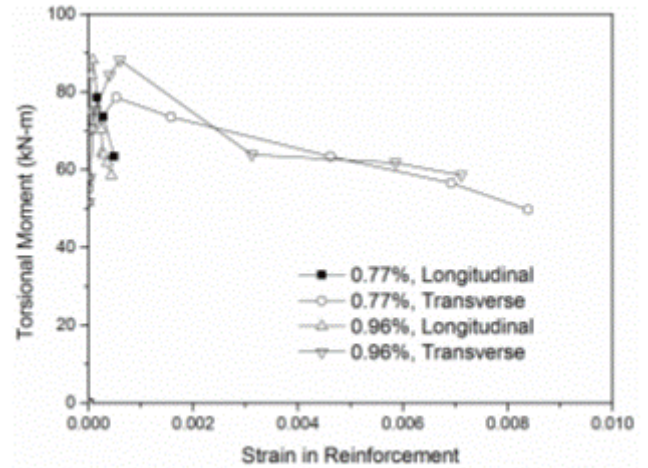
(b) Square Column
(axial compression = 1 MPa)

Fig. 2.6 Effect of Transverse Steel Ratio on Strain Level in Reinforcement

2.7.5 Thickness of Shear Flow Zone

The ultimate strength of reinforced concrete member under torsion can be predicted by the truss models, the modified compression field theory (MCFT) (Vecchio and Collins 1986), or the softened truss model (Hsu 1988; Pang and Hsu 1996; Hsu and Zhang 1997). These theories are based on Bredt's thin tube theory (Bredt 1896) which assumes that the torque resisted by the section acts as shear stress that flows around the perimeter of the cross section. The analysis of any member (hollow or solid) under torsion can be modelled as a thin-tube as shown in Fig. 2.7(a). The concrete core of a solid member is assumed to not contribute to the torsional resistance. These theories commonly assume reinforced concrete member as assemblies of two-dimensional membrane elements, also called panels, subjected to in-plane shear and normal stresses (Fig. 2.7(b)). Therefore, the behaviour of a reinforced concrete member under pure torsion can be predicted via the behaviour of membrane elements including additional equilibrium and compatibility equations. FE analysis can help in improving the predictions of these models by accurate estimation of shear flow thickness. The variation of shear stress at ultimate loads depends on the shape of cross section. Typical distribution of

38

shear stress for circular and rectangular cross section is shown in Fig. 2.8. The predicted shear flow distribution for circular and square columns at the cracking and peak torsional resistance is shown in Fig 2.9 and Fig. 2.10, respectively. The variation of shear stress was found to be highly nonlinear at peak torsional loading for both the circular and square cross sections. Higher shear stresses occur at the outer periphery of the cross section validating Bredt's thin tube theory. The results show that the calibrated FE models can be used for parametric studies to establish accurate estimation of shear flow thickness for developing simple analytical models for design purpose.
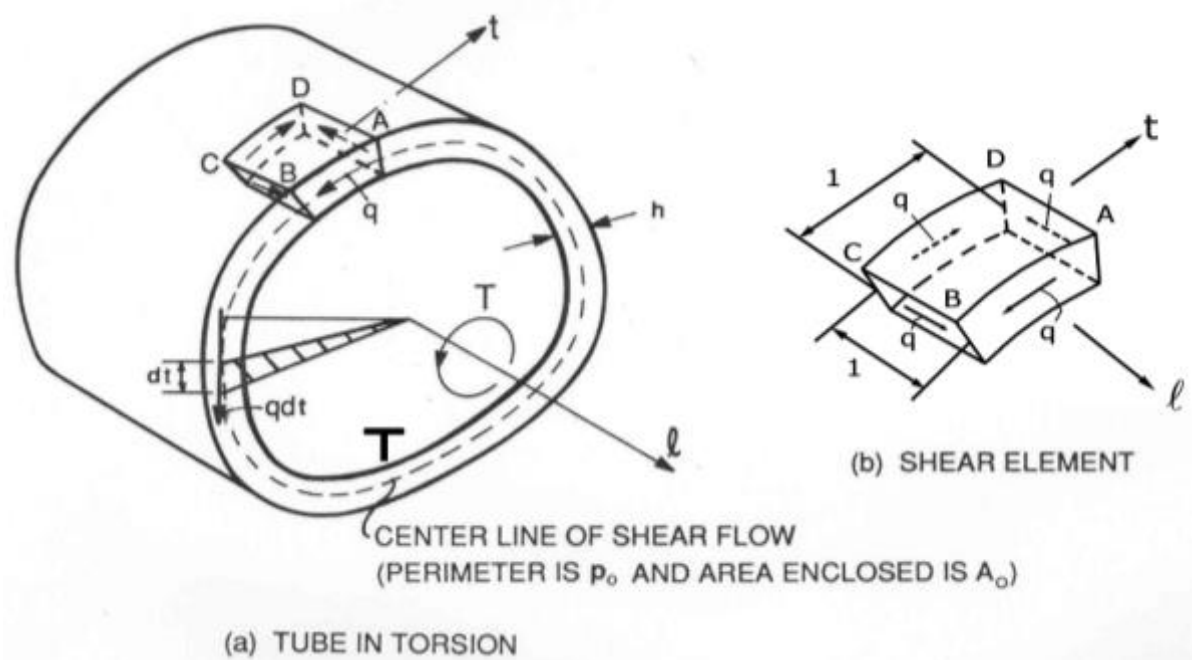
Fig. 2.7 Torsion of Thin Tube and Lever Arm Area A_o (Adapted from Hsu 1993)
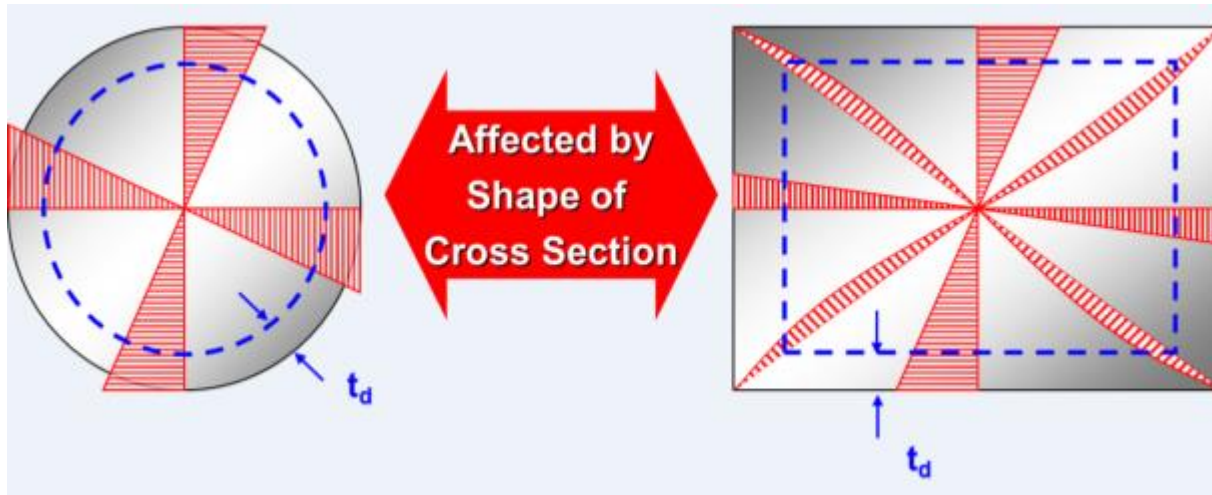
Fig. 2.8 Variation of shear stress for square and circular cross sections
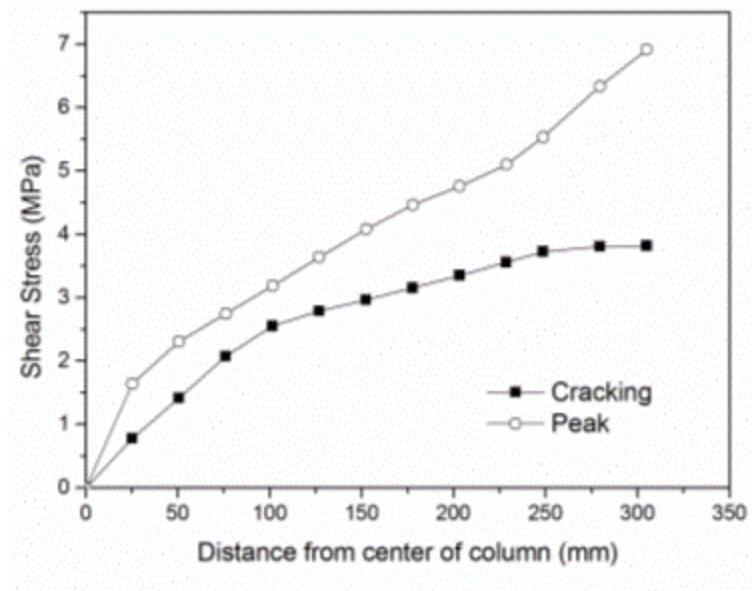
Fig 2.9 Variation of shear stress due to torsion in radial direction for circular sections
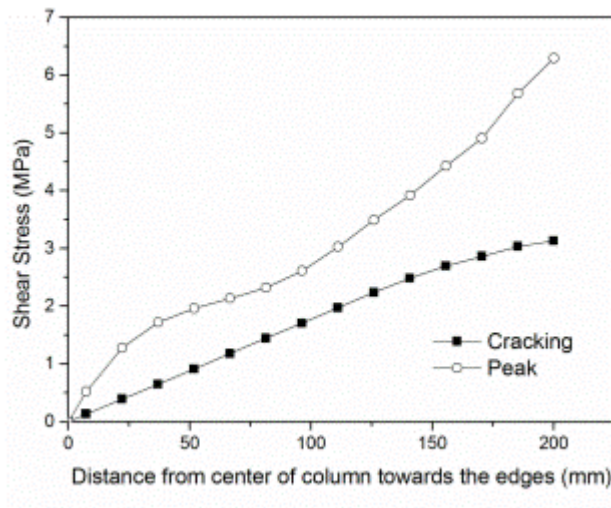
(a) Variation of shear stress towards the edges
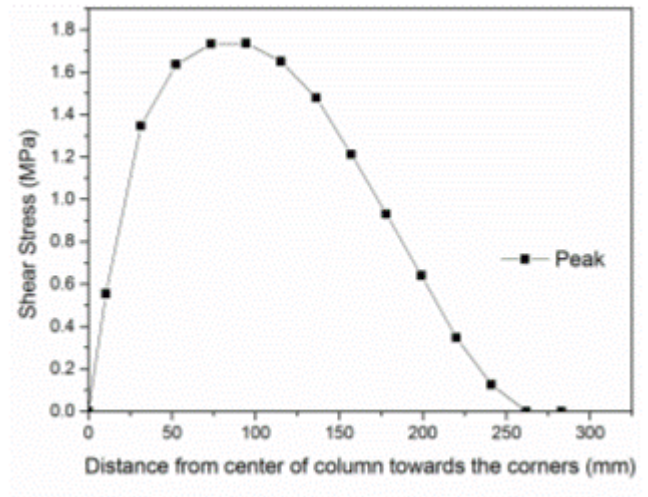
(b) Variation of shear stress in diagonal direction

Fig. 2.10 Variation of shear stress due to torsion in square sections

2.7.6 Damage and Spalling of Cover

Typically diagonal cracks start developing from near the mid-height of the column under applied torsion at lower levels of loading. The cracks spread and close in the form of inclined spiral as the loading is increased. Soon after the diagonal cracking, an apparent truss action is formed where the spirals act as tensile links. After significant yielding of spirals at a high level of torsional loading, a plastic zone forms near mid-height of the column. The progression of damage observed during testing is shown in Fig. 2.11 and 2.12.
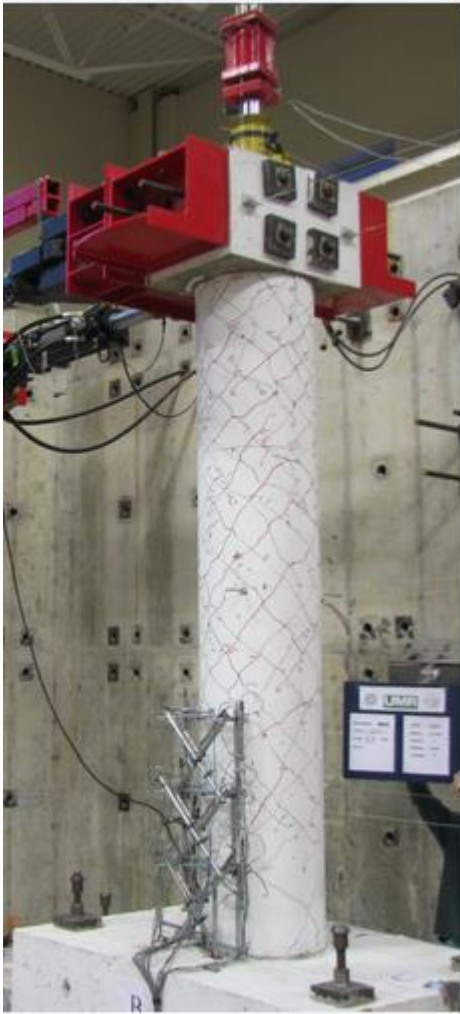
| (a) Transverse bar yield | (b) Peak torsional moment | (c) Overall failure |

Fig. 2.11 Damage in circular column under pure torsion

(a) Transverse bar yield (b) Peak torsional moment (c) Overall failure

Fig. 2.12 Damage in circular column under pure torsion

The damage state observed at ultimate load showed a good correlation with the finite element prediction as shown in Fig. 2.13. Tensile damage variable is used in this study to quantify degradation of the material. It is a non-decreasing quantity associated with the tensile failure of the material strength. The value of this variable is zero before any degradation of the material takes place and it reaches its maximum value of one at complete degradation of the

material. At an intermediate level of damage it assumes a value in between zero and one depending upon the level of damage. In essence, this parameter represents failure of material in a structure under loading in a quantitative sense. It was further observed that the effect of cross sectional shape played a major role on distribution of damage in the columns. Square columns exhibited a more localized damage (Fig. 2.13) owing to warping deformation compared to that of circular columns where the damage was predominantly distributed over a greater height of the columns.
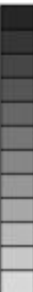
| Specimen Id | Experimental | FE Analysis | |
		Contour	Legend
H/D (6)-T/M (∞)-0.73%			DAMAGET (Avg: 75%) +9.973e-01 +9.165e-01 +8.357e-01 +7.549e-01 +6.741e-01 +5.932e-01 +5.124e-01 +4.316e-01 +3.508e-01 +2.700e-01 +1.892e-01 +1.084e-01 +2.760e-02
Missouri Square Specimen			DAMAGET (Avg: 75%) +9.973e-01 +9.142e-01 +8.311e-01 +7.480e-01 +6.649e-01 +5.817e-01 +4.986e-01 +4.155e-01 +3.324e-01 +2.493e-01 +1.662e-01 +8.311e-02 +0.000e+00

Fig. 2.13 Damage Distribution in Columns under Pure Torsion at Final Failure

2.8 CONCLUDING REMARKS

The results of nonlinear finite element analysis results for RC columns under combined torsion and axial compression are presented in this chapter. The generated FE model exhibited excellent convergence and numerical stability characteristics, requiring little computational time for analyses under torsional loading. The proposed model accurately simulated the overall experimental responses of columns under combined torsion and axial compression. Strength, stiffness, ductility, damage progression and failure modes are captured accurately. At low levels of axial compression, the cracking torsional moment increases significantly but ultimate torsional moment increases marginally. The increase in transverse reinforcement ratio increased the peak torsional strength. However, it reduced the twist component at the ultimate torsional moment. It also helps to limit the damage in columns under pure torsion. Effect of cross sectional shape plays a major role on distribution of damage in the columns. Square columns exhibited a more localized damage while the same in the circular columns was distributed over a larger length.

CHAPTER 3

BOUC – WEN BASED HYSTERESIS MODELLING OF CIRCULAR RC COLUMNS FAILING IN FLEXURE

3.1 GENERAL

Earthquake events in recent years have led to the collapse of many important bridges around the world. In general, the primary cause behind the failure of most of the bridges is inadequate capacity of the bridge columns under lateral loads. This requires one to assess the seismic vulnerability of the existing bridge columns. Seismic analysis is typically required for assessing the degree of damage and designing retrofit solutions (He et al. 2015). Seismic analysis of reinforced concrete (RC) structures requires hysteresis models that can accurately predict strength, stiffness, and ductility characteristics of the members under cyclic loading. Bridge columns should be properly designed to dissipate seismic energy adequately through inelastic deformation under vibrations during earthquakes (Goodnight et al. 2013, Prakash and Belarbi, 2010). The level of accuracy of seismic design depends on the accuracy of the hysteresis model. Owing to all these reasons it is of utmost importance to have a proper hysteresis model which can accurately predict the cyclic flexural behaviour of RC members considering strength and stiffness degradation along with the pinching effects.

Smooth differential models are a well-known modelling approach, where the response of a member to a reversed cyclic loading is represented by a set of linear ordinary differential equations. Among all SDMs studied previously, the one proposed by Bouc (1967) and Wen (1976, 1980) is most widely used owing to its versatility and robustness. The model was subsequently modified by Baber and Noori (Baber and Wen 1981, Baber and Noori 1985, 1986) to include the effect of system degradation and pinching and the improved model is

popularly known as Bouc - Wen - Baber - Noori (BWBN) model. In the past, Bouc - Wen type models have been used to predict the cyclic response of different structural systems such as, masonry walls (Clarke 2005), torsional – shear buildings (Omrani et al. 2010), reinforced concrete beams and beam-column joints (Kunnath 1997, Sengupta and Li 2013), concrete piles (Lin et al. 2002) and base isolation devices (Ismail et al. 2010). However, only limited studies have focused on predicting the flexural hysteresis behaviour of RC bridge columns.

Efficiency of BWBN model in predicting the response of a system greatly depends on accurate estimation of these unknown parameters. This requires adjusting the model parameters in such a way that the difference between the model output and the experimental measurements becomes minimal. Various system identification techniques can be applied to tune the model parameters so as to match the experimental measurements for proper approximation of the actual physical system. In the present study, a system identification tool box developed by Ortiz (2012) is used. This toolbox uses NSGA-II algorithm developed by Deb et al. (2002) for optimization. A good correlation is found between the predicted response and the experimental observation. The model was also able to capture the dissipated energy reasonably well. A sensitivity analysis was carried out to gauge the influence of different parameters to the accuracy of the model prediction. Each parameter was assigned a sensitivity ranking based on their relative sensitivity to model output. Finally, upper and lower bounds for each parameter were specified based on the range of their variation observed in this study.

3.2 BOUC-WEN-BABER-NOORI HYSTERESIS MODEL

3.2.1 Model Description

The formulation of BWBN model is founded on a single degree of freedom system containing a mass (m) connected in parallel with a linear viscous damper and a nonlinear hysteretic spring element as shown in Fig. 3.1.
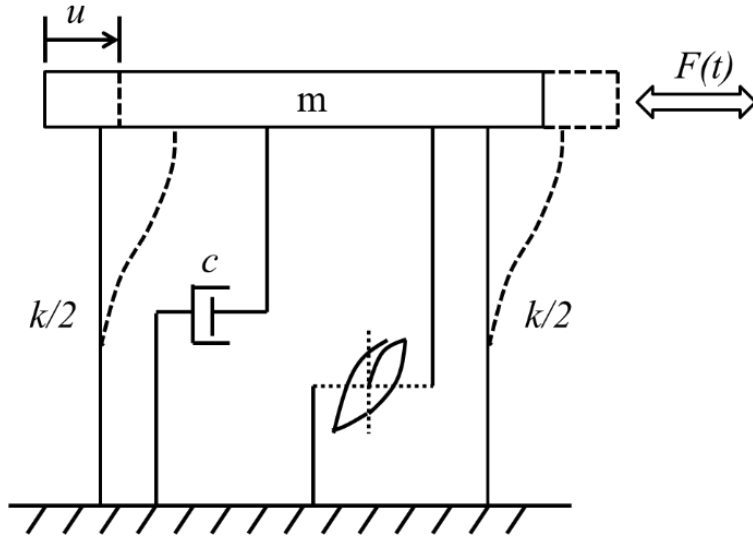
(a) Schematic Model
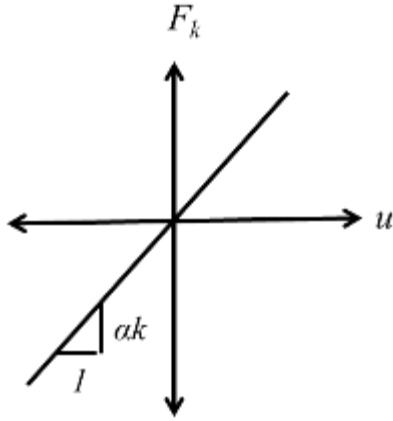
(b) Linear Restoring Force
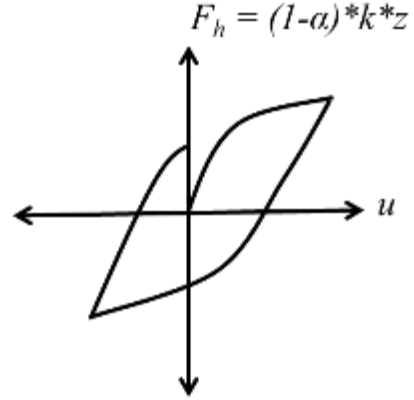
(c) Hysteretic Restoring Force

Fig. 3.1 SDF system representing BWBN Model

The equation of motion of the mass under a time dependent forcing function, *F(t),* is given by -

$$m\ddot{u} + c\dot{u} + R(u(t), z(t); t) = F(t) \tag{3.1}$$

where, u is relative displacement of the mass with respect to ground and c is linear viscous damping coefficient. The restoring force acting on the mass comprises the inertial restoring force ($m\ddot{u}$), the damping restoring force ($c\dot{u}$) and the non-damping restoring force,

($R(u(t),z(t);t)$), which is composed of linear restoring force $\alpha k u$ and hysteretic (nonlinear) restoring force $(1-\alpha)kz$ as shown in Eq. (3.2).

$$R(u(t), z(t);t) = F_k + F_h = \alpha k u + (1-\alpha)kz \tag{3.2}$$

where, k is the initial stiffness of the nonlinear spring, α is known as the rigidity ratio which varies in the range $0 \leq \alpha \leq 1$).

The mass-normalized equilibrium equation shown in Eq. (3.3) is obtained by dividing both sides of Eq. (3.2) by mass (m).

$$\ddot{u} + 2\xi_0\omega_0\dot{u} + \alpha\omega_0^2 u + (1-\alpha)\omega_0^2 z = f(t) \tag{3.3}$$

where, ξ_0 is linear damping ratio given by $c/2\sqrt{km}$. ω_0 is pre-yield natural frequency of the single degree of freedom system defined by $\sqrt{k/m}$. f_t is mass-normalized forcing function which is synonymous to acceleration of the system. The hysteretic displacement (z) is expressed as a first-order nonlinear differential equation as shown by Eq. (3.4).

$$\dot{z} = h(z)\left\{\frac{A(\varepsilon)\dot{u} - \nu(\varepsilon)(\beta|\dot{u}\|z|^{n-1}z + \gamma\dot{u}|z|^n)}{\eta(\varepsilon)}\right\} \tag{3.4}$$

where, $A(\varepsilon)$, β, and γ are parameters which control the shape and size of the hysteresis loop. n determines the smoothness of transition from elastic to the post-elastic part of hysteresis curve. Parameters $\nu(\varepsilon)$ and $\eta(\varepsilon)$ which represent strength and stiffness degradation are functions of dissipated energy ($\varepsilon(t)$) as shown in Eqs. (3.6)-(3.7).

$$A(\varepsilon) = A_0 - \delta_A\varepsilon(t) \tag{3.5}$$

$$\nu(\varepsilon) = 1 + \delta_\nu\varepsilon(t) \tag{3.6}$$

$$\eta(\varepsilon) = 1 + \delta_\eta \varepsilon(t) \tag{3.7}$$

where, δ_ν and δ_η define the rates of strength and stiffness degradation. The dissipated energy per unit mass, $\varepsilon(t)$, is a measure of the area under the hysteretic force (F_h) and displacement (u) curve as shown in Eq. (3.8).

$$\varepsilon(t) = \int_{u(0)}^{u(T)} F_h du = (1-\alpha)\omega_0^2 \int_{u(0)}^{u(T)} z du \frac{dt}{dt} = (1-\alpha)\omega_0^2 \int_0^T z(u,t)\dot{u}dt \tag{3.8}$$

The pinching function, $h(z)$ can be written as,

$$h(z) = 1 - \zeta_1 e\left[-(z\,\mathrm{sgn}(\dot{u}) - qZ_u)^2 / \zeta_2^2\right] \tag{3.9}$$

where,

$$\zeta_1(\varepsilon) = \zeta_0\left[1 - e^{-p\varepsilon}\right] \tag{3.10}$$

$$\zeta_2(\varepsilon) = (\psi_0 + \delta_\psi \varepsilon)(\lambda + \zeta_1) \tag{3.11}$$

ζ_0, p, q, ψ_0, δ_ψ and λ are pinching parameters constituting the pinching function. Z_u is the ultimate value of z, given by

$$Z_u = \pm\left[\frac{A}{\nu(\beta+\gamma)}\right]^{1/n} \tag{3.12}$$

The equations discussed in this section is expressed in state vector form as shown in Eq. (3.13).

$$y = \begin{Bmatrix} y_1 \\ y_2 \\ y_3 \\ y_4 \end{Bmatrix} = \begin{Bmatrix} u \\ \dot{u} \\ z \\ \varepsilon \end{Bmatrix} \tag{3.13}$$

It follows from the above discussion that the BWBN model can be represented by a set of ordinary differential equations (ODE) as given by Eqs. (3.14) - (3.17).

$$\dot{y}_1 = y_2 \tag{3.14}$$

$$\dot{y}_2 = -\alpha\omega_0^2 y_1 - 2\xi_0\omega_0 y_2 - (1-\alpha)\omega_0^2 y_3 + f(t) \tag{3.15}$$

$$\dot{y}_3 = h(z)\left\{ \frac{Ay_2 - \nu(\beta|y_2||y_3|^{n-1}y_3 + \gamma y_2|y_3|^n)}{\eta} \right\} \tag{3.16}$$

$$\dot{y}_4 = (1-\alpha)\omega_0^2 y_2 y_3 \tag{3.17}$$

When $A = \nu = \eta = h(z) = 1$ and Eq. (3.17d) is eliminated from the set of governing differential equations, the BWBN model is reduced to BW model comprising only 5 unknown parameters. Stiff ODEs like the ones presented above can be solved using various methods like Livermore solver (Sengupta 2014), semi implicit Rosenbrock method (Nithyadharan and Kalyanaraman 2013) or 4th order Runge – Kutta method (Ortiz et al. (2013)). In this study, the latter has been used for solving the linear ODEs.

3.3 OVERVIEW OF NSGA-II PROCEDURE

Various techniques have been attempted in previous studies for parameter identification of Bouc – Wen type model as shown in Table 3.1. It may be mentioned here that, all the methods suggested by various researchers minimize only the mean square error between estimated and experimental displacements. Ortiz et al. (2013) proposed a multi-objective optimization function by using NSGA-II algorithm. The multi-objective optimization involves minimizing the differences between estimated and measured displacements and the estimated and measured values of dissipated energies. The author (Oriz et al. 2003) found that this technique offered higher precision than all other existing methods. In this study, the same NSGA-II technique was adopted for optimization and a reasonably good match was observed between the predicted response and test data.

Table 3.1: Overview of various optimization techniques used in literature

Literature	Optimization Technique
Heine (2001)	Genetic Algorithm
Yang and Ma (2003)	Constrained Kalman Filter
Dimizas and Koumousis (2005)	Levenberg - Marquardt algorithm
Ye and Wang (2007)	Particle Swarm Optimization
Soeiro et al. (2007)	Levenberg - Marquardt algorithm + Stochastic Simulated Annealing Approach
Sengupta and Li (2013)	Genetic Algorithm
Nithyadharan and Kalyanaraman (2013)	Nelder and Mead's Simplex Algorithm
Mueller (2014)	Unscented Kalman Filter

Non-dominated Sorting Genetic Algorithm (NSGA-II), proposed by Deb et al. (2002), is one of the most referred multi-objective evolutionary algorithms that has been successfully applied on various optimization problems appearing from different fields. Unlike classical algorithms, evolutionary algorithms exploit the concept of working with population of candidate solutions where from the best set of Pareto solutions are picked up intelligently by several genetic operators working over several iterations. In binary NSGA-II, each of these solutions is presented in the form of binary strings. One example of this string where 4 decision variables are involved could be "{(001)(110)(111)(000)}", where the entire string within {} is one candidate solution and each of the decision variables is presented by the bits inside (). Presenting decision variables by 3 bits creates 2^3 discrete values which can be mapped between the lower (presented as 000) and upper bounds (presented as 111) of the decision variable. This clearly shows that increasing the number of bits for representing each of these decision variables is going to increase the precision of the decision variables involved. The first iteration is composed of candidate solutions (say, N_{Pop}^P parent solutions) that are created within the given bounds of the optimizing variables (or decision variables). Creating candidate solutions

within the given bounds helps not to handle bound constraints separately. Evaluating each of these solutions for their corresponding function values (fitness / objective function), the entire population is undergone the process of reproduction, where better solutions are selected and a new set of solutions (say, N_{Pop}^C parent solutions) are generated from them using genetic operators such as crossover and mutation. The extent of generation of new candidates is controlled by the probabilities of crossover and mutation. In crossover, two of the candidate parent solutions are selected randomly and a set of two new children solutions are generated by merging information of the given two parent solutions. This can be achieved by selecting a random cross site after keeping the two parent solutions one above the other and swapping the information appearing on one side of the cross site between them. In case of mutation, one of the bits in an optimizing variable in a candidate solution is selected randomly and changed. In this way, crossover creates new solution using information of existing solutions, whereas mutation creates solution disruptively. With the new population in place, the parent and children populations $(N_{Pop}^P + N_{Pop}^C)$ are merged and the entire set of population is evaluated for the fitness value. Using the fitness information, the population is next ranked on the basis of domination (termed as non-dominated sorting). In case of both objective minimization, a candidate solution "c" is asked to dominate solution "d", when both the objective values of solution "c" is less than that of solution "d". Following this definition, the set of solutions which dominates rest of the solutions are given a rank of 1 (N_{Pop}^{Rank-1}). Eliminating these N_{Pop}^{Rank-1} solutions from the set of $(N_{Pop}^P + N_{Pop}^C)$ solutions, non-dominated sorting is carried over again on rest of the solutions to find out the solutions in the rank 2 (N_{Pop}^{Rank-2}). This way the entire population is classified into several ranks and finally, the parents for the next generation, N_{Pop}^P are populated by picking low ranking solutions one after another (rank-1 first, then rank -2 and so on). The metric of crowding distance is used for the rank where all the solutions cannot be accommodated to be carried over to the next generation. Crowding distance

is the distance of a solution from its neighbors in the objective function space. This completes one iteration of NSGA-II and the entire process is repeated till the generation count reaches the final count ($N_{Gen, max}$) specified. For a relatively large value of $N_{Gen, max}$, final solutions with rank-1 are generated and the algorithm is assumed to be converged. The exploration operations of crossover, mutation and selection mechanisms like ranking-based selection and use of crowding distance metric help to generate non-dominated solutions which are well spread as well as near global Pareto solutions. The overall NSGA-II procedure is summarized in Fig. 3.2.
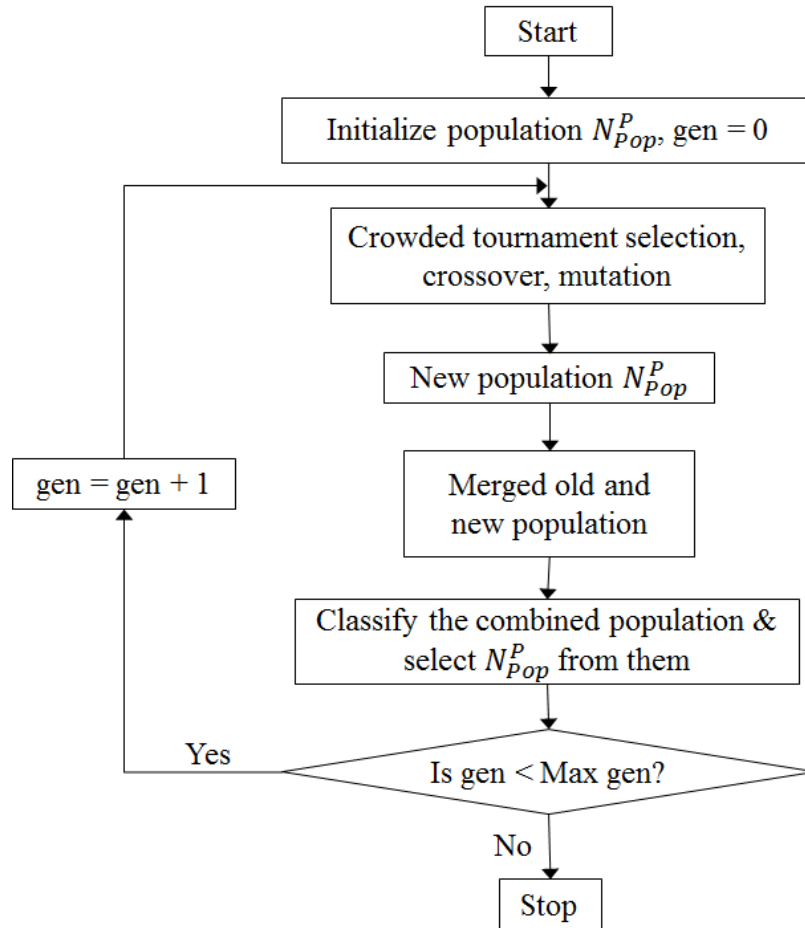
Fig. 3.2 Solution algorithm for NSGA-II

3.4 SYSTEM IDENTIFICATION WITH MULTI OBJECTIVE OPTIMIZATION

Ortiz et al. (2013) for the first time introduced multi objective optimization as a tool for identification of the model parameters. The authors proposed a set of objective functions involving displacement and dissipated energy as shown in Eqs. (3.18) - (3.20) and (3.23). The present study adopts the same objective functions as proposed by Ortiz et al. (2013) without any alteration.

1. The weighted difference between the experimental displacements ($u(t)$) and displacements predicted by the model ($\hat{u}(t \mid p)$).

$$f_1(p) = \sum_{i=1}^{l} \frac{|u(t_i) - \hat{u}(t_i \mid p)|}{w(t_i)} \tag{3.18}$$

where, $w(t)$ is a weighting function for normlaizing the displacements between $[-1, 1]$ and it is calculated using the envelope that linearly interpolates between the peak absolute values of the displacements (Ortiz et al. 2003). l is the number of elements in time series recorded in the laboratory. This objective function was widely used in the previous studies (Sengupta and Li (2013), Nithyadharan and Kalyanaraman (2013)) where parameters of BWBN model were identified using single objective optimization.

2. The maximum difference between the experimental values of displacement ($u(t)$) and displacements predicted by the model ($\hat{u}(t \mid p)$).

$$f_2(p) = \max_{1 \leq i \leq l} \left\{ |u(t_i) - \hat{u}(t_i \mid p)| \right\} \tag{3.19}$$

3. The difference between the total measured dissipated energy per unit mass ($\varepsilon_{tot}(t_l)$) in the experiments and the estimated total dissipated energy per unit mass ($\hat{\varepsilon}_{tot}(t_l \mid p)$) with BWBN model.

$$f_3(p) = \left| \varepsilon_{tot}(t_l) - \hat{\varepsilon}_{tot}(t_l \mid p) \right| \tag{3.20}$$

where $\varepsilon_{tot}(t_l)$ indicates the hysteresis curve area and can be expressed as the sum of elastic dissipated energy per unit mass ($\varepsilon_{el}(t_l)$) and hysteretic dissipated energy per unit mass ($\varepsilon(t_l)$) as shown below.

$$\varepsilon_{tot}(t_l) = \varepsilon(t_l) + \varepsilon_{el}(t_l) \tag{3.21}$$

$\varepsilon_{el}(t_l)$ is a measure of the area enclosed by elastic restoring force ($F^e(u(t))$) and displacement curve and can be written as:

$$\varepsilon_{el}(t_l) = \int_{u(0)}^{u(t)} \frac{F^e(u)}{m} dx = \alpha \frac{k}{m} \int_0^t x(\tau)\,\dot{x}(\tau)\,d\tau = \alpha \omega_0^2 \int_0^t x(\tau)\,\dot{x}(\tau)\,d\tau \tag{3.22}$$

4. The maximum difference between the total dissipated energy per unit mass ($\varepsilon_{tot}(t_l)$) calculated from load − displacement data, and the total dissipated energy per unit mass ($\hat{\varepsilon}_{tot}(t_l \mid p)$) estimated with BWBN model.

$$f_4(p) = \max_{1 \le i \le l} \left\{ \left| \varepsilon_{tot}(t_i) - \hat{\varepsilon}_{tot}(t_i \mid p) \right| \right\} \tag{3.23}$$

The parameter space D was restricted by two limiting vectors p_{min} and p_{max} such that $p_{min}(i) \le p(i) \le p_{max}(i)$, $1 \le i \le q$, where q is the number of parameters associated with the mathematical model. The stability of the differential equations was ensured by imposition of two linear inequalities such as $\beta + \gamma > 0$ and $\beta - \gamma > 0$. It is very common in multi-objective

optimization to encounter situations where different objective functions have different optimal solutions which compete with each other. These set of trade-off solutions are popularly known as Pareto optimal. The criteria adopted in this study for selecting a unique solution out of the entire set of Pareto optimal solutions is the minimum Euclidean distance from the origin to a normalized Pareto front as illustrated by Ortiz et al. (2013). The algorithm used in this study for multi objective optimization is shown in Fig. 3.3.
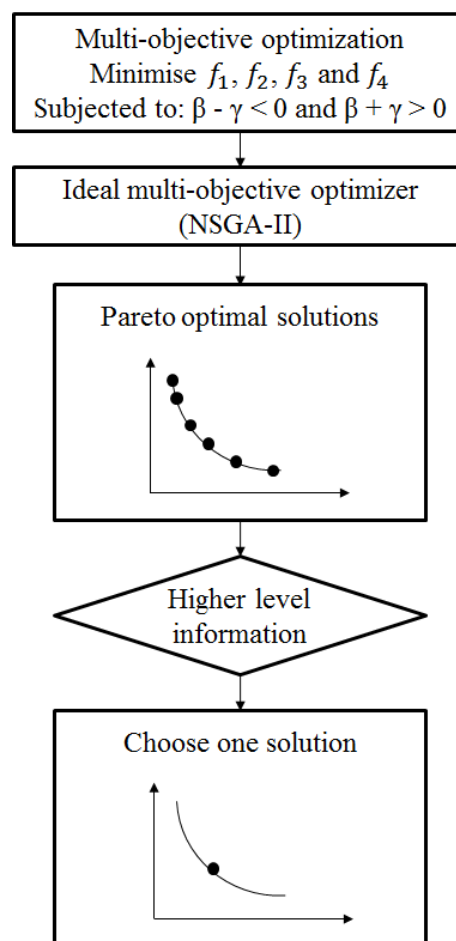
Fig. 3.3 Steps in multi objective optimization

3.5 RESULTS AND DISCUSSIONS

3.5.1 Prediction of Load – Displacement Behaviour

The load-displacement behaviour predicted by the analytical model are presented and compared with experimental data in Fig. 3.4. It is observed that, the model predicted the observed response of the tested specimens reasonably well. It can be also observed from the graphs that the model was able to capture the phenomena like strength and stiffness degradation along with pinching with a good accuracy. The converged values of the unknown parameters are summarised in Table 3.3 and 3.4.
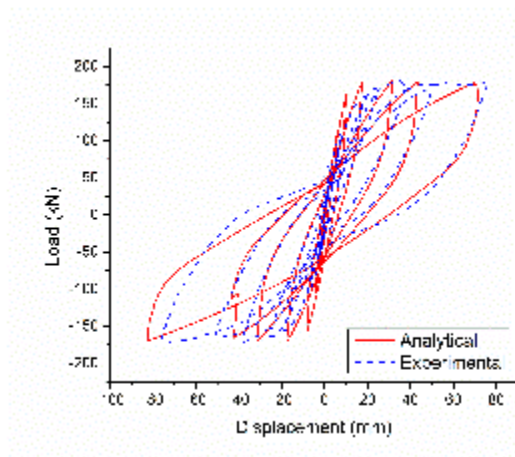
(a) Leh-H/D(4)- 1.5%-0.72%-7.2%
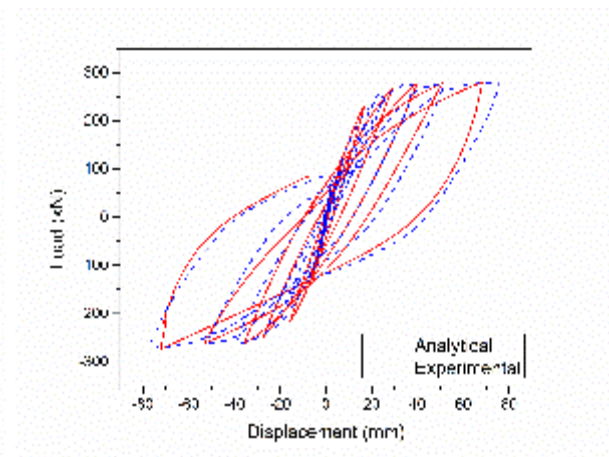
(b) Leh-H/D(4)- 0.75%-0.72%-7.2%
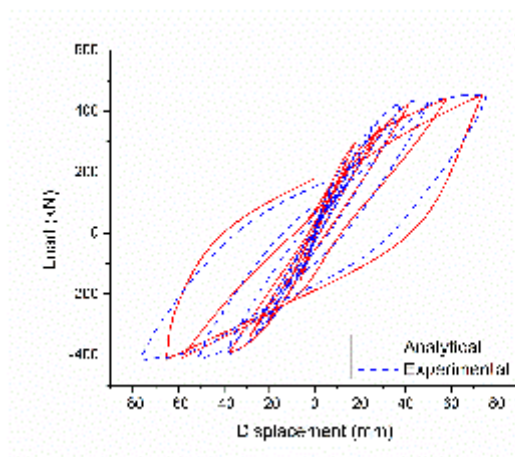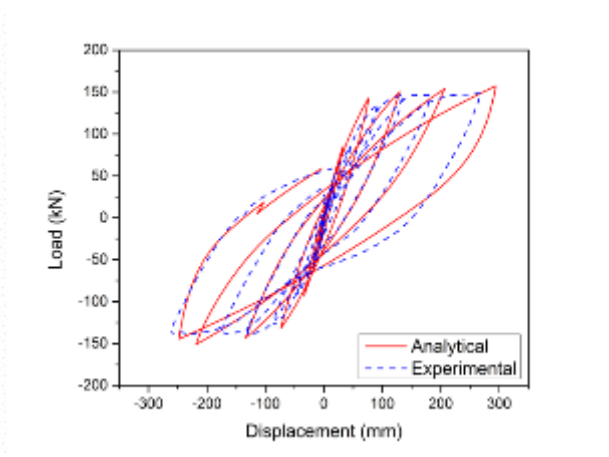
(c) Leh-H/D(4)- 2.98%-0.72%-7.2%

(d) Leh-H/D(8)- 1.5%-0.72%-7.2%
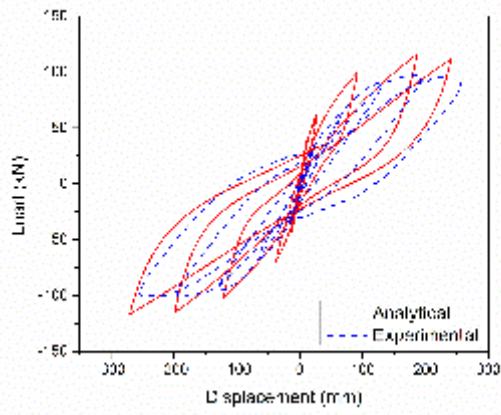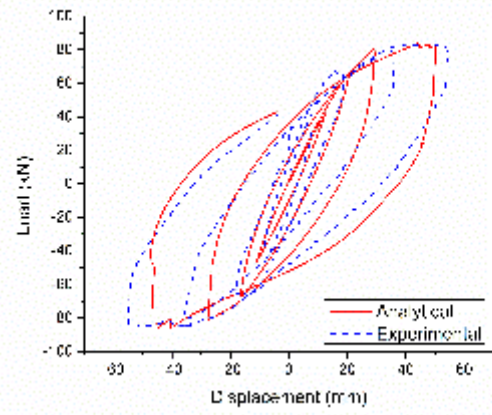
(e) Leh-H/D(10)- 1.5%-0.72%-7.2%   (f) Saat-H/D(6.58)-3.28%-1.54%-21%
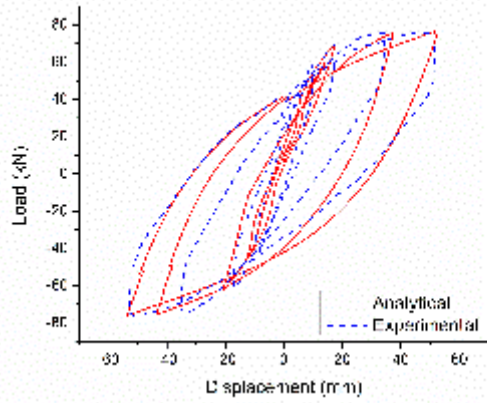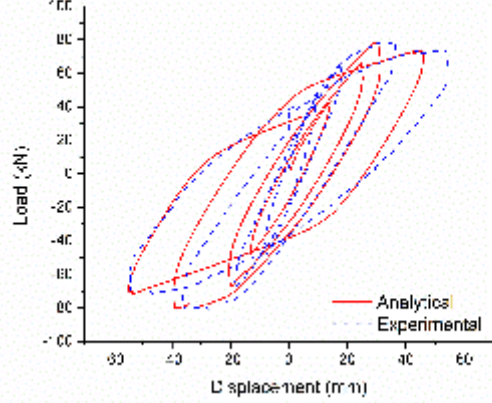
(g) Saat-H/D(6.58)-3.28%-1.75%-42%   (h) Saat-H/D(6.58)-3.28%-3.43%-42%

Fig. 3.4 Prediction of load – deformation behaviour

Table 3.3 Obtained model parameters for the bridge columns tested by Lehman and Moehle (2000)

	Leh-H/D(4)-1.5%-0.72%-7.2%	Leh-H/D(4)-0.75%-0.72%-7.2%	Leh-H/D(4)-2.98%-0.72%-7.2%	Leh-H/D(8)-1.5%-0.72%-7.2%	Leh-H/D(10)-1.5%-0.72%-7.2%
α	0.0407433	0.0964799	0.1191158	0.0286079	0.0130374
β	0.5095716	0.4627439	1.5016440	0.1315011	2.5675280
γ	-0.4690061	-0.0758199	-0.0900127	-0.0937927	-1.9861380
ξ	0.1234275	0.1104669	0.2358382	0.1156080	0.0645147
n	1.4426500	1.0033100	1.0671160	1.0006230	1.0104840
v_0	0.1427614	0.2604299	0.0003359	0.3416125	0.0187557
δ_v	0.2148782	0.2555180	0.0699940	0.0610115	0.0414266

A_0	2.5040620	5.3920180	3.2052890	2.4223650	2.7493890
δ_A	0.0664819	-0.2998774	-0.6900749	-0.0764594	-3.0650290
η_0	2.8164230	6.7927710	3.1466400	3.6640740	1.4726840
δ_η	3.3640030	5.4694450	6.6712000	2.2407170	11.1306300
p	4.3978310	0.0353988	8.1473140	3.1156360	2.0626950
ζ_0	-0.7742132	-6.0687180	-3.6594970	-2.6291620	0.6172936
ψ_0	-0.4146149	2.3848000	-7.5816870	1.1290900	-2.4245960
δ_ψ	2.5409530	1.7116370	0.6027874	-1.1896050	-1.2574620
λ	-0.7071068	2.1989540	1.9687790	1.5656850	1.9195990
q	3.0042070	7.3344820	5.1716300	-2.3739610	-0.4537854

Table 3.4 Obtained model parameters for the bridge columns tested by Saatcioglu and Baingo (1999)

	Saat-H/D(6.58)-3.28%-1.54%-21%	Saat-H/D(6.58)-3.28%-1.75%-42%	Saat-H/D(6.58)-3.28%-3.43%-42%
α	0.0373	0.0984	0.0675
β	0.1001	0.1005	0.1496
γ	-0.0032	0.1100	-0.0441
ξ	0.1716	0.1855	0.1338
n	1.2942	1.0108	1.6555
ν_0	0.1001	0.2609	0.1623
δ_ν	0.0625	0.2210	0.1986
A_0	2.0406	2.9066	1.9758
δ_A	-1.8902	-0.4232	-0.7356
η_0	3.6862	3.9791	5.7470
δ_η	3.3995	1.4025	3.3444
p	8.5244	5.0844	4.6596
ζ_0	0.8573	-0.5928	1.1464
ψ_0	3.4132	-0.8682	-2.5346
δ_ψ	-0.0301	-1.1569	-0.2323
λ	3.9872	3.4906	-1.0645
q	3.8576	0.9099	4.2282

3.5.2 Predictions of Dissipated Energy

Energy dissipation capacity is one of the most important parameters estimated from hysteresis curves. It is an important parameter for damage assessment and health monitoring of reinforced concrete structural members (Iranmanesh and Ansari 2013). Dissipated energy is a measure of the area under the load - deformation curve. The estimated and observed values of dissipated energy for all the columns are presented and compared in Fig. 3.5. Fig. 3.6 shows that, the analytical model used in this study can predict the energy dissipation capacity reinforced concrete bridge columns with reasonable accuracy.
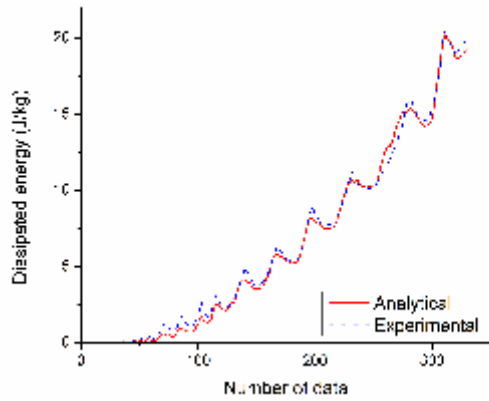
(a) Leh-H/D(4)- 1.5% -0.72% -7.2%
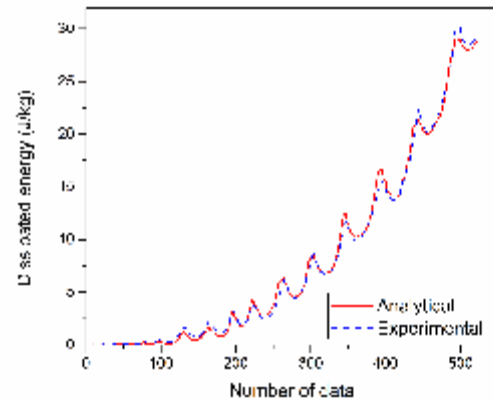
(b) Leh-H/D(4)- 0.75% -0.72% -7.2%
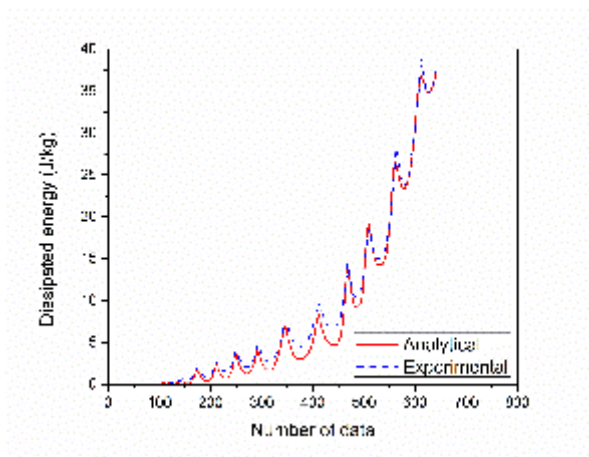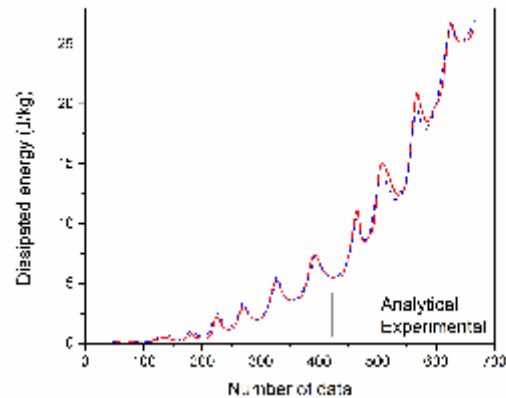
(c) Leh-H/D(4)- 2.98% -0.72% -7.2%

(d) Leh-H/D(8)- 1.5% -0.72% -7.2%
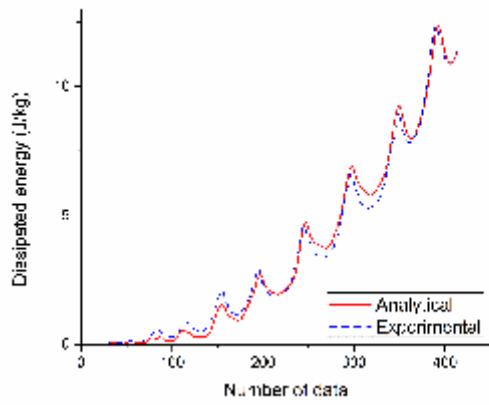
(e) Leh-H/D(10)- 1.5%-0.72%-7.2%
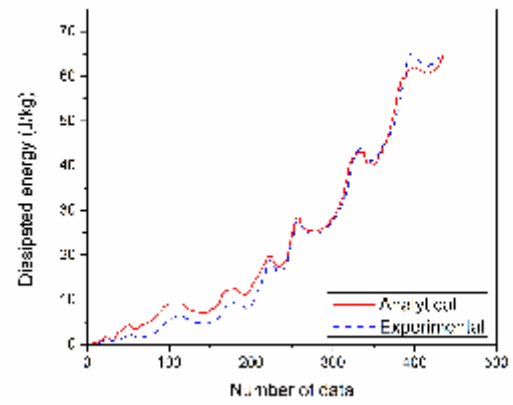
(f) Saat-H/D(6.58)-3.28%-1.54%-21%
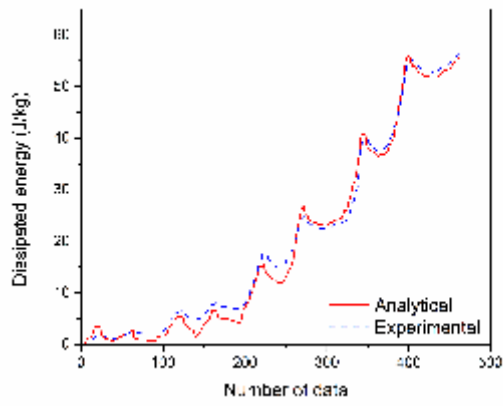
(g) Saat-H/D(6.58)-3.28%-1.75%-42%
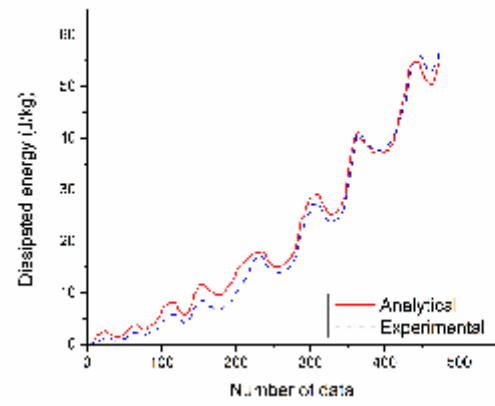
(h) Saat-H/D(6.58)-3.28%-3.43%-42%

Fig. 3.5 Prediction of dissipated energy
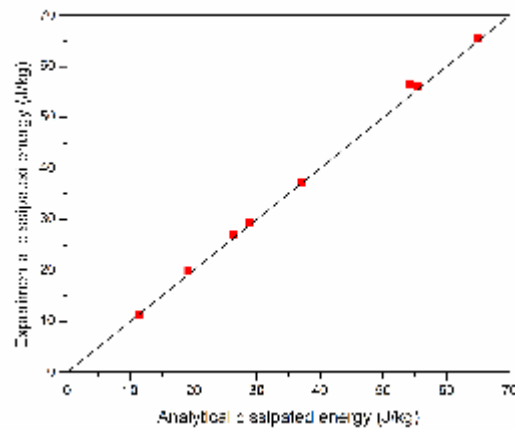
Fig. 3.6 Experimental and analytical hysteretic energy

3.5.3 Sensitivity Study on Parameters

In order to estimate the sensitivity of the model to the variation of the constituent parameters, sensitivity analysis was carried out. The parameters were gradually varied from their original values one by one keeping other parameters constant and the change in the model output was recorded. Let $[Y]$ be the hysteretic displacement for a given input forcing function. Then each parameter was varied from -50% to 50% of its original value. Now, due to variation of a parameter, if, for the same input forcing function, output displacement becomes $[Y']$, then the root mean square error (e) can be written as

$$e = \left(\sum_{i=1}^{n} (Y - Y')^2 \right)^{1/2}$$

(3.24)

In which, 'n' is the number of data point in the input forcing function. The root mean square error for each parameter within the range of its variation was plotted as shown in Fig. 3.7.
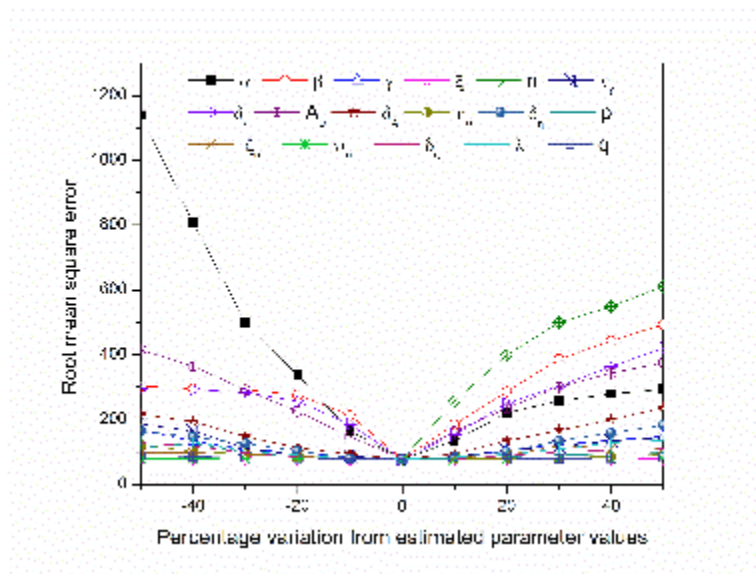
Fig. 3.7 Model sensitivity to parameter variation

The maximum error corresponding to variation of a parameter ($|e|$) can be obtained from the expression shown in Eq. (3.25).

$$|e| = \max(e) \qquad (3.25)$$

The maximum root mean square error associated with each parameter variation is summarized in Table 3.5. The parameters are ranked based on the magnitude of maximum root mean square error corresponding to each parameter. Parameters securing high position in the sensitivity ranking when deviated from their original values will lead to considerable error in the model prediction. On the hand, fluctuation of parameters with low sensitivity ranking will not result in any significant change in the model output. This study will help in judicious choosing of the possible lower and upper bounds of different parameters. Based on the results obtained from this study, the upper bound and lower bound of each parameter can be estimated as shown in Table 3.6.

Table 3.5: Sensitivity ranking of model parameters

Parameter	Maximum Root Mean Square Error	Rank
α	1139.82	1
β	493.65	3
γ	168.01	9
ξ	78.20	17
n	610.71	2
v_0	186.08	7
δ_v	420.37	4
A_0	415.07	5
δ_A	236.02	6
η_0	121.42	13
δ_η	182.31	8
p	125.92	12

ζ_0	119.09	14
ψ_0	78.36	16
δ_ψ	127.45	11
λ	135.73	10
q	88.59	15

Table 3.6: Lower Bound and Upper Bound of Parameters

Parameter	Lower Bound	Upper Bound
α	0.01	0.12
β	0.10	3.00
γ	-2.00	0.00
ξ	0.00	0.30
n	1.00	1.50
v_0	0.00	0.50
δ_v	0.00	0.30
A_0	2.00	6.00
δ_A	-3.00	0.10
η_0	1.00	7.00
δ_η	2.00	12.0
p	0.00	9.00
ζ_0	-7.00	1.00
ψ_0	-8.00	3.00
δ_ψ	-2.00	3.00
λ	-1.00	3.00
q	-3.00	8.00

3.6 CONCLUDING REMARKS

BWBN model was used in this study to predict the hysteresis behaviour of circular bridge columns failing in flexure. The model was found to predict the observed cyclic behaviour of tested specimen with reasonable accuracy. Complex phenomena like system

degradation and pinching are also captured well. Energy dissipated by the columns through hysteresis which is pivotal for determining seismic capacity of members also showed a good correlation with experimental data. Sensitivity analysis was carried out to estimate the sensitivity of model to variation of each parameter and sensitivity ranking was prepared based on maximum root mean square error associated with each parameter. Finally, an approximate upper bound and lower bound for each parameter was specified based on its range of variation observed in this study.

CHAPTER 4

PARAMETER IDENTIFICATION OF BOUC-WEN TYPE MODELS USING HOMOTOPY OPTIMIZATION

4.1 GENERAL

Efficiency of Bouc – Wen type models in predicting the response of a system greatly depends on accurate estimation of the unknown parameters. This requires adjusting the model parameters in such a way that the difference between the model output and the experimental measurements is minimised. Various system identification techniques can be applied to tune the model parameters so as to match the experimental measurements following which the model can be presented as a good approximation of the actual physical system.

Minimisation of an objective function with a single minimum can be achieved by classical optimisation theories like the steepest descent algorithm, Gauss - Newton algorithm, Levenberg - Marquardt algorithm etc. These non-stochastic algorithms are robust and they converge rapidly. However, the objective function of BW type models generally contains multiple local minima. If non-stochastic approach is used to minimise the objective function of BW type models, it will most likely converge to a local minimum rather than the global minimum. Owing to this limitation involved in non-stochastic approaches, previous studies on BW type models used stochastic methods such as genetic algorithm and simulated annealing for minimisation of the objective function. However, it was observed that stochastic approaches require a large number of iterations to converge and thus, are time-consuming. In recent times, particle swarm optimisation and constrained Kalman Filter have been used successfully to minimise the objective function of BW type models. Though they perform better than other stochastic approaches, they can hardly match the speed and robustness of non-stochastic

approaches. This study investigates the scope of extending the non-stochastic approaches to finding the global minimum of the objective function of BW type models.

This study investigates the scope of minimising the objective function of BW type models using a non-stochastic algorithm which outperforms the stochastic algorithms in terms of computation speed and efficiency. It has been shown in this study that using a special technique called 'homotopy', it is possible to attain the global minimum of a function through non-stochastic approach in situations where usual deterministic methods fail. In general, the algorithm begins by finding the global minimum of a less complicated approximation of the original function and then deforming the function into the original function in a series of steps. Minimum of the deformed function at one step is found starting from the minimizers found at the previous step. It is particularly suitable for highly nonlinear problems for which initial solution estimates are difficult to obtain. However, application of this method may be inappropriate for mildly nonlinear problems or problems for which initial estimate of the solution is easily obtainable (Watson and Haftka 1989).

Homotopy is used in several areas of mathematics, including optimization and nonlinear root finding. It is robust, accurate, numerically stable and almost universally applicable. It can converge from any arbitrary starting points almost assuredly (Watson and Haftka 1989). In the past, homotopy technique has been applied to complex optimisation problems involving protein structures (Dunlavy and O'Leary 2005) and to finding the equilibrium configuration of an elastica (Watson and Wang 1981). However, it has never been used in solving Bouc-Wen type models, which is a widely used as a mathematical tool for predicting hysteresis behaviour of any physical system. The study presented in this chapter shows that the application of homotopy can be successfully extended to parameter

identification of Bouc Wen type models. It makes the application of the model more viable and cost effective.

4.2 INTRODUCTION TO HOMOTOPY

Say the objective function of an optimization problem is $F(p)$ which has multiple local minima. The objective is to find parameters p^* which yield the global minimum of the objective function. As per homotopy optimization theory, the objective function is modified by addition of a simpler approximation of the original function $F(p)$ as shown in Eq. 4.1.

$$H(p, \lambda) = (1 - \lambda)F(p) + \lambda G(p) \tag{4.1}$$

It should be noted that, $G(p)$ should be convex in the unknown parameters, and, the arguments of the global minimum of $G(p)$ should be easily obtainable or known a priory. Caution should be exercised while selecting $G(p)$ as its choice affects the performance of this theory (Dunlavy and O'Leary 2005). The morphing parameter λ is varied gradually from 1 to 0. Let ${}^{\lambda}p^*$ denote the arguments of global minimum corresponding to morphing parameter λ. When $\lambda = 1$, the global minimum of the objective function $H(p, 1)$ is simply the global minimum of $G(p)$, which is known. Once $H(p, 1)$ is minimised, λ is reduced by a small amount $\delta\lambda$, and $H(p, 1 - \delta\lambda)$ is minimised using ${}^{1}p^*$ as initial guesses. Then λ is further reduced by $\delta\lambda$, and $H(p, 1 - 2\delta\lambda)$ is minimised using ${}^{1-\delta\lambda}p^*$ as intial guesses. This process is continued until λ is reduced to 0 and the objective function $H(p, \lambda)$ is morphed back to its original form $F(p)$. As λ is varied slowly, the objective function at any step is obtained by a slight modification of the objective function in the previous step, and the arguments of global minimum at any step are used as initial guesses for the next step, the iteration will most likely converge to the global minimum of the original objective function.

4.3 PARAMETER IDENTIFICATION USING HOMOTOPY OPTIMIZATION

4.3.1 Theory

Say an experimental system is governed by a set of ordinary differential equations given by

$$\dot{x}_e = f(x_e, p_e, t) \tag{4.2}$$

where, $x_e = [x_{1e}(t), x_{2e}(t), \ldots\ldots x_{ne}(t)]^T$ is a vector containing the time series of n independent coordinates, and, $p_e = [p_{1e}(t), p_{2e}(t), \ldots\ldots p_{ke}(t)]^T$ is a set of the parameters for the experimental system. Let the mathematical approximation of the experimental system, be represented as

$$\dot{x} = f(x, p, t) \tag{4.3}$$

where, $x = [x_1(t), x_2(t), \ldots\ldots x_m(t)]^T$, $m \leq n$. The objective is to identify the model parameters $p_e = [p_1(t), p_2(t), \ldots\ldots p_k(t)]^T$ such that the difference between the predicted response, $x_1(t)$ and the response measured during experiment, $x_{1e}(t)$ is minimised. The objective function can therefore be expressed as

$$J(p) = \frac{1}{2} \int_0^T (x_{1e}(t) - x_1(p,t))^2 \, dt \tag{4.4}$$

Homotopy optimization generally converges to a local minimum. However, through proper selection of the coupling term $G(p)$ (Eq. 4.1), it is possible to enhance the probability of convergence to the global minimum. In case of optimization problems involving parameter identification, appropriate selection of $G(p)$ is difficult as the shape of the objective function ($F(p)$) is not known a priori owing to its dependence on the solution of the differential equation (Eq. 4.3). Unlike algebraic problems, where the minimum value of the objective

function is not known, in case of parameter identification problems the minimum value of the objective function is zero provided the mathematical model accurately represents the physical system. However, in practice, mathematical models invariably involve some approximations rendering the final value of the objective function assuming a sufficiently small value rather than an absolute zero. Making use of this knowledge, the homotopy parameter is introduced implicitly in the objective function and explicitly in the governing differential equation as shown in Eqs. 4.5 and 4.6 (Vyasarayani et al. 2011).

$$J(p, \lambda) = \frac{1}{2} \int_0^T \left(x_{1e}(t) - x_1(p, \lambda, t) \right)^2 dt \qquad (4.5)$$

$$\dot{x} = f(x, p, t) + \lambda \, \mathrm{K} \, e(t) \qquad (4.6)$$

where, $e(t) = [e_1(t), e_2(t), \ldots \ldots e_n(t)]^T$ is the error vector, whose k^{th} element is defined as $e_k(t) = x_{ke}(t) - x_k(t)$. Since only one independent coordinate was measured during experiment, therefore, the error vector reduces to $e(t) = [e_1(t), 0, \ldots \ldots, 0]^T$ in this study. For large value of K, the coupling term acts as a high gain observer (Khalil 1999; Vyasarayani et al. 2012) and the simulated response synchronizes with experimental data with a synchronization error $J(p, \lambda)$. Irrespective of the initial parameter guess, by selecting appropriate K the error $J(p, \lambda)$ can be made arbitrarily small. As we continue homotopy optimization the parameters get closer and closer to the actual values as λ is decreased. At every step of the optimization problem we ensure that $J(p, \lambda)$ remains small. Thereby when λ becomes zero, i.e, during the last step of homotopy optimization, the value of $J(p, \lambda)$ will remain small.

The algorithm begins by assuming some initial guesses for the model parameters. The morphing parameter λ is set to 1, and the differential equation of Eq. 4.6 is solved using 4th order Runge - Kutta method (Ortiz et al. 2013) to get the simulated model output. Then, the

objective function shown in Eq. 4.5 is minimised using `fmincon', which is an inbuilt optimization function in MATLAB environment. The arguments of minimum of $J(p,1)$ are used to solve the differential equation of Eq. 4.6 with modified λ which is obtained by reducing the initial value by a small amount $\delta\lambda$. Then, the modified objective function is optimized again to get the arguments of its minimum. This process is continued till λ is reduced to 0, and the objective function gets rid of any coupling term. The arguments of minimum of the last step are reported as the global minimum of the original objective function.

4.3.2 Numerical Example

Application of homotopy method in parameter identification of a physical system can be illustrated with the help of a numerical example. Let a simple pendulum be set to free oscilation by displacing it from its initial static equilibrium position to a position where the string of the pendulum makes an angle of $30°$ with the vertical. The differential equations representing the experimental system can be written as

$$\dot{x}_{1e} = x_{2e} \tag{4.7a}$$

$$\dot{x}_{2e} = -p_e \sin(x_{1e}) \tag{4.7b}$$

where, p_e is a parameter that governs the behaviour of the experimental system. x_{1e} and x_{2e} are experimental values of displacement and velocity of the simple pendulum which are obtained by solving Eq. 4.7 for time span $t \in [0, 40]$ assuming a value of 10 for parameter p_e. The mathematical model depicting the free vibration of the simple pendulum is presented in Eq. 4.8.

$$\dot{x}_1 = x_2 \tag{4.8a}$$

$$\dot{x}_2 = -p\sin(x_1) \tag{4.8b}$$

The initial conditions are given by : $x_1(0) = \pi/6$ and $x_2(0) = 0$. The objective is to identify the unknown system parameter p. This presents an optimization problem which is defined as follows.

$$p^* = \min_{\text{arg}} \int_0^{40} \left(x_{1e}(t) - x_1(p, \lambda, t)\right)^2 dt \tag{4.9}$$
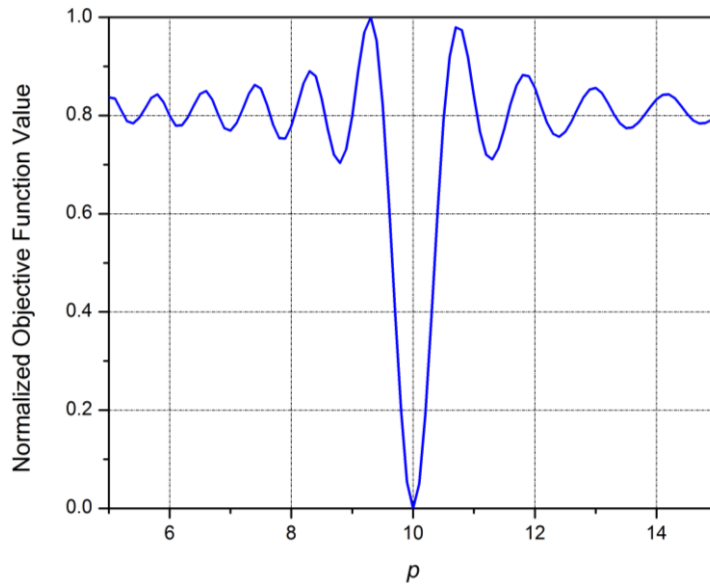
Fig. 4.1 Normalized objective function for simple pendulum

The shape of the objective function is estimated by a direct search as shown in Fig. 4.1. It can be observed that the objective function has multiple local minima. Any deterministic approach will fail to converge to the global minimum unless the initial guess for p is close to 10.
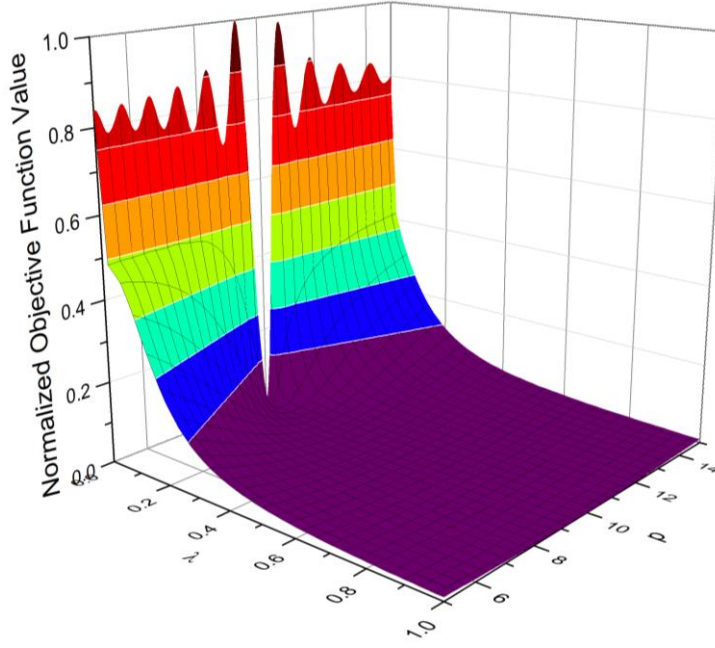
Fig. 4.2 Normalized objective function for simple pendulum for $0 \leq \lambda \leq 1$

Solution of this problem using homotopy technique is presented in this section to demonstrate that this technique can ensure convergence starting from a remote initial guess in case of objective functions with multiple local minima. To apply this technique, the governing differential equations (Eq. 4.8) are modified by addition of coupling terms as shown in Eq. 4.10.

$$\dot{x}_1 = x_2 + \lambda K_1 (x_{1e} - x_1) \tag{4.10a}$$

$$\dot{x}_2 = -p \sin(x_1) + \lambda K_2 (x_{1e} - x_1) \tag{4.10b}$$

An initial value of 15 was assumed for parameter p. Coupling parameters K_1 and K_2 were equated to 10. It can be seen in Fig. 4.2 that, the modified objective function is convex at $\lambda = 1$. As λ is reduced slowly the objective function deforms and morphs backs to the original objective function at $\lambda = 0$. The final value of parameter p was found to be 10.00 suggesting that the global minimum has been attained. On the hand, without homotopy technique and starting from the same initial value, parameter p converges to a local minimum at $p = 14.74$.

74

4.4 NUMERICAL EXPERIMENT: BW MODEL (5 PAREMETERS)

A numerical example is presented to illustrate the role of homotopy in convergence of BW type models. The example is adopted from a previous study performed by Ortiz et al. (2013). Hysteresis of a system with mass, m = 500 kg and stiffness, k = 6 kN/mm is studied under a time-varying cyclic load given by $F(t) = t \sin(2\pi t)$ as shown in Fig. 4.3.
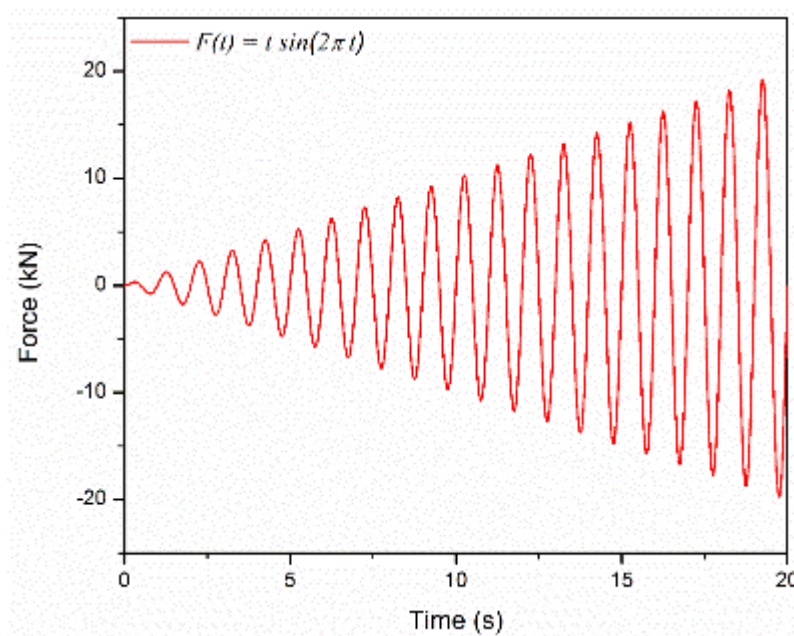
Fig. 4.3 External excitation force used in the simulation

Response of the system under the given load was estimated with true values of the parameters as shown in Table 4.1. Then the model parameters were identified following the algorithm presented earlier in this chapter. Several trials were conducted starting from different initial guesses for the parameters which varied from 50% to 150% of the true values. The final values of parameter obtained from different simulations is summarised in Table 4.1.

Table 4.1 : Identified parameters for different initial guesses (BW model)

Parameter		α	B	γ	ξ	n
True Values		0.2000	2.0000	-1.0000	0.0500	1.2000
Initial guesses / True values	0.5	0.2047	3.6553	-2.1526	0.0742	2.6867
	0.6	0.2035	1.0044	0.8198	0.0898	3.3651
	0.7	0.2088	1.4195	0.4020	0.1888	2.2971
	0.8	0.2040	0.7227	1.9156	0.1487	4.8216
	0.9	0.2064	3.0492	-1.0848	0.1428	3.4076
	1.1	0.2097	3.7867	-1.5037	0.1218	3.4488
	1.2	0.2023	2.1364	-0.9119	0.0500	1.6115
	1.3	0.2012	2.1051	-0.8465	0.0112	2.5199
	1.4	0.2001	0.8510	0.5822	0.0137	4.8806
	1.5	0.2065	2.0056	0.0955	0.1299	3.9351

It is observed that different initial guesses resulted in to different final values suggesting that the global minimum was not achieved. However, the model output, namely displacement of the system, when compared with the estimated values, invariably showed a very good correlation for all cases of initial guesses. This leads to the conclusion that, that the objective function of this model has multiple local minima which overall produce same results as that of the global minima. In can also be inferred from the results that Homotopy can converge from far flung initial values which is unique for this optimisation technique. In this study the comparison of estimated and simulated values of displacement is presented only for initial guesses 50% and 150% of true values (Fig. 4.4). The results for other cases of initial cases are provided in the annexure. The simulated load – displacement behaviour is compared with estimated data and a reasonably good agreement was observed. The simulated values of dissipated energy also matched favourably with estimated behaviour.
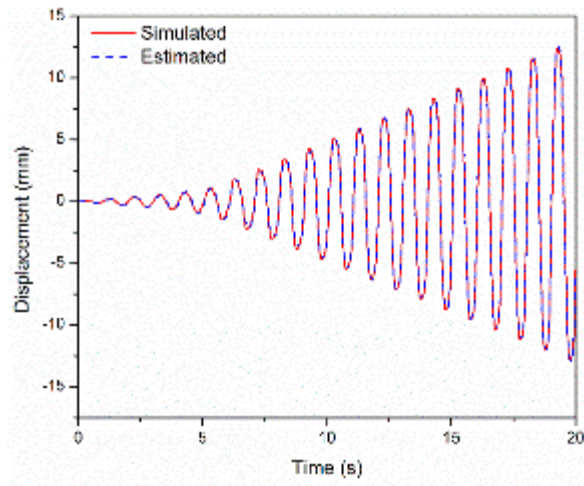
(a) Displacements (0.5)
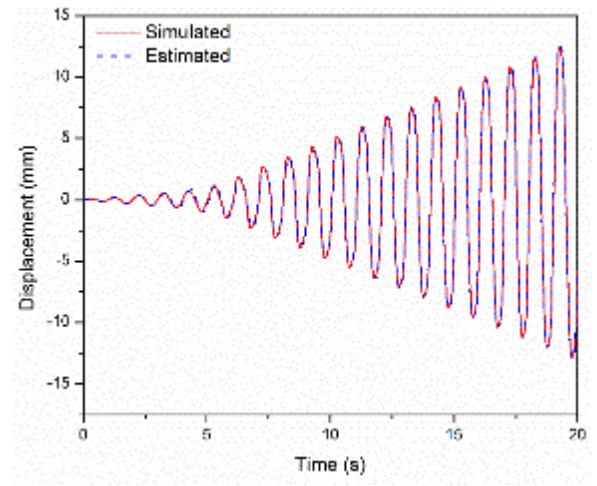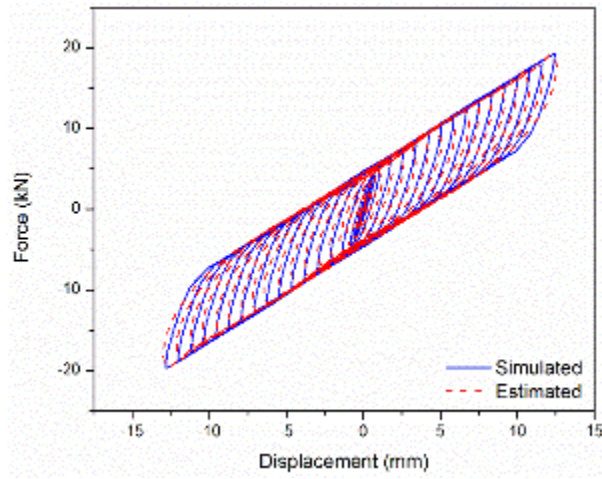
(b) Displacements (1.5)

(c) Hysteresis Cycles (0.5)
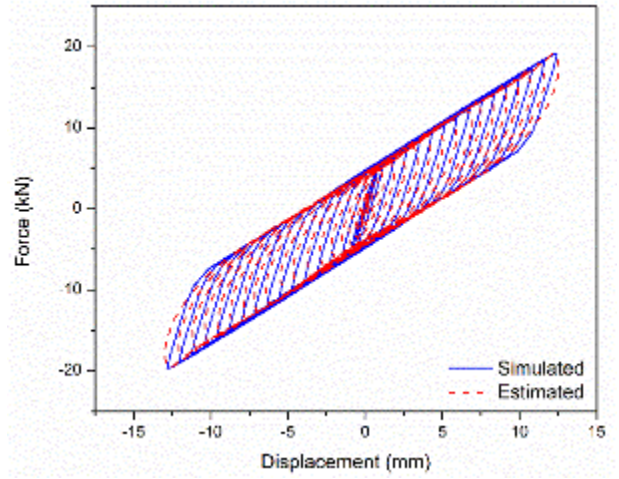
(d) Hysteresis Cycles (1.5)
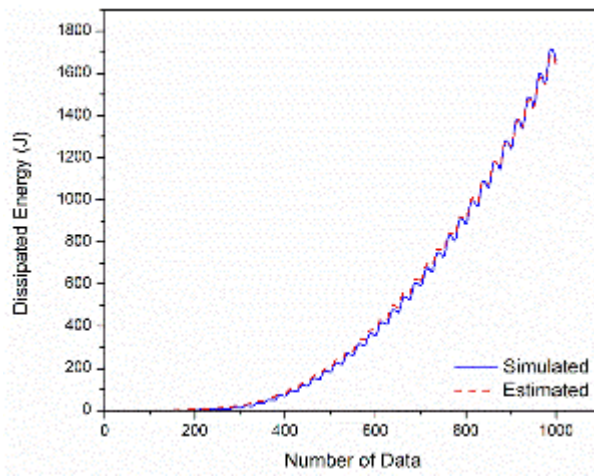
(e) Dissipated Energy (0.5)
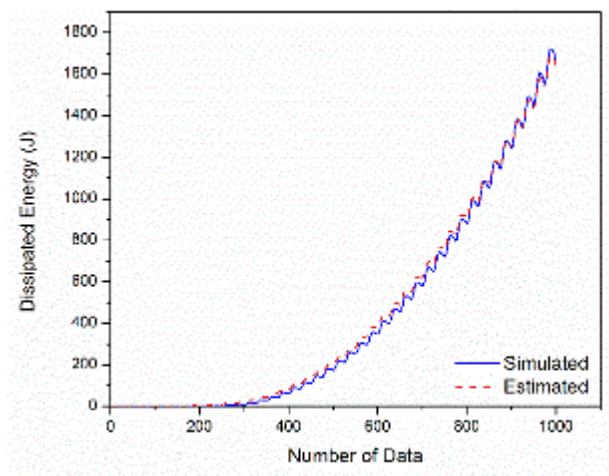
(f) Dissipated Energy (1.5)

Fig. 4.4 Comparison of simulated and estimated behaviour (Numbers in the parenthesis denote the ratio of initial guesses to true values)

Fig. 4.5 Convergence of model parameters (initial guesses = 0.5 times the true values)

Fig. 4.6 Variation of homotopy parameter and corresponding objective function during optimisation process (initial guesses = 0.5 times the true values)

Variation in parameter values with iteration number is presented in Fig. 4.5. Values of the parameters at the onset of iteration indicate the initial guesses for the parameters. It was observed that, after certain number iterations all the parameters converged to their final values. The minimisation of the objective function and the homotopy parameter with respect to the iteration number is also plotted as shown in Fig. 4.6. It is observed that the value of the objective function at the end of the final iteration is trivial suggesting that the simulated values of displacement are sufficiently close to the estimated response. It may be noted further that the number of iterations required for convergence of the objective function at different stages of homotopic morphing is different. When the homotopy parameter is reduced to zero, the original objective function is retrieved, minimisation of which marks the end of the simulation.

4.5 NUMERICAL EXPERIMENT: BWBN MODEL (17 PARAMETERS)

The second part of the numerical experiment comprised repeating the same exercise as presented in section 4.4 for 17 parameter BWBN model. Displacement values were estimated using the true values as presented in Table 4.2. Next, unknown model parameters were identified following algorithm explained in section 4.3.. The initial guesses were varied from 50% to 150% of the true values and close correlation was observed between model output and simulated response (Fig. 4.7) for all cases. The variation of model parameters, objective function and homotopy parameter with respect to iteration number is presented Figs. 4.8 and 4.9.

Table 4.2 : Identified parameters for different initial guesses (BWBN model)

Parameter		α	β	γ	ξ	n	A_0
True Values		0.2	2	-1	0.05	1.2	1.1
Initial guesses / True values	0.5	0.2131	2.3526	-1.5026	0.0202	1.0220	1.3385
	0.6	0.2165	1.5159	-0.3518	0.0200	1.0884	1.0717
	0.7	0.2176	2.1064	-1.3949	0.0200	1.0177	1.4657
	0.8	0.2143	1.7364	-0.7046	0.0200	1.0353	0.9206
	0.9	0.2178	2.2998	-1.2755	0.0211	1.1182	1.6017
	1.1	0.2136	2.3391	-1.1414	-0.0182	1.1005	1.2065
	1.2	0.2123	2.3885	-1.2649	0.0200	1.2143	1.3752
	1.3	0.2062	2.8952	-1.1447	0.0831	3.0802	1.6700
	1.4	0.2108	2.7195	-1.5710	0.0200	1.3595	1.5439
	1.5	0.2118	2.8898	-1.7366	0.0200	1.3761	1.6525
Parameter		v_0	δ_v	δ_A	η_0	δ_η	p
True Values		1.2	0.4	0.1	1.3	0.5	2
Initial guesses / True values	0.5	1.8151	-0.0725	0.7229	1.4941	-0.9293	2.9559
	0.6	1.0760	0.0019	0.7848	1.1375	0.6776	1.2028
	0.7	2.4427	-0.8219	1.1927	1.3648	1.7722	3.2176
	0.8	1.0377	0.3970	0.2537	0.9812	0.4749	1.6483
	0.9	1.9076	-0.6803	1.3326	1.7206	-1.4294	2.3397
	1.1	1.1940	0.4900	0.1274	1.2854	0.4659	2.6372
	1.2	1.4839	0.6163	0.3101	1.4994	0.5863	2.3815
	1.3	1.6910	1.1307	0.6633	1.7428	1.6730	5.7418
	1.4	1.6327	0.7383	0.4516	1.7222	0.7118	2.7707

		ς_0	ψ_0	δ_ψ	λ	q	
	1.5	1.7520	0.8047	0.4686	1.8397	0.7421	2.9203
Parameter		ς_0	ψ_0	δ_ψ	λ	q	
True Values		1	0.5	0.6	0.9	1	
Initial guesses / True values	0.5	1.0543	0.2019	2.3729	1.4038	1.8052	
	0.6	0.8564	0.3891	0.4972	0.6115	0.3726	
	0.7	0.3992	1.3454	0.1547	1.2175	-0.3239	
	0.8	1.2268	0.3951	0.5588	0.7354	0.7836	
	0.9	1.0658	-0.1883	2.1266	1.3666	0.8466	
	1.1	0.5812	0.6157	0.7249	1.6408	1.9290	
	1.2	1.0990	0.4335	0.6554	1.0040	1.2859	
	1.3	0.9928	-0.7029	-1.1638	1.1392	0.4665	
	1.4	1.0645	0.4231	0.7636	1.1361	1.5110	
	1.5	1.0701	0.3351	0.7784	1.1626	1.6646	
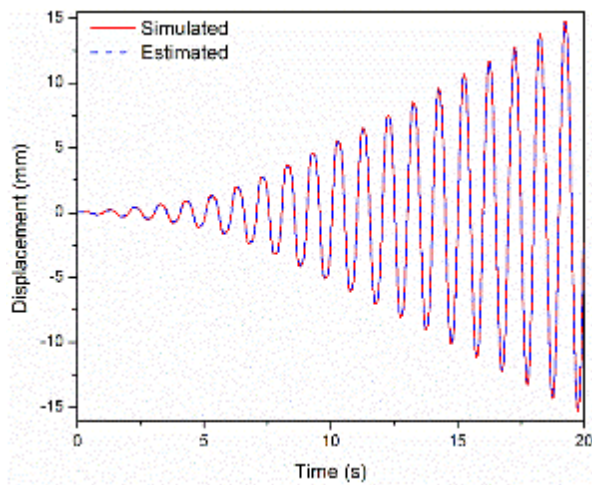
(a) Displacements (0.5)   (b) Displacements (1.5)
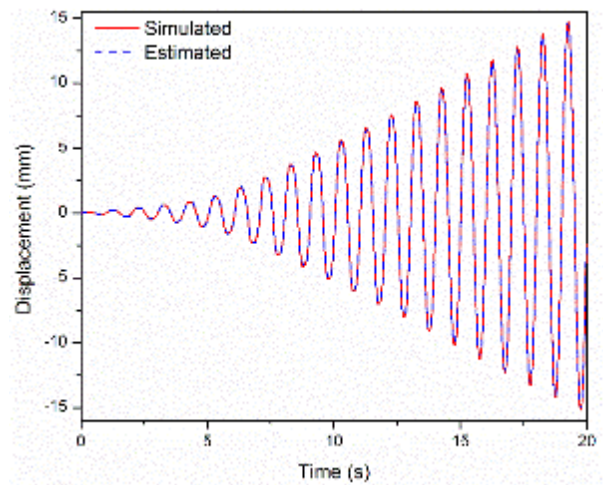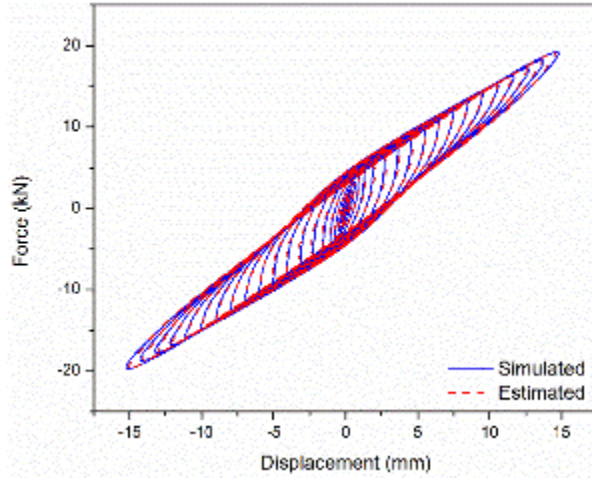
(c) Hysteresis Cycles (0.5) (d) Hysteresis Cycles (1.5)
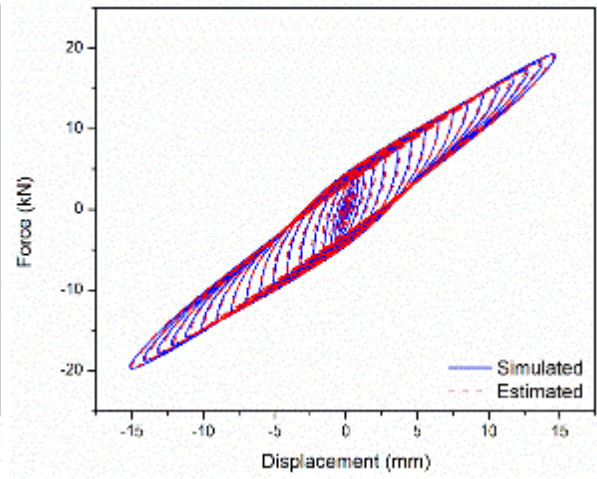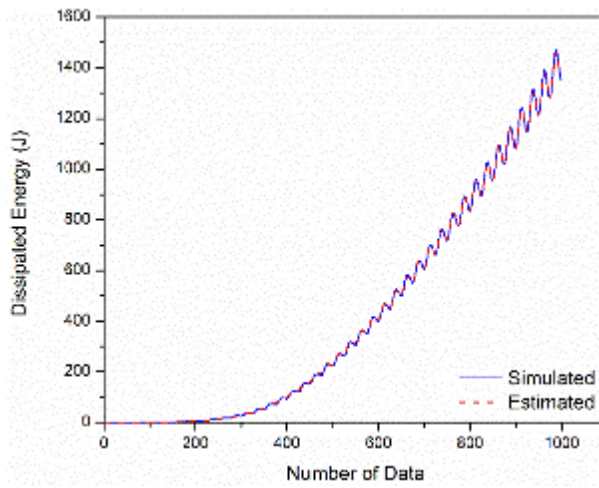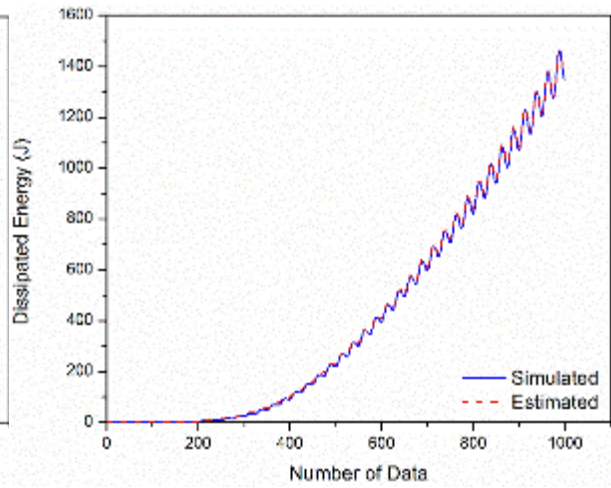
(e) Dissipated Energy (0.5) (f) Dissipated Energy (1.5)

Fig. 4.7 Comparison of simulated and estimated behaviour (Numbers in bracket denote the ratio of initial guesses to true values
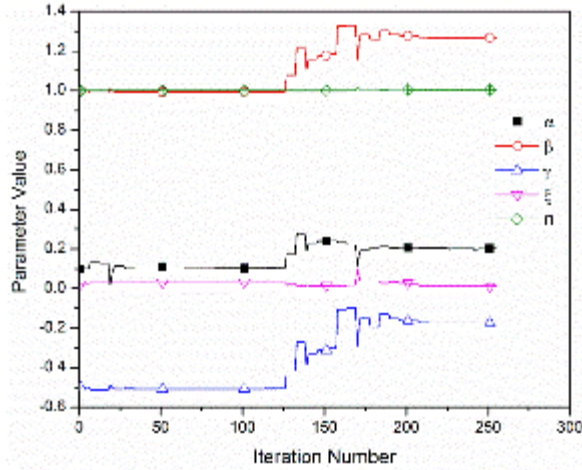
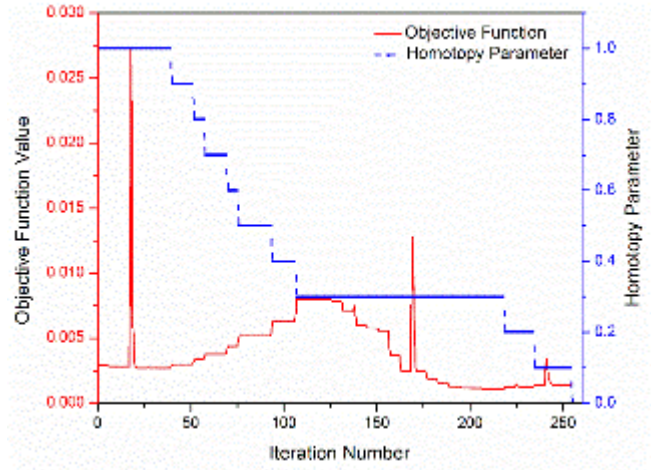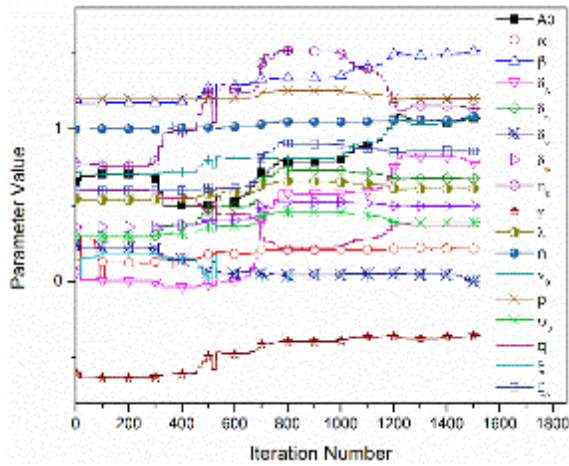Fig. 4.8 Convergence of model parameters (initial guesses = 0.5 times the true values)
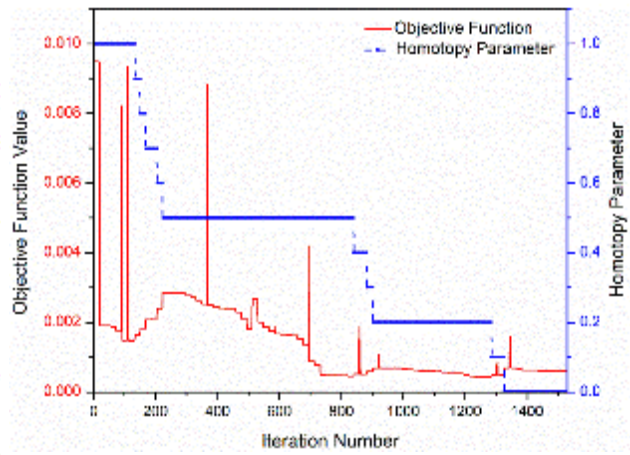
Fig. 4.9 Variation of homotopy parameter and corresponding objective function during optimisation process (initial guesses = 0.5 times the true values)

The estimated parameters were then used to predict the response of the system under Northridge earthquake (1994) ground motion data. The estimated response was reasonably close to the actual response as shown in Fig. 4.10. It leads to the conclusion that parameters obtained from certain loading protocol can predict the response under any other loading protocol. In other words, the model parameters are system properties and are not subjected to variation with change in loading pattern.
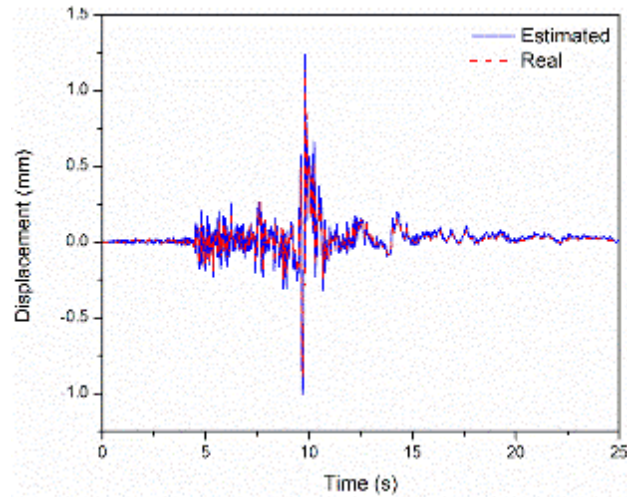
Fig. 4.10 Displacement under Northridge earthquake (1994) ground motion

4.6 EXPERIMENTAL CORROBORATION: BWBN MODEL (17 PARAMETERS)

Homotopy technique was employed to predict the hysteresis response of a circular reinforced reinforced concrete column (Leh-H/D(4)- 1.5%-0.72%-7.2%) tested by Lehman and Moehle (2000) under cyclic lateral load. The column was tested as a cantilever under a time varying lateral shown in Fig. 4.11.
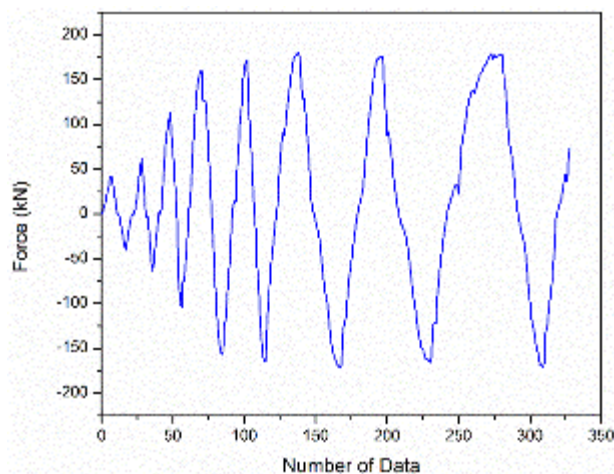
Fig. 4.11 Applied force on the tested column specimen
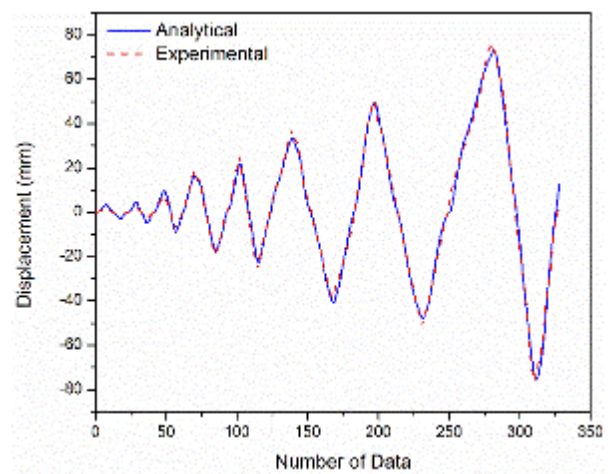
Fig. 4.12 Comparison of analytical and experimental displacements

Table 4.3 : Identified model parameters for the tested column specimen

Parameter	α	β	γ	ξ	n	A_0
Final Value	0.0214	0.1206	-0.0829	0.2997	3.4631	0.0037
Parameter	v_0	δ_v	δ_A	η_0	δ_η	p
Final Value	0.0969	0.7096	0.0847	2.9577	3.8494	1.0608
Parameter	ς_0	ψ_0	δ_ψ	λ	q	
Final Value	-1.2442	-6.5865	3.3767	0.1486	0.8921	
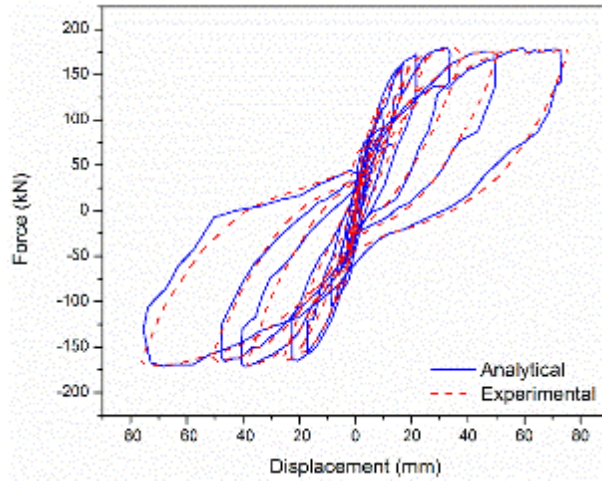
Fig. 4.13 Comparison of analytical and experimental hysteresis cycles
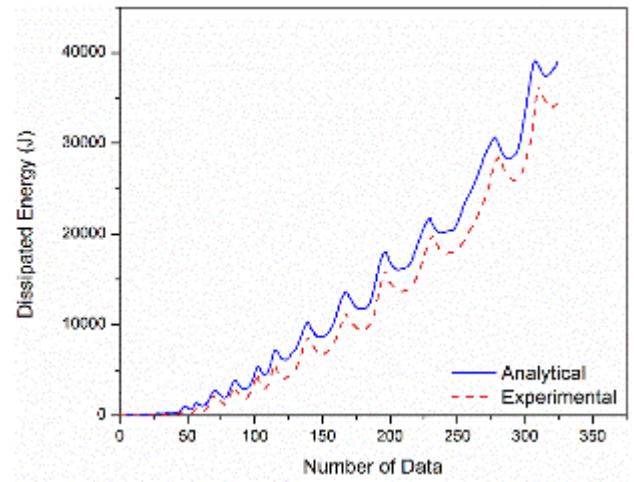
Fig. 4.14 Comparison of analytical and experimental dissipated energy

The response of the column was predicted using the algorithm presented in this chapter. The predicted behaviour compared favourably with the observed response (Fig. 4.12). Overall force displacement behaviour (Fig. 4.13) and dissipated energy (Fig. 4.14) were also captured accurately by the analytical model. The final values of model parameters are reported in Table 4.3. Convergence of parameters and variation of objective function and homotopy parameter with respect to iteration number were estimated as mentioned in previous sections and are presented in Figs. 4.15 and 4.16.
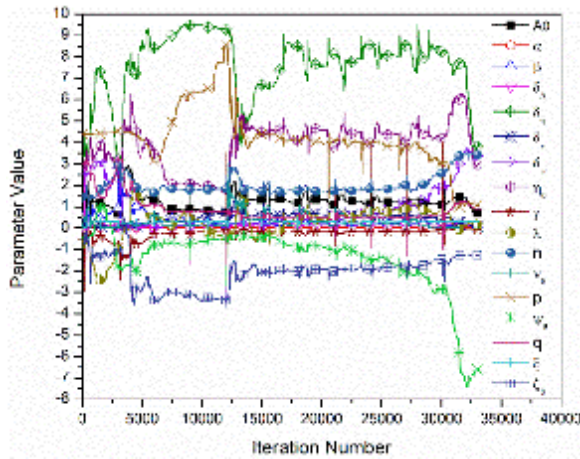
Fig. 4.15 Convergence of model parameters
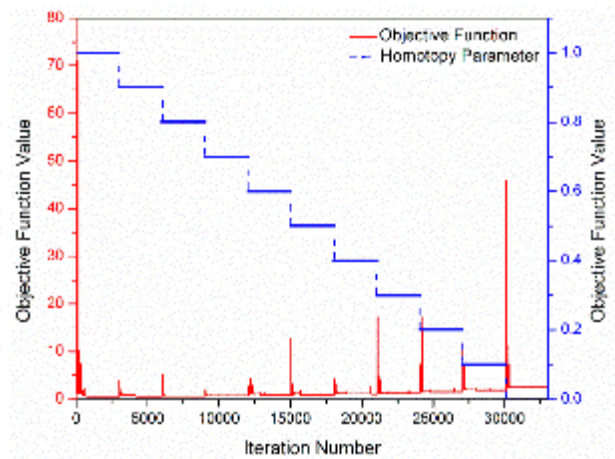
Fig. 4.16 Variation of homotopy parameter and corresponding objective function during optimisation process

4.7 CONCLUDING REMARKS

In this study, the parameters of Bouc - Wen type models have been identified using homotopy optimization in combination with local search algorithms. Through numerical examples, it has been shown that homotopy technique can successfully identify the parameters of Bouc – Wen type models. In the numerical test cases considered in this study, the identified parameters did not match closely with the actual values. However, the objective function was adequately minimized and the simulated response compared favourably with estimated response. To investigate the correlation between model parameters and the loading protocol, the response of a system under Northridge earthquake ground motion was predicted using the parameters identified with a sinusoidal loading function. The predicted response closely matched the estimated one suggesting that the Bouc Wen type model parameters are insensitive to loading protocol. Experimental data of a reinforced concrete column tested under cyclic lateral loading was used for experimental validation of this optimization approach. The response of the column under given loading was estimated using BWBN model with the help

of homotopy optimization. The predicted behaviour matched the observed behaviour reasonably well.

CHAPTER 5

DEVELOPMENT OF AN IMPROVED POLYGONAL HYSTERESIS MODEL FOR CIRCULAR RC COLUMNS UNDER TORSION

5.1 GENERAL

Reinforced concrete bridge columns are subjected to torsional loading under various conditions (Mondal and Prakash 2015d). Torsion in columns can be induced by skewed or horizontally curved bridges, bridges with unequal spans or column heights, and bridges with outrigger bents. Torsional moment needs special attention in design as it may otherwise trigger brittle shear dominated failure of members. Collapse of many important bridges around the world caused by recent earthquakes has put forth the necessity to assess the seismic vulnerability of the existing bridge columns. Seismic analysis of reinforced concrete (RC) structures requires hysteresis models that can accurately predict strength, stiffness, and ductility characteristics of the members under cyclic loading. Bridge columns should be properly designed to adequately dissipate seismic energy through inelastic deformation under vibrations during earthquakes (Prakash and Belarbi 2010; Goodnight et al. 2013). The level of accuracy of seismic design depends on the accuracy of the hysteresis model. Owing to all these reasons it is of utmost importance to have a proper hysteresis model which can accurately predict the cyclic flexural behavior of RC members considering strength and stiffness degradation along with the pinching effects.

Polygonal hysteresis models are a well-established modeling approach, where the response of a member to cyclic loading is governed by a set of control points and paths defined by piecewise linear or nonlinear functions. One of the best known polygonal hysteresis models

available in literature is Clough and Johnston (1966) model, which is characterized by a bilinear primary curve. It considers strain hardening in post yielding regime and takes into account stiffness degradation under load reversals. Takeda model (Takeda et al. 1970) represents a tri-linear primary curve marked by a stiffness change at cracking point. It is governed by some loading – unloading rules formulated based on experimental observations. In the pivot hysteresis model developed by Dowell et al. (1998), the envelope curve under monotonic loading has four branches characterized by elastic stiffness, strain hardening, strength degradation and linearly decreasing residual strength. The loading and unloading are governed by two pivot points which determine the level of softening with increasing displacement and the degree of pinching on load reversal. Other notable works on PHM include Fukada (1969), Aoyama (1971), Atalay and Penzien (1975), Nakata et al. (1978), and Mansur and Hsu (2005). However, all these models were developed for shear and flexure and are incapable of predicting the behavior under torsion (Wang et al. (2014) owing to high degree of pinching and degradation involved in torsional loading. Very few researchers have, in deed, focused on the analytical modeling of the hysteresis behavior exhibited by RC members under cyclic torsion. Tirasit and Kawashima (2007a) and Wang et al. (2014) have recently proposed some PHMs for RC columns under torsional loading. In both of the studies, a semi-empirical primary curve was used, where the yield torsional moment was estimated using space truss analogy ((Rahal and Collins 1995; Mo and Yang 1996) and post-yield behavior was obtained from empirical relations derived on the basis of experimental observations. In this study, an entirely mechanics based primary curve is proposed using SMMT (softened membrane model for torsion) (Hsu 1993) which is more reliable than any empirical model. Moreover, the previous studies did not consider any slope change in the primary curve at the cracking point, in contrast to the actual behavior observed during experiments. The present study tends to eliminate this discrepancy by introducing a slope change at the cracking point. Loading - unloading rules are proposed

based on statistical analysis of experimental data which are at variance with the previous models. An additional control point has been introduced in the unloading branch to better predict the actual behavior. It was observed that the proposed model closely predicts the measured load – displacement behavior.

5.2 MODEL DESCRIPTION

Any PHM is governed by primary (backbone) curve (Fig. 5.1 and 5.2) and loading/unloading rules (Fig. 5.3). A number of control points (Figs. 5.3(b) and 5.3(d)) are fixed which regulate the hysteresis loops. Paths joining successive control points are called branches ((Figs. 5.3(a) and 5.3(c))). Transition from one control point to another is governed by a set of rules which are determined empirically from experimental data (Figs. 5.4-5.10). The details of the model are described below.

(a) H/D(6)-T/M(∞)-0.73%   (b) H/D(3)-T/M(∞)-1.32%
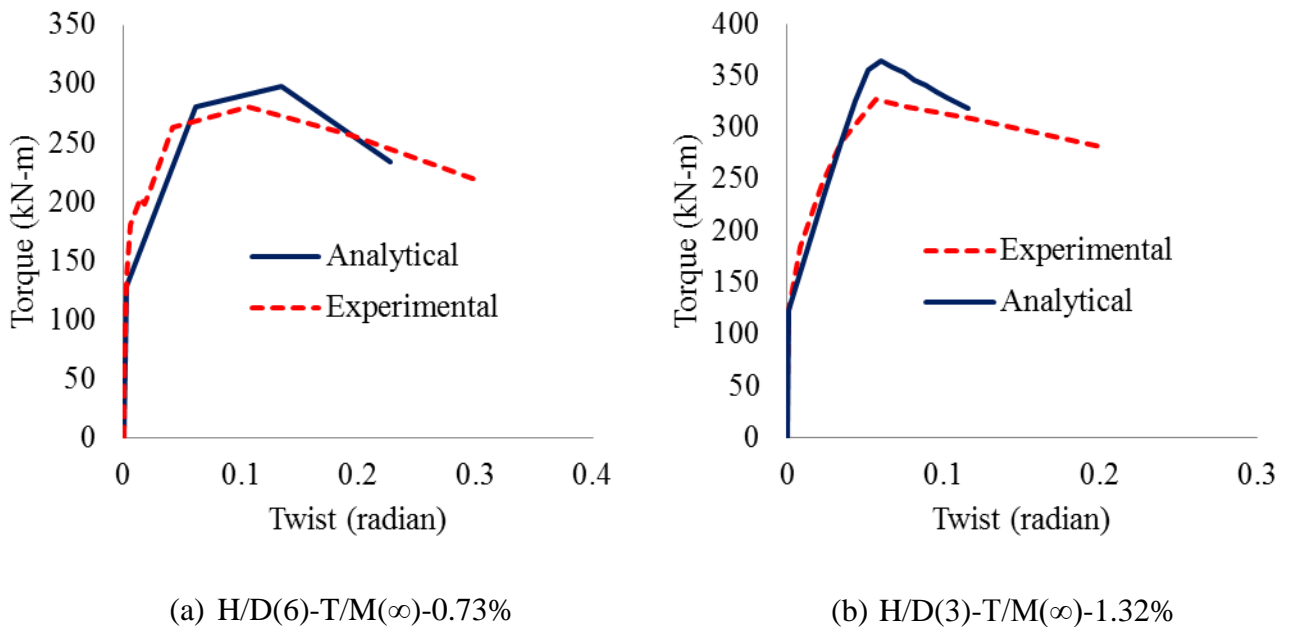
Fig. 5.1 - Primary Curve under Torsion (Anand et al. 2016)
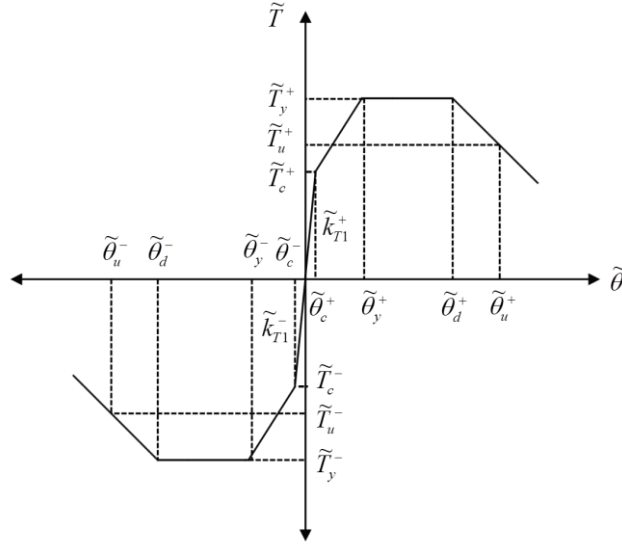
Fig. 5.2 - Idealized Primary Curve
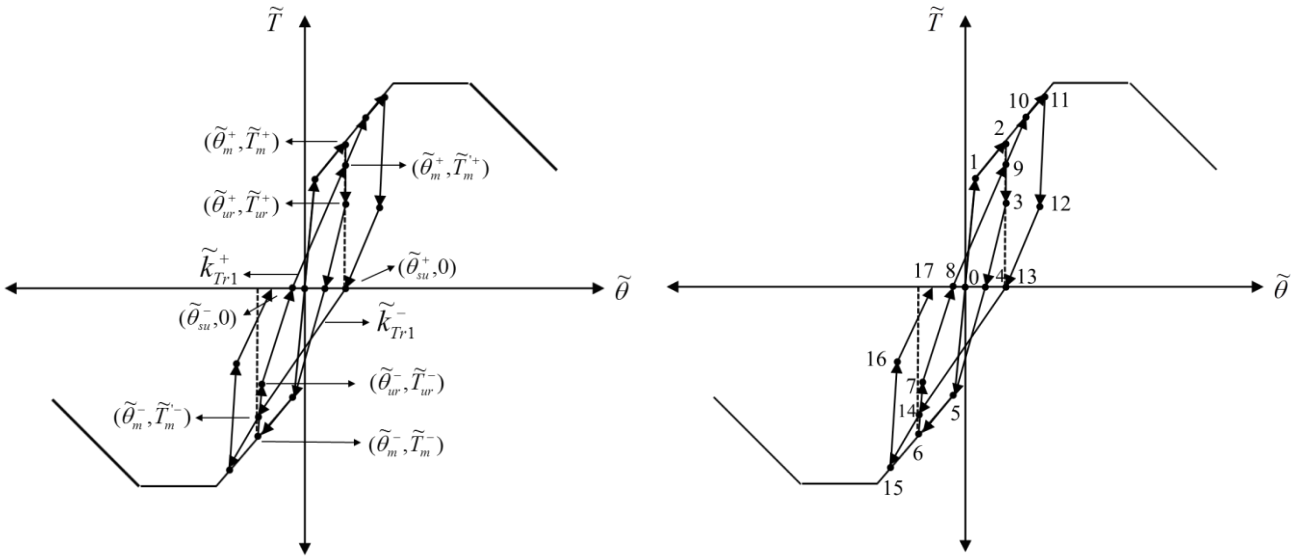
(a) Definition of parameters ($\tilde{\theta}_c < \tilde{\theta}_m < \tilde{\theta}_y$)

(b) Hysteresis paths ($\tilde{\theta}_c < \tilde{\theta}_m < \tilde{\theta}_y$)
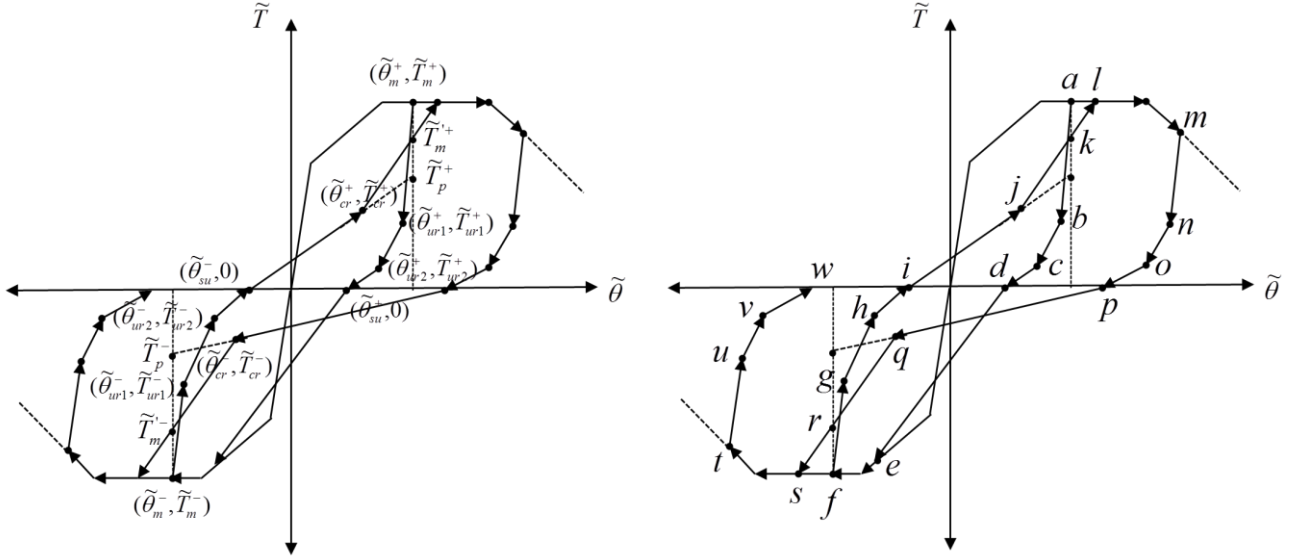
(c) Definition of parameters ($\tilde{\theta}_m > \tilde{\theta}_y$) (d) Hysteresis paths ($\tilde{\theta}_m > \tilde{\theta}_y$)

Fig. 5.3 Characteristics of hysteresis loops

5.2.1. Primary Curve

Primary curve is the envelope of the cyclic load – displacement behavior. It is assumed to be identical to the behavior under monotonic loading. In previous studies (Tirasit and Kawashima 2007a and Wang et al. 2014), the primary curve was estimated using a semi-empirical model, where the yield torsional moment was calculated using space truss analogy. However, in the present study, a more rational analytical model, known as SMMT (Softened Membrane Model for Torsion), was used to obtain the backbone curve. The details of SMMT are nicely explained by Anand et al. 2016. The authors used the same specimens as used in this study to show that SMMT can accurately predict backbone curve under cyclic torsion. Therefore, the backbone curves (Fig. 5.1) are directly adopted from the aforementioned study without any alteration. A change in slope in primary curve at the cracking point has been introduced in this model which was ignored by the previous researchers (Tirasit and Kawashima 2007a and Wang et al. 2014). The primary curve obtained from SMMT is idealized

as piecewise linear functions representing elastic stiffness, strain hardening, yield plateau, and strength deterioration as shown in Fig. 5.2.

5.2.2 Unloading Rules

1. The unloading path follows the initial stiffness of the primary curve (path $1 \rightarrow 0$, $5 \rightarrow 0$) if torsion at the beginning of the unloading is less than the cracking torsion ($\tilde{T}_m \leq \tilde{T}_c$), and $\tilde{T}_c$ has not been previously exceeded in either direction.

2. After cracking, the unloading path becomes a function of internal variables such as displacement (rotational) ductility ($\tilde{\theta}_m / \tilde{\theta}_c$ for $\tilde{\theta}_c < \tilde{\theta}_m < \tilde{\theta}_y$, $\tilde{\theta}_m / \tilde{\theta}_y$ for $\tilde{\theta}_m > \tilde{\theta}_y$) and current deformation level. From a given unloading point on the primary curve ($\tilde{\theta}_m, \tilde{T}_m$), the hysteresis path is directed towards ($\tilde{\theta}_{ur1}, \tilde{T}_{ur1}$) (path $2 \rightarrow 3$, $6 \rightarrow 7$, $11 \rightarrow 12$, $15 \rightarrow 16$, $a \rightarrow b$, $f \rightarrow g$, $m \rightarrow n$, $t \rightarrow u$) which is estimated using the expressions shown in Eq. 1 (Figs. 5.4 and 5.5).

$$\tilde{\theta}_{ur1} / \tilde{\theta}_m = -0.0028\left(\tilde{\theta}_m / \tilde{\theta}_c\right) + 1.0498 \qquad \text{for } \tilde{\theta}_c < \tilde{\theta}_m < \tilde{\theta}_y \qquad (1a)$$

$$= -0.0004\left(\tilde{\theta}_m / \tilde{\theta}_y\right) + 1.0047 \qquad \text{for } \tilde{\theta}_m > \tilde{\theta}_y \qquad (1b)$$

$$\tilde{T}_{ur1} / \tilde{T}_m = -0.0009\left(\tilde{\theta}_m / \tilde{\theta}_c\right) + 0.8527 \qquad \text{for } \tilde{\theta}_c < \tilde{\theta}_m < \tilde{\theta}_y \qquad (1c)$$

$$= -0.0006\left(\tilde{\theta}_m / \tilde{\theta}_y\right) + 0.8623 \qquad \text{for } \tilde{\theta}_m > \tilde{\theta}_y \qquad (1d)$$

3. In case of unloading beyond the yield point ($\tilde{\theta}_m > \tilde{\theta}_y$), from ($\tilde{\theta}_{ur1}, \tilde{T}_{ur1}$), the unloading path leads to ($\tilde{\theta}_{ur2}, \tilde{T}_{ur2}$) (path $b \rightarrow c$, $g \rightarrow h$, $n \rightarrow o$, $u \rightarrow v$), which is given by Eq. 2 (Fig. 5.6).

$$\tilde{\theta}_{ur2} / \tilde{\theta}_m = 0.0363\left(\tilde{\theta}_m / \tilde{\theta}_c\right) + 0.7101 \qquad (2a)$$

$$\tilde{T}_{ur2} / \tilde{T}_m = -0.0126\left(\tilde{\theta}_m / \tilde{\theta}_c\right) + 0.3243 \qquad (2b)$$

4. Next, the hysteresis loop proceeds straight towards $(\tilde{\theta}_{su},0)$ on the zero load axis (path $3 \rightarrow 4$, $7 \rightarrow 8$, $12 \rightarrow 13$, $16 \rightarrow 17$, $c \rightarrow d$, $h \rightarrow i$, $o \rightarrow p$, $v \rightarrow w$). The reloading point $(\tilde{\theta}_{su},0)$ can be calculated as shown in Eq. 3 (Fig. 5.7).

$$\tilde{\theta}_{su}/\tilde{\theta}_m = -0.0015(\tilde{\theta}_m/\tilde{\theta}_c) + 0.2358 \qquad \text{for } \tilde{\theta}_c < \tilde{\theta}_m < \tilde{\theta}_y \qquad (3a)$$

$$= 0.1012(\tilde{\theta}_m/\tilde{\theta}_y) + 0.0848 \qquad \text{for } \tilde{\theta}_m > \tilde{\theta}_y \qquad (3b)$$
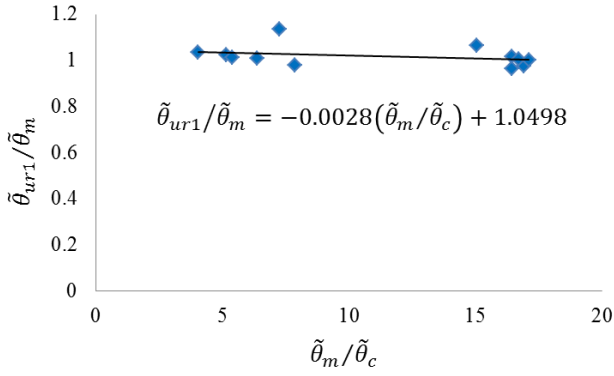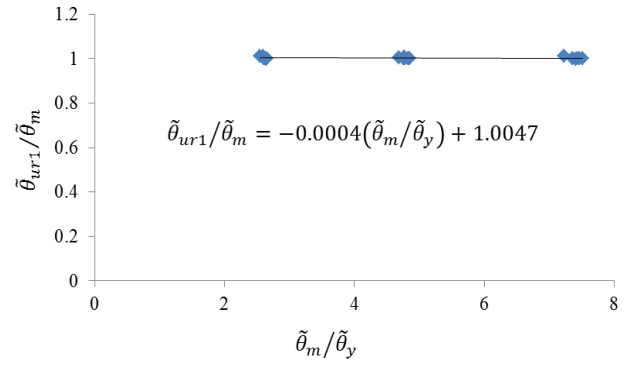
(a) $\tilde{\theta}_c < \tilde{\theta}_m < \tilde{\theta}_y$ (b) $\tilde{\theta}_m > \tilde{\theta}_y$

Fig. 5.4 - Dependence of $\tilde{\theta}_{ur1}/\tilde{\theta}_m$ on ductility ratio

$$\tilde{\theta}_{ur1}/\tilde{\theta}_m = -0.0028(\tilde{\theta}_m/\tilde{\theta}_c) + 1.0498$$

$$\tilde{\theta}_{ur1}/\tilde{\theta}_m = -0.0004(\tilde{\theta}_m/\tilde{\theta}_y) + 1.0047$$
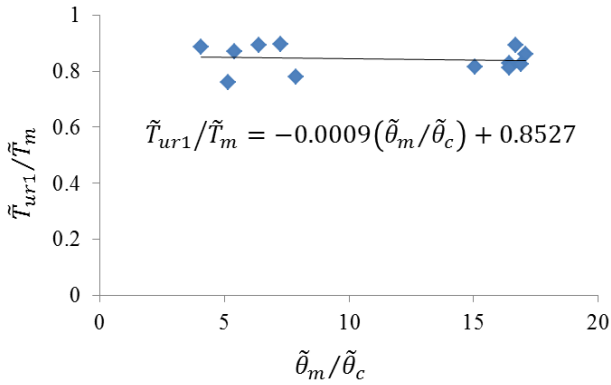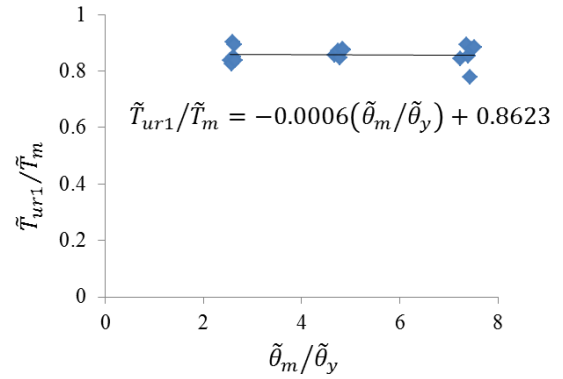
(a) $\tilde{\theta}_c < \tilde{\theta}_m < \tilde{\theta}_y$ (b) $\tilde{\theta}_m > \tilde{\theta}_y$

Fig. 5.5 - Dependence of $\tilde{T}_{ur1}/\tilde{T}_m$ on ductility ratio

$$\tilde{T}_{ur1}/\tilde{T}_m = -0.0009(\tilde{\theta}_m/\tilde{\theta}_c) + 0.8527$$

$$\tilde{T}_{ur1}/\tilde{T}_m = -0.0006(\tilde{\theta}_m/\tilde{\theta}_y) + 0.8623$$

Fig. 5.6 - Dependence of $\tilde{\theta}_{ur2}/\tilde{\theta}_m$ and $\tilde{T}_{ur2}/\tilde{T}_m$ on $\tilde{\theta}_m/\tilde{\theta}_y$

(a) $\tilde{\theta}_c < \tilde{\theta}_m < \tilde{\theta}_y$

(b) $\tilde{\theta}_m > \tilde{\theta}_y$
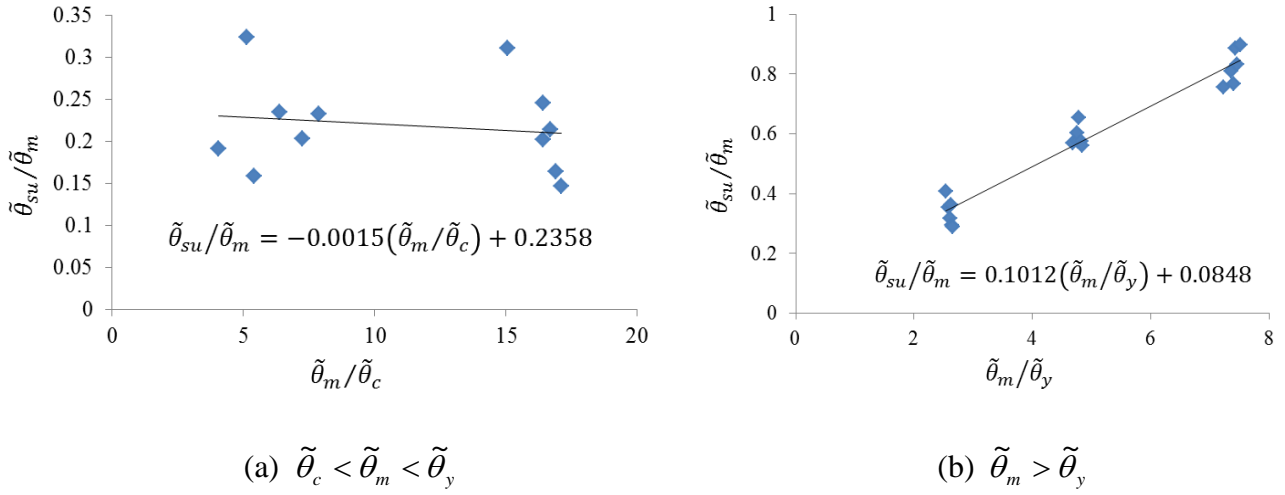
Fig. 5.7 - Dependence of $\tilde{\theta}_{su}/\tilde{\theta}_m$ on ductility ratio

5.2.3. Loading/reloading Rules

1. Initial loading and reloading follow the primary curve (path $1 \rightarrow 0$, $5 \rightarrow 0$) until the load is reversed at a level higher than the cracking load.

2. After cracking, the first loading in the opposite direction is directed towards the cracking load in the opposite direction (path $4 \rightarrow 5$).

3. When cracking load on both directions has been reached, the reloading path, till yielding, follows a straight line (path $8 \rightarrow 9$, $13 \rightarrow 14$) having a slope given by Eq. 4 (Fig. 5.8).

$$\tilde{k}_{Tr1}/\tilde{k}_{T1} = 0.7513\left(\tilde{\theta}_m/\tilde{\theta}_c\right)^{-0.786} \tag{4}$$

4. After yielding, reloading path up to $\tilde{\theta}_{cr}$ ($i \to j$, $p \to q$) follows a straight line passing through ($\tilde{\theta}_m, \tilde{T}_p$), which is estimated using Eq. 5 (Fig. 5.9).

$$\tilde{\theta}_{cr}/\tilde{\theta}_m = (-0.0067n + 0.0766)(\tilde{\theta}_m/\tilde{\theta}_y) + (0.0782n + 0.0037) \tag{5a}$$

$$\tilde{T}_p/\tilde{T}_m = (-0.0783n + 0.9425)(\tilde{\theta}_m/\tilde{\theta}_y)^{(0.1155n-1.3943)} \leq 1 \tag{5b}$$

where, n is counter indicating number of cycles repeated at unloading point $\tilde{\theta}_m$. n is assigned a value of 1 when first unloading takes place at a given deformation level ($\tilde{\theta}_m$) and incremented every time load is reversed from any deformation level falling within the range of $(1 \pm 0.05)\tilde{\theta}_m$. n is computed separately for each direction of loading.

5. After ($\tilde{\theta}_{cr}, \tilde{T}_{cr}$), the loading path heads towards ($\tilde{\theta}_m, \tilde{T}'_m$) (path $j \to k$, $q \to r$). Calculation of $\tilde{T}'_m$ is governed by Eq. 6 (Fig. 5.10).

$$\tilde{T}'_m/\tilde{T}_m = -0.05557(\tilde{\theta}_m/\tilde{\theta}_y) + (0.0177n + 0.9842) \tag{6}$$

6. Beyond the intersection of reloading branch with primary curve, the loading path follow the primary curve (path $l \to m$, $s \to t$).
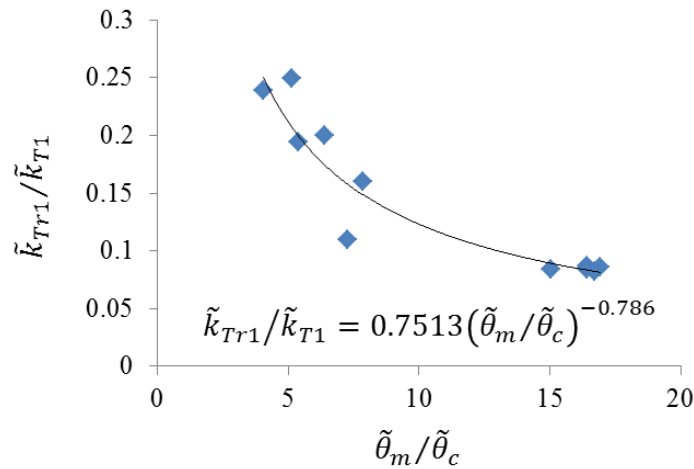
Fig. 5.8 - Dependence of $\tilde{k}_{Tr1}/\tilde{k}_{T1}$ on $\tilde{\theta}_m/\tilde{\theta}_c$

$$\tilde{\theta}_{cr}/\tilde{\theta}_m = (-0.0067n + 0.0766)(\tilde{\theta}_m/\tilde{\theta}_y) + (0.0782n + 0.0037)$$

$$\tilde{T}_p/\tilde{T}_m = (-0.0783n + 0.9425)(\tilde{\theta}_m/\tilde{\theta}_y)^{(0.1155n - 1.3943)}$$
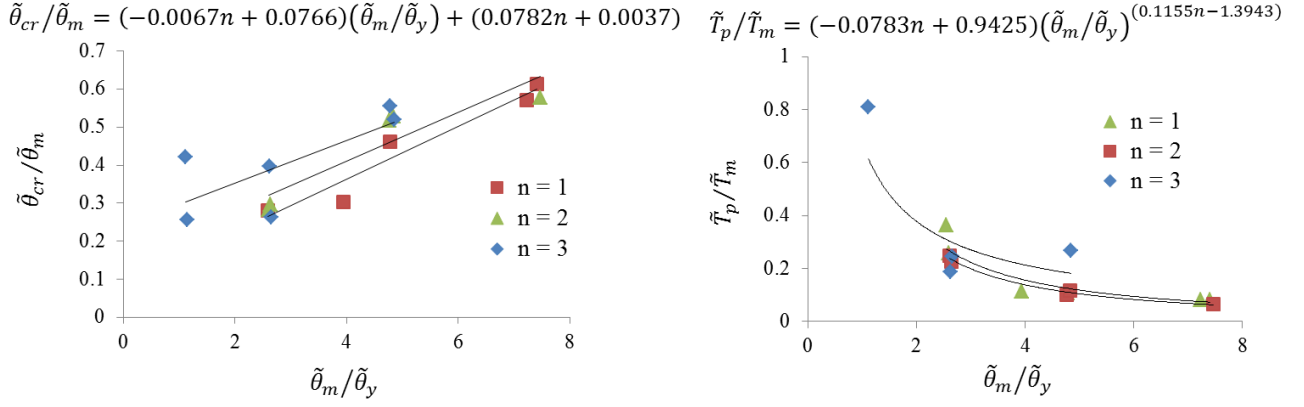
Fig. 5.9 - Dependence of $\tilde{\theta}_{cr}/\tilde{\theta}_m$ and $\tilde{T}_p/\tilde{T}_m$ on $\tilde{\theta}_m/\tilde{\theta}_y$

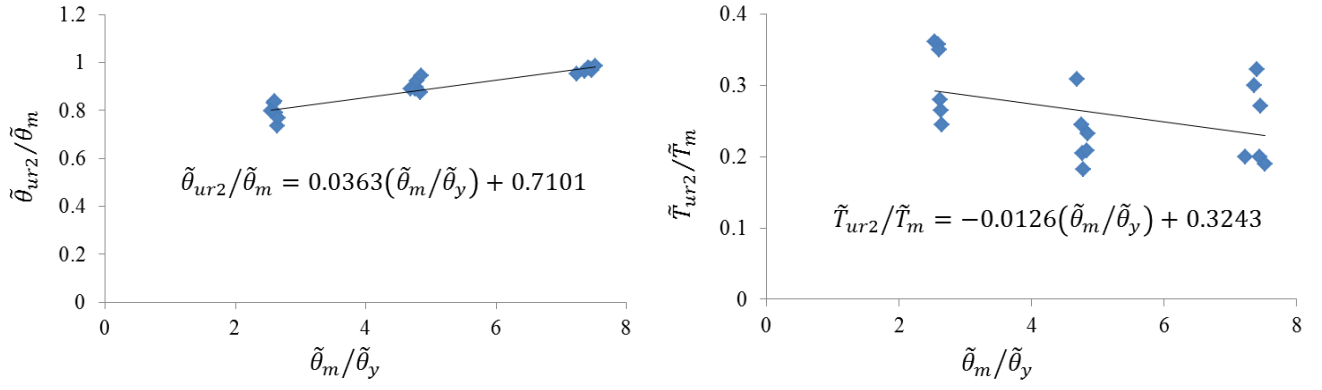$$\tilde{T}'_m/\tilde{T}_m = -0.05557(\tilde{\theta}_m/\tilde{\theta}_y) + (0.0177n + 0.9842)$$
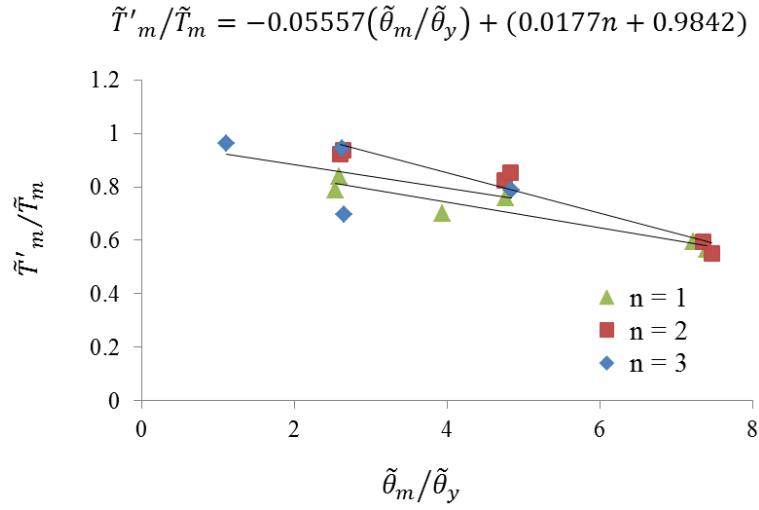
Fig. 5.10 - Dependence of $\tilde{T}'_m/\tilde{T}_m$ on $\tilde{\theta}_m/\tilde{\theta}_y$

5.3 RESULTS

5.3.1. Predictions of Load – Displacement Behavior

The torque-twist behavior predicted by the analytical model are presented and compared with experimental data in Fig. 5.11. It is observed that, the model predicted the experimental response of the columns reasonably well. It can also be seen from the graphs that the model was able to capture complex phenomena like strength and stiffness degradation along with pinching with appreciable accuracy.

(a) H/D(6)-T/M(∞)-0.73%   (b) H/D(3)-T/M(∞)-1.32%
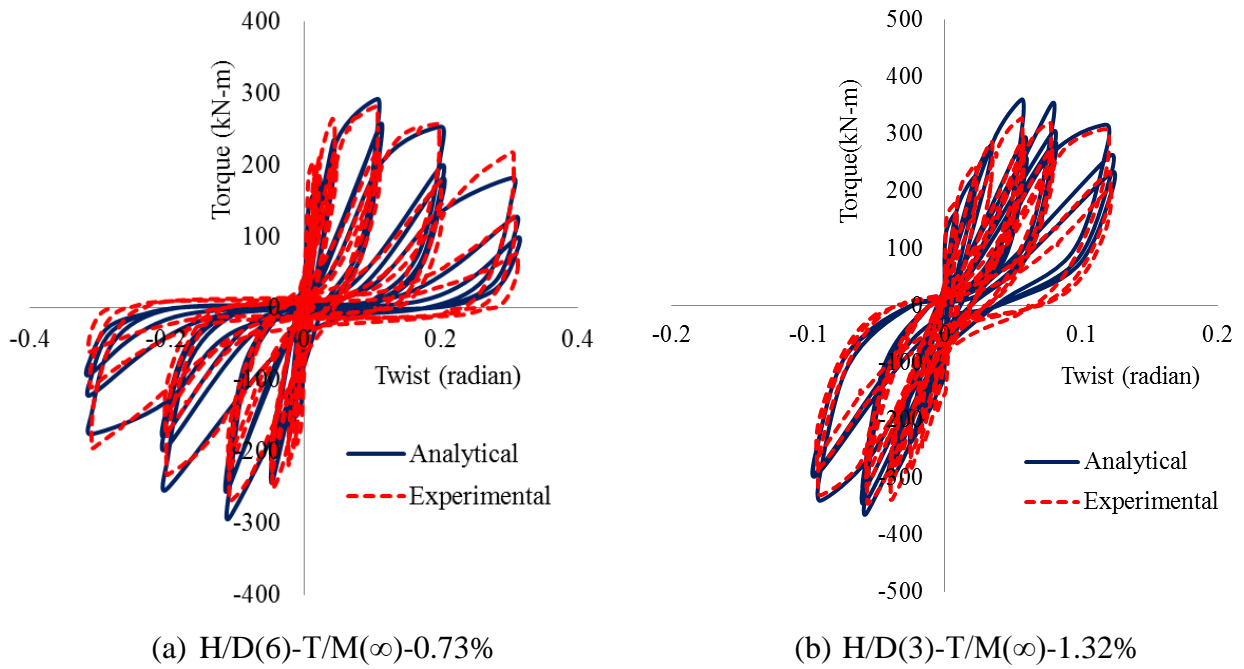
Fig. 5.11 Prediction of Torsional Hysteresis

5.4 CONCLUDING REMARKS

In this study, an improved PHM is proposed for reinforced concrete circular columns subjected to torsion. Unloading and reloading rules are derived based on experimental observations. Primary curve is proposed to be estimated from SMMT. A slope change has been suggested at the cracking point unlike in the previous models. An additional point is also introduced in the unloading branch for more accurate prediction of the hysteresis loops. The analytical torque – twist behavior showed close correlation with experimental data. The proposed model can be extended in future to predict the hysteretic response of bridge columns under combined loading including torsion.

CHAPTER 6
CONCLUSIONS

6.1 GENERAL

This study evaluated existing modeling strategies and proposed new models for analysis of RC columns under monotonic and cyclic loading. A finite element study was carried out to predict the behavior of columns under monotonic torsional loading. Behavior of columns under cyclic lateral loading was predicted using BWBN model. A homotopy based optimization technique is proposed to identify the parameters of Bouc – Wen type models using local search algorithms. Finally, a polygonal hysteresis model is developed to estimate behavior circular columns under cyclic torsion.

6.2 CONCLUSIONS

6.2.1 Finite Element Analysis

The results of nonlinear finite element analysis for RC columns under combined torsion and axial compression are presented Chapter 2. It discussed the effects of increasing the transverse reinforcement ratio and axial compression on strength, stiffness, and damage characteristics for both square and circular columns. The effect of cross sectional shape on torsional behaviour of RC columns was also discussed. The generated FE model exhibited excellent convergence and numerical stability characteristics, requiring little computational time for analyses under torsional loading. Within the scope of parameters considered in this study, the results lead to the following major conclusions:

- The FE model generated in this study accurately simulates the overall experimental responses of columns under combined torsion and axial compression. Strength, stiffness, ductility, damage progression and failure modes are captured accurately.

Computed parameters, such as reinforcement strains and member deformations are also simulated well.

- At low levels of axial compression, the cracking torsional moment increases significantly but ultimate torsional moment increases marginally. Future studies should focus on experimentally investigating the influence of higher levels of axial compression on the torsional capacity of RC bridge columns for further validation.

- The increase in transverse reinforcement ratio increased the peak torsional strength. However, it reduced the twist component at the ultimate torsional moment. It also helps to limit the damage in columns under pure torsion.

- Effect of cross sectional shape plays a major role on distribution of damage in the columns. Square columns exhibited a more localized damage while the same in the circular columns was distributed over a larger length.

- FE analysis can help to rationally estimate the shear flow thickness for developing simple analytical models from design point of view. This is scope for further work.

6.2.2 Prediction of Flexural Hysteresis using BWBN Model

BWBN model was used in this study to predict the hysteresis behaviour of circular bridge columns failing in flexure. The model was found to predict the observed cyclic behaviour of tested specimen with reasonable accuracy. Complex phenomena like system degradation and pinching are also captured well. Energy dissipated by the columns through hysteresis which is pivotal for determining seismic capacity of members also showed a good correlation with experimental data. Sensitivity analysis was carried out to estimate the sensitivity of model to variation of each parameter and sensitivity ranking was prepared based on maximum root mean square error associated with each parameter. Finally, an approximate

upper bound and lower bound for each parameter was specified based on its range of variation observed in this study.

The scope of this study was limited to circular columns failing predominantly in flexure. Circular columns showing other modes of failure were not considered in this study and are a scope of future study. Future investigations should also focus on extension of this model to other shapes of cross section. A regression analysis can be carried out to propose a simplistic relation between the model parameters and various loading as well as sectional parameters such as aspect ratio, longitudinal and transverse reinforcement ratio, level of axial compression etc. This will enable the user to estimate the model parameters and thereby predict the cyclic behaviour of any reinforced concrete columns without any system identification tool or an efficient solver.

6.2.3 Parameter Identification of Bouc – Wen Type Models using Homotopy Optimization

This study addresses the problem of high computational time associated with stochastic algorithms that are generally used to solve the Bouc – Wen model. It invokes the theory of homotopy to solve this problem using non-stochastic algorithm without compromising with the accuracy of final results. Through numerical examples and experimental data, it is shown that BW type model can also be solved using non-stochastic algorithms such as homotopy techniques. It is advantageous than the former in the sense that it saves time and thereby reduces the cost of computation. The key findings of this study within the range of parameters investigated are as follows:

1) Stochastic algorithms, which are iterative and time consuming, can be replaced by a homotopy based non-stochastic algorithm which is fast and computationally efficient.

2) Homotopy ensures convergence even with initial guesses far from the true values of the parameters.

3) Homotopy can produce accurate results even in case of objective function with multiple local minima.

Homotopy technique presented in this chapter can possibly be extended to other civil engineering problems such as identification of material properties of a medium, detection of vibration signatures such as frequency, mode shape and damping ratio. It can also be used in health monitoring of civil infrastructures through identification of damage in structural elements. Active and semi-active control of smart structures may also be benefitted by the application of this technique.

6.2.4 Polygonal Hysteresis Model for Torsion

In this study, an improved PHM is proposed for reinforced concrete circular columns subjected to torsion. Unloading and reloading rules are derived based on experimental observations. Primary curve is proposed to be estimated from SMMT. A slope change has been suggested at the cracking point unlike in the previous models. An additional point is also introduced in the unloading branch for more accurate prediction of the hysteresis loops. The analytical torque – twist behavior showed close correlation with experimental data. The proposed model can be extended in future to predict the hysteretic response of bridge columns under combined loading including torsion. Future studies should also focus on computer implementation of this hysteresis model to realize its utility fully.

REFERENCES

Abaqus Analysis User's Manual 6.11. Dassault Systèmes Simulia Corporation, Providence, RI, USA.

Atalay, M. B., and Penzien, J. (1975). "The Seismic Behavior of Critical Regions of Reinforced Concrete Components Influenced By Moment, Shear and Axial Force." Report No. UCB/EERC/75/19, University of California, Berkeley.

Aoyama, H. (1971). "Analysis on a School Building Damaged During the Tockachi - Oki Earthquake." *Proc. of Kanto District Symp.*, Arch. Inst. of Japan, Tokyo, Jan.

Baber, T. T. and Wen, Y. K. (1981). "Random Vibration of Hysteretic Degrading Systems." *J Eng. Mech. Div. ASCE,*107(6):1069–89.

Baber, T. T. and Noori, M. (1985). "Random Vibration of Degrading Pinching Systems." *J Eng. Mech.*, 111(8):1010–26.

Belarbi, A. Prakash, S., Li, Q. (2009). "Cyclic behavior of square versus circular RC columns under combined loading including torsion." *Proceedings of the 25th US-Japan Bridge Engineering Workshop*, Japan, (CD-Rom).

Bouc, R. (1967). "Forced Vibration of Mechanical Systems with Hysteresis." Proc. 4th conference on Nonlinear Oscillations (extended abstract).

Bishara, A., and Peir, J.C. (1973). "Reinforced Concrete Rectangular Columns in Torsion." *Journal of Structural Division*, Vol. 94, No. ST 12, pp. 1409-1421.

Bredt, R. (1896). "Kritische Bemerkungen zur Drehungselastizitat." *Zeitschrift des Vereines Deutscher Ingenieure*, 40 (28) 785–790; 40 (29) 813–817 (in German).

Chaudhari, S. V., and Chakrabarti, M. A. (2012). "Modeling Of Concrete For Nonlinear Analysis Using Finite Element Code ABAQUS." *International Journal of Computer Applications*, Volume 44, No.7, pp. 0975-8887.

Claeson, C. and Johansson, M. (1999). "Finite element analysis of confined concrete columns." *Proceedings of the fifth international symposium on utilization of high-strength/high-performance concrete*, Sandefjord, Norway.

Clarke, R. (2005). "Non-Bouc Degrading Hysteresis Model for Nonlinear Dynamic Procedure Seismic Design." *Journal of Structural Engineering*, 10.1061/(ASCE)0733-9445(2005)131:2(287), 287-291.

Clough, R. W. and Johnston, S. B. (1966). "Effect of stiffness degradation on earthquake ductility requirements." *Proc. Japan Earthquake Engineering Symposium*, Tokyo, Japan, pp. 195–198.

Cocchi, G. M., and Volpi, M. (1996). "Inelastic Analysis of Reinforced Concrete Beams Subjected to Combined Torsion, Flexural and Axial loads." *Computers and Structures*, 61, 479-494.

Deb, K., Pratap, A., Agarwal, S., and Meyarivan, T. (2002). "A Fast and Elitist Multiobjective Genetic Algorithm: NSGA-II." *IEEE Transaction on Evolutionary Computation*, 6(2), pp. 182–97.

Delso, J. M., Stavridis, A., and Shing, B. (2011). "Modeling the Bond-Slip Behavior of Confined Large Diameter Reinforcing Bars." *III ECCOMAS Thematic Conference on Computational Methods in Structural Dynamics and Earthquake Engineering COMPDYN*, Corfu, Greece.

Dimizas, P. C., and Koumousis, V. K. (2005). "System Identification of Non-Linear Hysteretic Systems with Application to Friction Pendulum Isolation Systems." *Proc. of 5th GRACM international congress on computational mechanics*, Limassol (Vol. 29).

Dowell, R. K., Seible, F., and Wilson, E. L. (1998). Pivot Hysteresis Model for Reinforced Concrete Members. *ACI Structural Journal*, Vol. 95 (5), pp. 607-617.

Dunlavy, D. M., and O'Leary, D. P. (2005). "Homotopy Optimization Methods for Global Optimization." Report SAND2005-7495, Sandia National Laboratories.

Fink, J., Petraschek, T., and Ondris, L. (2007). "Push-Out Test Parametric Simulation Study of a New Sheet-Type Shear Connector." Zentraler Informatikdienst (ZID) der Technischen Universitat Wien, pp. 131-153.

Floros, D., and Ingason, O. A. (2013). "Modeling and Simulation of Reinforced Concrete Beams: Coupled Analysis of Imperfectly Bonded Reinforcement in Fracturing Concrete." Master's Thesis 2013:42, Department of Applied Mechanics: Division of Solid Mechaics, Goteborg, Sweden.

Foliente, G. C. (1993). "Stochastic Dynamic Response of Wood Structural Systems." PhD Thesis. Virginia Polytechnic Institute and State University, Blacksburg, Virginia.

Fukada, Y. (1969). "A Study on the Restoring Force Characteristics of Reinforced Concrete Buildings." *Proc. of Kanto District Symp.*, Arch. Inst. of Japan, Tokyo, Japan, No. 40, (in Japanese).

Ganganagoudar, A., Mondal, T. G., and Prakash, S. S. (2016). Improved Softened Membrane Model for Reinforced Concrete Circular Bridge Columns under Torsional Loading. *Journal of Bridge Engineering*, p.04016037.

Goodnight, J., Kowalsky, M., and Nau, J. (2013). "Effect of Load History on Performance Limit States of Circular Bridge Columns." *Journal of Bridge Engineering*, 10.1061/(ASCE)BE.1943-5592.0000495, 1383-1396.

Goel, R. K., and Chopra, A. K. (1994). "Seismic Response of the US 101/Painter Street Overpassing Using Strong Motion Records." *SMIP94 Seminar on Seismological and Engineering Implications of Recent Strong-Motion Data*, California Division of Mines and Geology, Sacramento, CA.

Greene, G. G. (2006). "Behavior of Reinforced Concrete Girders under Cyclic Torsion and Torsion Combined with Shear: Experimental Investigation and Analytical Models." Ph.D. Thesis, Department of Civil, Architectural, and Environmental Engineering, University of Missouri, Rolla, 227 pp.

He, R., Yang, Y., and Sneed, L. (2015). "Seismic Repair of Reinforced Concrete Bridge Columns: Review of Research Findings." *Journal of Bridge Engineering*, 10.1061/(ASCE)BE.1943-5592.0000760, 04015015.

Heine, C. P. (2001). "Simulated Response of Degrading Hysteretic Joints with Slack Behavior." PhD Thesis. Virginia Polytechnic Institute and State University, Blacksburg, Virginia.

Hsu, T. T. C. (1968a). "Torsion of Structural Concrete - Behavior of Reinforced Concrete Rectangular Members." *Torsion of Structural Concrete, SP-18, American Concrete Institute*, Detroit, MI.

Hsu, T. T. C, and Moy, Y. L. (1985). "Softening of Concrete Torsional Members Theory and Tests." *Journal of the American Concrete Institute*, 82, 290-303.

Hsu, T.T.C. (1988). "Softening Truss Model Theory for Shear and Torsion." *Structural Journal of the American Concrete Institute*, 85 (6) 624–635.

Hsu, T.T.C. (1993). "Unified Theory of Reinforced Concrete", CRC Press Inc., Boca Raton, FL, 329 pp.

Hsu, T.T.C. and Zhang, L.X. (1997). "Nonlinear Analysis of Membrane Elements by Fixed-Angle Softened-Truss Model." *Structural Journal of the American Concrete Institute*, 94 (5) 483–492.

Hsu, H. L., and Liang, L. L. (2003). "Performance of Hollow Composite Members Subjected to Cyclic Eccentric Loading." *Earthquake Engineering and Structural Dynamics*, 32, 443-461.

Hsu, H. L., and Wang, C. L. (2000). "Flexural-Torsional Behavior of Steel Reinforced Concrete Members Subjected to Repeated Loading." *Earthquake Engineering and Structural Dynamics*, 29, 667-682.

Hurtado, G. (2009). "Effect of Torsion on the Flexural Ductility of Reinforced Concrete Bridge Columns." Ph.D. Thesis, Department of Civil and Environmental Engineering, University of California, Berkeley.

Iranmanesh, A. and Ansari, F. (2014). "Energy-Based Damage Assessment Methodology for Structural Health Monitoring of Modern Reinforced Concrete Bridge Columns." *Journal of Bridge Engineering*, 10.1061/(ASCE)BE.1943-5592.0000569, A4014004.

Isakovic, T., Fischinger, M., and Fajfar, P. (1998). "Torsional Behavior of Single Column Bent Viaducts." *Sixth U.S. National Conference on Earthquake Engineering (6NCEE).*

Ismail, M., Rodellar, J., and Ikhouane, F. (2010). "An Innovative Isolation Device for Aseismic Design." *Engineering Structures*, 32(4), pp. 1168–83.

Iwan, W. D. (1973). "A Model for the Dynamic Analysis of Deteriorating Structures." *Proc. of 5th World Congress on Earthquake Engineering*, Rome, H, pp. 1782-1791.

Jakobsen, B., Hjorth-Hansen, E., and Holand, I. (1984). "Cyclic Torsion Tests of Concrete Box Columns." *Journal of Structural Engineering*, ASCE, 110, 803-822.

Jankowiak, T., and Lodygowski T. (2005). "Identification of Parameters of Concrete Damage Plasticity Constitutive Model." *Foundations of Civil and Environmental Engineering*, No. 6.

Johnson, N. S., Saiidi, M., and Sanders, D. H. (2006). "Large-Scale Experimental and Analytical Seismic Studies of a Two-Span Reinforced Concrete Bridge System." CCEER Report No. 06-02, Center for Civil Engineering Earthquake Research, University of Nevada, Reno, NV.

Khalil, H. K. (1999). High-Gain Observers in Nonlinear Feedback Control. Lecture Notes in Control and Information Sciences: New Directions in Nonlinear Observer Design, H. Nijmeijer and T. I. Fossen, eds., Vol. 244, Springer, New York, pp. 249-268.

Kmiecik, P., and Kamiński M. (2011). "Modeling of Reinforced Concrete Structures and Composite Structures with Concrete Strength Degradation taken into Consideration." *Archives Of Civil And Mechanical Engineering*, Vol. 11, No. 3.

Kunnath S. K., Mander J. B, and Fang L. (1997). "Parameter Identification for Degrading and Pinched Hysteretic Structural Concrete Systems." *Engineering Structures*, 19(3) : 224–32.

Kunnath, S. K., Reinhorn, A. M., and Park, Y. J. (1990). "Analytical modeling of inelastic seismic response of R/C structures." *Journal of Structural Engineering*, 116(4), 996–1017.

Kustu, O., and Bouwkamp, J. G. (1973). "Behavior of Reinforced Concrete Deep Beam-Column Sub-assemblages under Cyclic Loads." Report No. UCB/EERC/73/ 08, University of California, Berkeley.

Lampert, P., and Collins, M. P. (1972). "Torsion, Bending, and Confusion : An Attempt to Establish the Facts." *Journal of the American Concrete Institute*, 69, 501-504.

Lampert, P. (1973). "Post cracking Stiffness of Reinforced Concrete Beams in Torsion and Bending." *Analysis of Structural Systems for Torsion.* SP-35, American Concrete Institute, Detroit, MI.

Lehman, D. E., and Moehle, J. P. (2000). "Performance-Based Seismic Design of Reinforced Concrete Bridge Columns." *Proc. of 12th World Earthquake Engineering Conference*, New Zealand (pp. 215-223).

Leung, M. B., and Schnobrich, W. C. (1987). "Reinforced Concrete Beams Subjected to Bending and Torsion." *Journal of Structural Engineering, ASCE*, 113, 307-320.

Lin, S., Liao, J., Liang, T., and Juang, C. (2002). "Use of Bouc-Wen Model for Seismic Analysis of Concrete Piles." *Deep Foundations*, pp. 372-384.

Mansour, M. and Hsu, T. (2005). "Behavior of Reinforced Concrete Elements under Cyclic Shear. I: Experiments." J. Struct. Eng., 10.1061/(ASCE)0733-9445(2005)131:1(44), 44-53.

Mitchell, D. and Collins, M. P. (1974). "Diagonal Compression Field Theory - A Rational Model for Structural Concrete in Pure Torsion." *Journal of the American Concrete Institute, 71,* pp. 396-408.

McLean, D. L., and Buckingham, G. C. (1994). "Seismic Performance of Bridge Columns with Interlocking Spiral Reinforcement." Report WA-RD 357.1, Washington State Department of Transportation, Olympia, WA.

Meng, J. Y., and Lui, E. M. (2000). "Torsional Effects on Short-Span Highway Bridges." *Computers and Structures*, 75, 619-629.

Mo, Y. L., Yang, R. Y. (1996). Response of reinforced/prestressed concrete box structures to dynamically applied torsion. *Nuclear engineering and design*, 165(1), 25-41.

Mondal, T. G., and Prakash, S. S. (2015a). "Effect of Tension Stiffening on the Behaviour of Reinforced Concrete Circular Columns under Torsion." *Engineering Structures Journal*, Elsevier, 92, pp. 186-195.

Mondal, T. G., and Prakash, S. S. (2015b). "Effect of Tension Stiffening on the Behaviour of Square RC Columns under Torsion." *Structural Engineering and Mechanics Journal*, Techno-press, Vol. 54, No. 3, pp. 501-520.

Mondal, T. G., and Prakash, S. S. (2015c). "Improved Softened Truss Model for Behaviour of Reinforced Concrete Circular Columns under Combined Torsion and Axial Compression." *Magazine of Concrete Research*, ICE (UK), Vol. 67, No. 1, 12 pp.

Mondal, T. G., Prakash, S. S. (2015d). "Nonlinear Finite Element Analysis of RC Bridge Columns under Torsion with and without Axial Compression." *Journal of Bridge Engineering*, 21(2), 04015037.

Mueller, A. (2014) "Real-Time Hybrid Simulation with Online Model Updating." Master's Thesis, Western Michigan University, Paper 506.

Mullapudi T. R. S., and Ayoub, A. (2009). "Non-Linear Finite Element Analysis of RC Bridge Columns using the Softened Membrane Model." *Structures Congress 2009 : Don't Mess with Structural Engineers*, ASCE, 223 pp.

Muto, K., et al. (1973). "Earthquake Resistant Design of a 20-story Reinforced Concrete Building." *Proc. of 5th World Conference on Earthquake Engineering*, Rome, Italy, II, pp. 1960-1969.

Nagata, S., Kawashima, K., and Watanabe, G. (2004). "Seismic Performance of Reinforced Concrete C-Bent Columns Based on a Hybrid Loading Test." *First International Conference on Urban Earthquake Engineering*, Tokyo, Japan.

Nelson, R. B., Saiidi, M., and Zadeh, S. (2007). "Experimental Evaluation of Performance of Conventional Bridge Systems." CCEER Report No. 07-04, Center for Civil Engineering Earthquake Research, University of Nevada, Reno, NV.

Nakata, S., Sproul, T., and Penzien, J. (1978). "Mathematical Modeling of Hysteresis Loops for Reinforced Concrete Columns." Report No. UCB/EERC/78/11, University of California, Berkeley, California.

Nithyadharan, M., & Kalyanaraman, V. (2013). "Modelling Hysteretic Behaviour of Cold-Formed Steel Wall Panels." *Engineering Structures*, 46, pp. 643-652.

Ogata, T., Suda, K., and Masukawa, J. (2000). "Transverse Reinforcement and Ductility of Reinforced Concrete High Pier with Hollow Section." *12th World Conference on Earthquake Engineering (12WCEE)*.

Omrani, R., Hudson, R., and Taciroglu, E. (2010). "Parameter Identification for Hysteretic Models of Torsional-Shear Buildings." *Structures Congress*, pp. 417-428.

Ortiz G. A. (2012). "Toolbox for Computing the Parameters of the Bouc-Wen-Baber-Noori Model of Hysteresis." available at *http://sourceforge.net/projects/boucwenbabernoo/*.

Ortiz G. A., Daniel D. A., and Bedoya-Ruiz D. (2013). "Identification of Bouc-Wen Type Models using Multi-Objective Optimization Algorithms." *Journal of Computers and Structures*, V. 114, pp. 121-132.

Otsuka, H., Takeshita, E., Yabuki, W., Wang, Y., Yoshimura, T., and Tsunomoto, M. (2004). "Study on the Seismic Performance of Reinforced Concrete Columns Subjected to Torsional Moment, Bending Moment and Axial Force." *13th World Conference on Earthquake Engineering (13WCEE).*

Ozcebe, G. and Saatcioglu, M. (1989). "Hysteretic shear model for reinforced concrete members." *Journal of Structural Engineering*, 115(1), 132–148.

Paevere P. J. (2002). "Full-scale Testing, Modeling and Analysis of Light-frame Structures under Lateral Loading," PhD thesis. Department of Civil and Environmental Engineering, University of Melbourne, Australia.

Pang, X. B. and Hsu, T.T.C. (1996). "Fixed-Angle Softened-Truss Model for Reinforced Concrete." *Structural Journal of the American Concrete Institute*, 93 (2) 197–207.

Prakash, S. S. (2009). "Seismic Behavior of RC Circular Columns under Combined Loading Including Torsion." Department of Civil Engineering, Missouri University of Science and Technology, Missouri, USA.

Prakash, S. S., Belarbi, A., and You, Y. M. (2010). "Seismic performance of circular RC columns subjected to axial, bending, and torsion with low and moderate shear." *Engineering Structures Journal*, Elsevier Vol. 32, No. 1. Pages 46-59.

Prakash, S.S., and Belarbi, A. (2010). "Towards damage-based design approach for RC bridge columns under combined loadings using damage index models", *Journal of Earthquake Engineering,* Taylor & Francis Group Journals, Vol. 14, No. 3, pages 363 – 389.

Prakash, S. S., Li, Q., and Belarbi, A. (2012). "Behavior of circular and square RC bridge columns under combined loading including torsion." *ACI Structural Journal*, Vol. 109, No. 3, pages 317-328.

Rabbat, B. G., and Collins, M. P. (1978). "A Variable Angle Space Truss Model for Structural Concrete Members Subjected to Complex Loading." *Douglas McHenry International Symposium on Concrete and Concrete Structures.* SP-55, American Concrete Institute, Detroit, MI.

Rabbat, B. G., and Russell, H. G. (1985). "Friction Coefficient of Steel on Concrete or Grout." *Journal of Structural Engineering*, ASCE 111(3): 505-515.

Rahal, K. N., and Collins, M. P. (1996). "Simple Model for Predicting Torsional Strength of Reinforced and Prestressed Concrete Sections." *ACI Structural Journal*, 93, 658-666.

Rao, S. S. (1983). Optimization: Theory and Applications. Wiley, New York.

Saadeghvaziri, M.A., and Fouch, D.A. (1990). "Behavior of RC Columns under Non-proportionally Varying Axial load." *Journal of Structural Engineering*, ASCE, V.116, No 7, pp. 1835-1856.

Saatcioglu, M., and Baingo, D. (1999). "Circular High-Strength Concrete Columns under Simulated Seismic Loading." *Journal of Structural Engineering*, 125(3), pp. 272-280.

Sengupta, P. and Li, B. (2013). "Modified Bouc-Wen Model for Hysteresis behavior of RC Beam-Column Joints with Limited Transverse Reinforcement", *Engineering Structures*, Vol. 46, pp. 392-406.

Sengupta, P. (2014). "Hysteresis Models and Fragility Assessments of Reinforced Concrete Structural Components." School of Civil & Environmental Engineering, Nanyang Technological University, Singapore.

Serban, R., Freeman, J. S. (2001). "Identification and Identifiability of Unknown parameters in Multibody Dynamic Systems." *Multibody System Dynamics*, V. 5, pp. 335-350.

Soeiro F. J. C., Stutz L. T., Tenenbaum R. A., and Neto A. J. S. (2007). "Estimation of Parameters in the Bouc-Wen Model for Magneto-Rheological Dampers using a Hybrid Method." *Proceedings of 19th International Congress of Mechanical Engineering*.

Takayanagi, T., and Schnobrich, W. C. (1977). "Computed Behavior of Coupled Shear Walls." *Proc. of 6th World Congress on Earthquake Engineering*, New Delhi, India, IH, 3069-3074.

Takeda, T., Sozen, M. A., and Nielsen, N. N. (1970). "Reinforced concrete response to simulated earthquakes." *Journal of Structural Engineering*, 96(12), 2557–2573.

Tani, S., and Nomura, S. (1973). "Response of Reinforced Concrete Structures Characterized by Skeleton curve and Normalized Characteristic Loops to Ground Motion." *Proc. of 5th World Conference on Earthquake Engineering*, Rome, Italy, II, pp. 2136-2139.

Tirasit, P., and Kawashima, K. (2005). "Seismic Torsion Response of Skewed Bridge Piers." *Journal of Earthquake Engineering*, JSCE 116, (CD-ROM).

Tirasit, P. (2006). "Seismic Performance of Reinforced Concrete Columns of Bridges under Combined Flexural and Torsional Loading." Department of Civil Engineering, Tokyo Institute of Technology, Japan.

Tirasit, P., and Kawashima, K. (2006). "Seismic Torsion Response of Skewed Bridge Piers," *Journal of Earthquake Engineering*, JSCE pp. 357-364, 2006.

Tirasit, P., and Kawashima, K. (2007a). "Seismic performance of square reinforced concrete columns under combined cyclic flexural and torsional loadings." *Journal of Earthquake Engineering*, 11, 425-452.

Tirasit, P., and Kawashima, K. (2007b). "Effect of nonlinear torsion on the performance of skewed bridge piers." *Journal of Earthquake Engineering*, 12, 980-998.

Vecchio, F. J., and Collins, M. P. (1986). "The Modified Compression-Field Theory for Reinforced Concrete Elements Subjected to Shear." *Journal of the American Concrete Institute*, 83, 219-231.

Venkappa, V., and Pandit, G. S. (1987). "Cyclic Torsion Tests on Reinforced Concrete Beams." *Journal of Structural Engineering, ASCE*, 113, 1329-1340.

Vyasarayani C. P., Uchida T., Carvalho A., and McPhee J. (2011). "Parameter Identification in Dynamic Systems using the Homotopy Optimization Approach." *Journal of Multibody System Dynamics*.

Watson, L.T., Haftka, R.T. (1989). "Modern Homotopy Methods in Optimization." *Computer Methods Applied Mechanics Engineering*, V. 74, pp. 289-305.

Watson, L.T., Wang, C.Y. (1981). "A homotopy Method Applied to Elastica Problems." *International Journal of Solid and Structures*, V. 17, pp. 29–37.

Wang, P., Han, Q., and Du, X. (2014). Seismic performance of circular RC bridge columns with flexure–torsion interaction. *Soil Dynamics and Earthquake Engineering*, 66, pp.13-30.

Wen, Y. K. (1976). "Method for Random Vibration of Hysteretic Systems." *J Eng. Mech. Div. ASCE*, 102(EM2):249–63.

Wen, Y. K. (1980). "Equivalent Linearization for Hysteretic Systems under Random Excitation." *Journal of Applied Mechanics ASME*, 47:150–4.

Yang, Y., Ma, F. (2003). "Constrained Kalman Filter for Nonlinear Structural Identification." *Journal of Vibration and Control*, 9, pp. 1343–57.

Ye, M., and Wang, X. (2007). "Parameter estimation of the Bouc–Wen hysteresis model using particle swarm optimization." *Smart Materials and Structures*, 16(6), pp. 2341–9.

Zhengying L., Albermani F., Chan R. W. K., and Kitipornchai S. (2011). "Pinching Hysteretic Response of Yielding Shear Panel Device." *Engineering Structures*, V. 33, pp. 993–1000.

Zimmermann, S. (2001). "Finite Elemente und ihre Anwendung auf physikalisch und geometrisch nichtlineare Probleme." Report TUE-BCO 01.05. Technische Universitat Eindhoven, Niederlande.